Scholar Commons
USF University of South Florida

University of South Florida
Scholar Commons

Graduate Theses and Dissertations | Graduate School

2011

Interface Engineered Diamond Coatings for Dry Machining Applications

Humberto Arturo Gomez Vega
University of South Florida, humgomez@uninorte.edu.co

Follow this and additional works at: http://scholarcommons.usf.edu/etd


Part of the American Studies Commons, Materials Science and Engineering Commons, and the Mechanical Engineering Commons

Scholar Commons Citation
Gomez Vega, Humberto Arturo, "Interface Engineered Diamond Coatings for Dry Machining Applications" (2011). *Graduate Theses and Dissertations.*
http://scholarcommons.usf.edu/etd/3121

This Dissertation is brought to you for free and open access by the Graduate School at Scholar Commons. It has been accepted for inclusion in Graduate Theses and Dissertations by an authorized administrator of Scholar Commons. For more information, please contact scholarcommons@usf.edu.

www.manaraa.com

Interface Engineered Diamond Coatings for Dry Machining Applications

by

Humberto A. Gomez Vega

A dissertation submitted in partial fulfillment
of the requirements for the degree of
Doctor of Philosophy
Department of Mechanical Engineering
College of Engineering
University of South Florida

Major Professor: Ashok Kumar, Ph.D.
Delcie Durham, Ph.D.
Rajiv Dubey, Ph.D.
Jing Wang, Ph.D.
Hariharan Srikanth, Ph.D.
Manoj Ram, Ph.D.
Marco Sanjuan, Ph.D

Date of Approval:
October 28, 2011

Keywords: Delamination, Adhesion, Wear, CVD, Surface

Copyright © 2011, Humberto A. Gomez Vega

www.manaraa.com

DEDICATION

For Samantha. You came to our life during the writing of this dissertation and gave me the strength and joy to culminate my dream. For my wife Sandra for walking next to me during this journey. For my parents for believing in my capabilities and being always there.

www.manaraa.com

ACKNOWLEDGMENTS

I would like to thank to Dr. Ashok Kumar, for giving me all the opportunities I had during my doctoral studies and providing his guidance and constant support. I would also like to thank to Dr. Delcie Durham, for her timely and invaluable suggestions during my research. I would like to highly acknowledge Dr. Anil Sachdev, Dr. Xingcheng Xiao, and Dr. Michael Lukitsch at General Motors R&D Center for the opportunity of being part of the new GM family and their professional guidance during my research. I have to thank my committee members, Dr. Rajiv Dubey, Jing Wang, Hariharan Srikanth, and Marco Sanjuan for their professional feedback regarding my dissertation. I deeply thank to Dr. Manoj Ram for all his significant research advice and motivation during my career path. Thank you to Dr. Wilfrido Moreno for serving as the Chair of my doctoral defense.

I would like to thank to Dr. Jessica Weber and all of my lab-mates for all their help during my research activities. A special thank to Mr. Bernard Batson, for providing priceless support and advice for me and my wife Sandra. Thank you to Ms. Susan Britten and Ms. Shirley Tervort of the Mechanical Engineering office for all their administrative help. I would also like to thank to all NREC staff, for their support and guidance during this research. I would like to thank Dr. Kevin Chou at the University of Alabama, for his advice and support. The financial support for this research came from the NSF GOALI/Collaborative Research Award # 0928823.

www.manaraa.com

TABLE OF CONTENTS

www.manaraa.com

www.manaraa.com

LIST OF TABLES

www.manaraa.com

www.manaraa.com

LIST OF FIGURES

www.manaraa.com

www.manaraa.com

www.manaraa.com

www.manaraa.com

www.manaraa.com

www.manaraa.com

www.manaraa.com

ABSTRACT

Several studies have been propose to improve the adhesion of diamond films on cemented carbide tool materials, however a systematic study in identifying the role of the factors that affect the final diamond adhesion and the resulting machining performance of the tool under real manufacturing conditions is still unexplored. CVD diamond film's extraordinary qualities bring little benefit if the film fails to adhere sufficiently to the substrate. Inadequate adhesion undermines tool performance and longevity, causing unpredictable behavior under load and possibly leading to unexpected failure of the tool in the production line. This dissertation investigates the effects of different surface pretreatments on the adhesion and performance of CVD diamond coated WC-Co turning inserts for the dry machining of high silicon aluminum alloys.

Different interfacial characteristics between the diamond coatings and the modified WC-Co substrate were obtained by the use of two different chemical etchings and a CrN/Cr interlayer, with the aim to produce an adherent diamond coating by increasing the interlocking effect of the diamond film, and halting the catalytic effect of the cobalt present on the cemented carbide tool. A systematic study is analyzed in terms of the initial cutting tool surface modifications, the deposition and characterization of microcrystalline diamond coatings deposited by HFCVD synthesis, the estimation of the resulting diamond adhesion by Rockwell indentations and Raman spectroscopy, and

www.manaraa.com

finally, the evaluation of the dry machining performance of the diamond coated tools on A390 aluminum alloys. Scanning electron microscopy (SEM), metallographic analysis, and x-ray diffraction techniques were used to characterize the morphology, cobalt content, and nature of the substrate surfaces before and after each pretreatment; optical interferometry was utilized to characterize the surface roughness. After successfully diamond depositions, the films were characterized again using SEM, Raman spectroscopy, XRD, Electron Probe Microscopy Analysis (EPMA), and optical interferometry.

The experiments show that chemical etching methods exceed the effect of the CrN/Cr interlayer in increasing the diamond coating adhesion under dry cutting operations. This dissertation provided new insights about optimizing the surface characteristics of cemented carbides to produce adherent diamond coatings in the dry cutting manufacturing chain of high silicon aluminum alloys.

An alternative method to measure the practical adhesion on commercial diamond coatings that can be correlated with the machining performance is proposed to be used when other methods (scratch, nanoindentation, microindentation, pin-on-disk, etc.) are not viable.

This research is the first comprehensive and systematic work that links the surface/subsurface integrity of cutting tools with their ability to produce an adherent diamond coating capable to dry machine high silicon aluminum alloys.

www.manaraa.com

CHAPTER 1. INTRODUCTION

1.1. Research Overview

Capturing the unique properties of carbon in its crystalline diamond structure requires knowledge of both material science and manufacturing techniques. The final diamond coating performance not only depends on the diamond properties itself, but also on the substrate surface characteristics that it is deposited on. In addition to the adhesion of the coating to the underlying substrate base, a compromise between fracture toughness and wear resistance is required for cutting applications.

Cemented carbide tools enriched with cobalt binder levels from 3 - 13 wt% to provide high fracture strength are the most commonly used tool materials for machining applications. When diamond is deposited on these substrates, Co represents an issue to the final diamond adhesion as a consequence of the carbon-cobalt solubility (0.2 – 0.3 wt %) at diamond CVD temperatures as shown in Figure 1.1, which promotes the diffusion of carbon in cobalt and produces a weak non-diamond layer at the interface, preventing diamond nucleation and creating voids with a detrimental effect on the final diamond adhesion.

www.manaraa.com

In order to overcome these issues, any proposed solution must suppress the detrimental effect of cobalt, maximize the adhesion by increasing the mechanical interlocking between the coating and the substrate, and enhance the interface toughness.

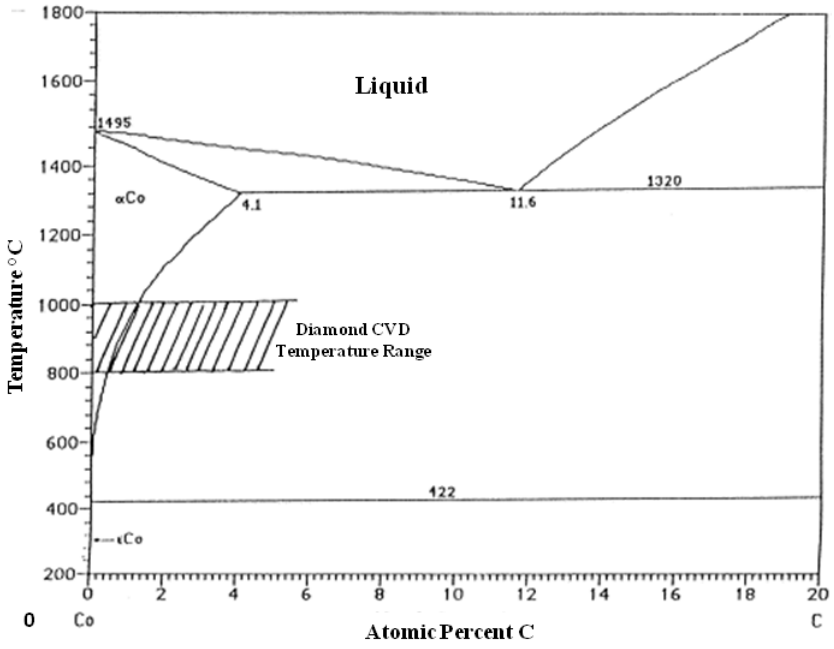

Figure 1.1. Phase diagram of Co – C system depicting the interdiffusion range at standard diamond CVD conditions on WC-Co substrates. Adapted from Mallika and Komanduri [1]

Numerous solutions have been evaluated in scientific literature to increase the diamond adhesion when deposited on cobalt cemented carbide substrates, however, the majorities do not take into account the practical conditions encountered when using commercial carbide tools existing in the market as the substrate material of interest. In most of these research studies, substrate samples correspond to WC-Co coupons with surface conditions that differ from the commercial tools and cutting inserts. Moreover, the pretreatment effects in the surface/subsurface modifications of the carbide tool

www.manaraa.com

materials used as a substrate for further diamond deposition have not been systematically evaluated, specifically, in terms of the Co depletion/halting approach effect with respect to the resulting dry machining performance. This type of analysis may exist as the internal know-how of CVD diamond tool makers, who normally optimize the process variables for particular customer applications.

The present study proposes a systematic approach, supported from the fundamental aspects required in producing an adherent diamond coating on cemented carbides, followed by the modification of the substrate surface/subsurface characteristics, analyzed along the resulting diamond quality in terms of adhesion, and finally concluded from the machining behavior of the diamond coatings under a real dry machining scenario. Most of the traditional studies conclude about diamond adhesion from evaluating the results obtained by final indentation or scratch techniques on the coatings. In contrast, the present approach provides a comparison between indentation techniques and the dry machining results by using diamond coatings that have been deposited using the same growth characteristics and thicknesses (25 – 30 μm) than the commercial microcrystalline diamond (MCD) tools found in the market.

Despite the recent interest in the use of nanocrystalline diamond (NCD) coatings in cutting tools due to their tribological advantages, or the evaluation of multilayered MCD/NCD architectures, this dissertation is mainly focused on the interfacial aspects required to achieve an optimal diamond coating adhesion. Different surface pretreatments are evaluated in terms of the effects produced on the carbide substrate surface textures and subsurface modifications when using chemical etchings or physical vapor deposited

www.manaraa.com

(PVD) inter-diffusion barrier layers to overcome the effects of the Co binder. A final correlation between the substrate pretreatments and the failure of the diamond coating under indentation and dry machining cutting operations is analyzed. The synergy between the fundamental and practical aspects of surface engineering principles tailored to improve the practical adhesion of diamond is presented in this dissertation, and will positively impact the final performance regardless of the diamond coating architecture. The overall research approach is summarized in Figure 1.2.

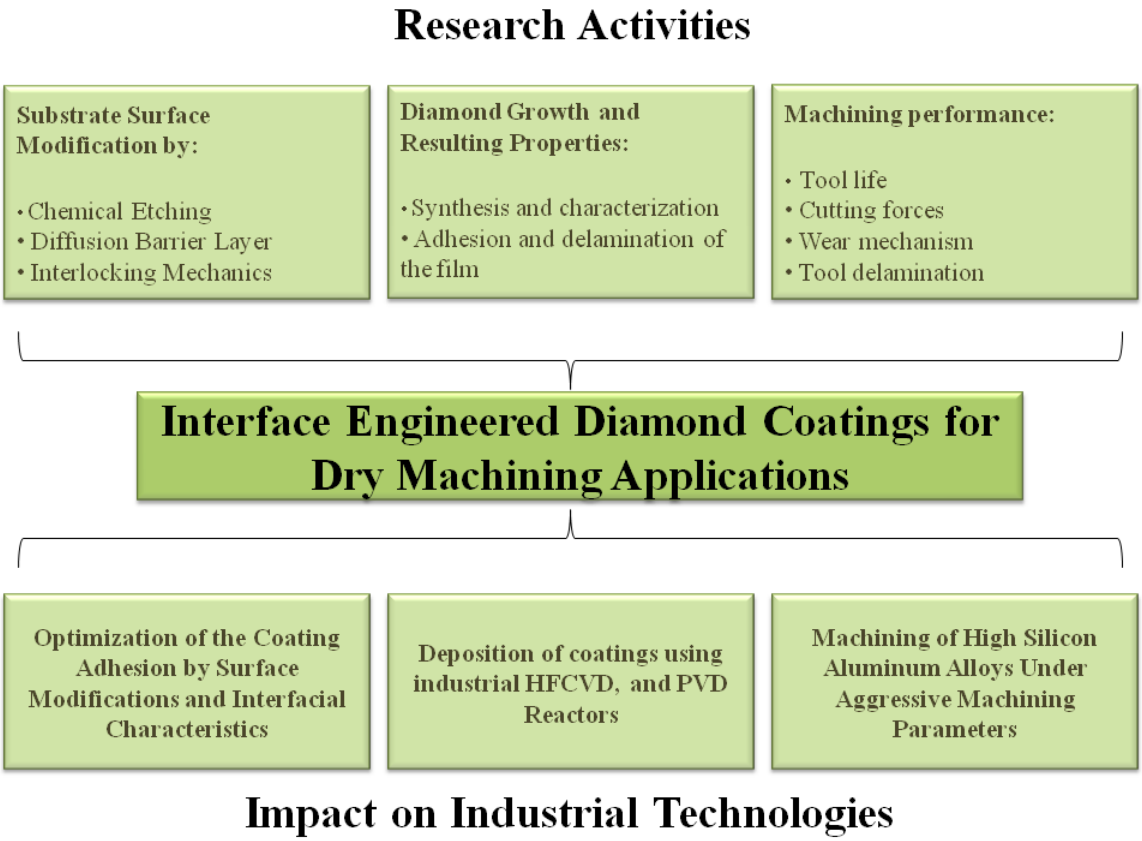

Figure 1.2. Proposed research approach

www.manaraa.com

In order to fulfill the aforementioned approach, the main objective of this research can be stated as to investigate the performance of newly developed CVD diamond coated tools, by modifying the surface characteristics of commercial cemented carbide tools, with the aim to improve the interfacial conditions necessary to achieve an adherent diamond coating intended for dry machining-cutting operations.

Several interface engineering approaches have been reported in the last 15 years with the aim of reducing the undesired catalytic effect of cobalt on diamond adhesion. In order to maximize the practical adhesion of diamond coatings on cemented carbides, any approach must halt the interdiffusion effect of cobalt. The most widely successful techniques discussed in the literature are related to the cobalt removal in depths ranging in about 3 – 10 μm from the substrate surface by using chemical etching methods, or by halting the cobalt effect on the surface by depositing interdiffusion barrier layers, that also diminish the thermal stresses caused during the diamond growth.

In the present research, the effects of these interfacial approaches will be correlated with the dry machining performance when using specific experimental conditions intended to analyze their effects in the substrate (cutting tool) with the aim to:

- Establish the amount of surface/subsurface integrity preexisting in the commercial tool and how influences the optimization of the subsequent surface pretreatment methods
- Characterize the effect of two chemical etching methods in the surface/subsurface morphology of the tool

www.manaraa.com

- Evaluate a potential re-diffusion of Co from the bulk to the pretreated surface during the deposition of diamond coatings when chemical pretreatment methods are used
- Characterize the role of CrN/Cr interdiffusion barrier layers in the adhesion improvement of diamond coatings deposited in cemented carbide substrates
- Study the delamination process of diamond coatings during indentation methods and its correlation with each surface pretreatment
- Quantify the resulting tool life and machining performance of the pretreated diamond coated cutting tools under specific dry cutting conditions
- Analyze the corresponding wear failure mechanism of the diamond coated tools after dry machining operations

1.2. Diamond Structure and Synthesis

Diamond is a cubic modification of crystalline carbon known as the diamond lattice and arranged as two interpenetrating face centered cubic Bravais lattices derived from a sp^3 covalent chemical bond as shown in Figure 1.3. There are eight atoms per unit cell distributed among eight corners, six face centers, and four other lattice positions for a total of $1.77E10^{23}$ atoms/cm^3, which corresponds to the highest atomic density of any material.

www.manaraa.com

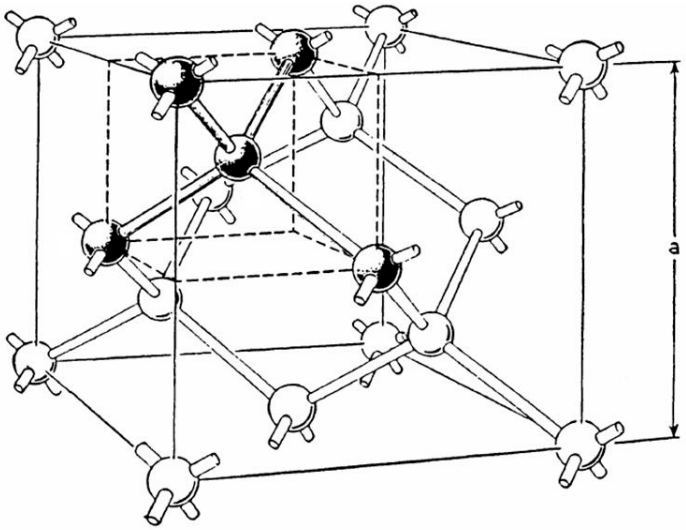

Figure 1.3. Crystal diamond structure viewed as two interpenetrating face centered cubic (FCC) Bravais lattices. The near distance between neighbor atoms is 1.54 Å and the lattice parameter a is 3.567 Å at 298 K [2]

There are many exceptional properties of diamond in addition to being the hardest known material. Diamond also has the lowest compressibility, the highest elastic modulus, the highest thermal conductivity of all solids in the temperature range of 90 to 1200 K. It also has the lowest specific heat of all solids in the temperature range of 0 to 800 K, a considerably higher mobility associated with holes for p-type doped diamond than the hole-mobility of either silicon or gallium arsenide, and also, pure diamond has the largest optical transmission bandwidth of any solid material [3]. A summary of some diamond properties is compiled in Table 1.1.

www.manaraa.com

Table 1.1. Summary of properties of diamond compared with reference materials

PROPERTIES	DIAMOND	REFERENCE MATERIAL	COMMENTS FOR DIAMOND
KNOOP HARDNESS	5700 – 10,400 kg/mm^2	**Hardened Steel**: 400 Kg/mm^2	Depending of the crystallographic orientation of the sample
MOHS HARDNESS	10	**Steel tool**: 6 – 7	10 is the largest value of the scale
YOUNG'S MODULUS	1050 GPa	**Tungsten Carbide WC**: 450 – 650 GPa	Five times higher than steel
THERMAL CONDUCTIVITY	20 W/cm-K	**Copper:** 4.01 W/cm-K	At room temperature
SPECIFIC HEAT	6.195 J/mol-K	**Aluminum**: 24.2 J/mol-K	At 300 K
ENERGY BAND GAP	5.47 eV	**Silicon:** 1.11 eV	At 300 K
DIELECTRIC CONSTANT	5.7	**Neoprene**: 6.7	At 20 °C

The new developments in characterization techniques during the last century, and the improvement in scientific apparatuses by the use of new materials, reliable manufacturing processes, and new concepts in physics, made a significant impact in the synthetic diamond production. One of the most important contributions was made by

www.manaraa.com

Percy William Bridgman in the field of high-pressure physics. Bridgman synthesized numerous new materials by pressurizing all different kinds of compounds in his anvil by using a revolutionary non-extruding gasket device. However, Bridgman was not able to produce synthetic diamond, but his developments on high pressure systems opened a new era in physics that allows the final achievement of producing synthetic diamonds in the near future.

The final successful diamond synthesis was only possible by doing innovative modifications to the existing Bridgman's apparatus, which allowed producing high pressures and high temperatures at stable conditions for significant periods of time. Afterward, the so called "belt" apparatus was designed by H. T. Hall in 1953, capable of reaching pressures of 3,000,000 psi and temperatures up to approximately 5,000 °C at the same time [4]. Using these capabilities, F. Bundy was able to make a significant contribution to the diamond field by proposing the new pressure-temperature phase diagram of carbon shown in Figure 1.4 [5]. Later on, the final goal was achieved by scientists (H. Nerad, F. Bundy, H. Strong, R. Wentorf, Etc.) at the *General Electric Company* in 1955, when they announced the results from a reproducible synthesis process of artificial diamond [6].

Today, it is possible to synthesize commercial diamond at high pressure (HP) and high temperature (HT) states. This HP-HT synthesis process is mostly used in industrial applications to produce polishing, grinding, cutting, and sawing products. However, at these conditions it is not possible to deposit diamond over large surface areas. The importance and interest of diamond synthesis at low pressure is based on the unique

www.manaraa.com

properties that can be achieved using this method to deposit conformal functional coatings on the surface of solid materials, including new thin film architectures and nanosized films based on the deposition of microcrystalline (MCD) or nanocrystalline (NCD) structured diamond by using low pressure synthesis methods like Chemical Vapor Deposition (CVD).

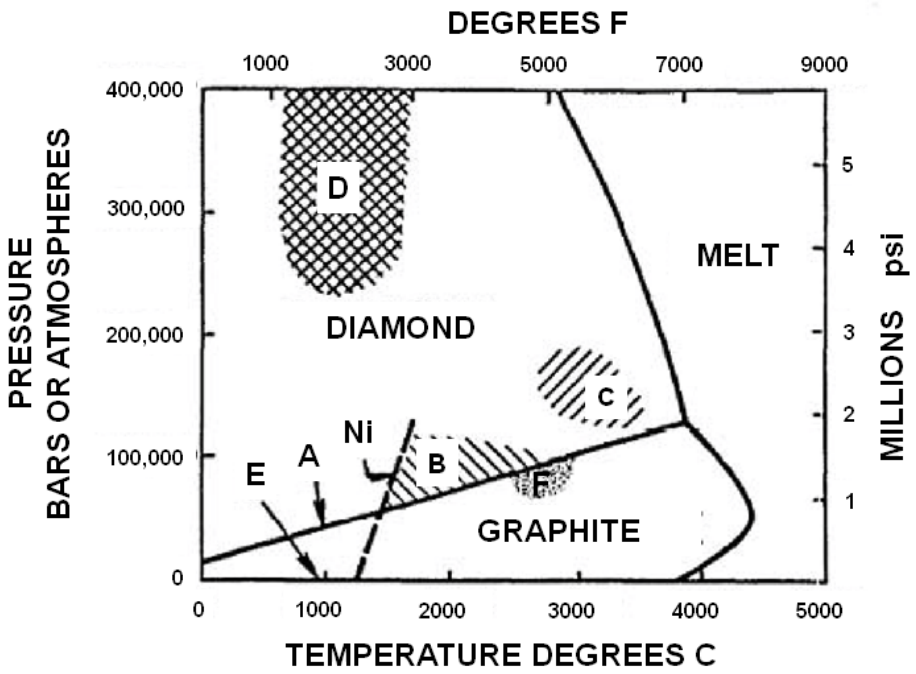

Figure 1.4. Pressure-temperature phase diagram of carbon. Diamond is a stable form of carbon only above line A. Scientist of General Electric synthesized diamond on region B using Ni as a catalyst. C represents a synthesis region with no metal solvent used by Bundy, D is a high pressure but lower temperature synthesis region, and E represents the metastable growth of diamond film conditions at low pressure-low temperature [5]

A CVD process uses a gaseous feedstock containing a carbon source and an input of energy to the system which breaks the carbonaceous gas in diverse subspecies for the donation of carbon atoms to the substrate, then promoting the growing of a diamond film

www.manaraa.com

over the surface when specific low pressure-temperature conditions are used. This film is used to enhance the mechanical, electrical, thermal, optical, or electrochemical properties of different materials in specific product designs, including new kinds of electrodes, electronic devices, sensors, high quality loudspeakers, thermal management applications, bearings, and cutting tools.

More details about the diamond CVD synthesis and characterization will be discussed in Chapter 3, with particular interest in the growth mechanism and characterization of the diamond coatings deposited by Hot Filament Chemical Vapor Deposition (HFCVD) technique, which is the synthesis process used to deposit the diamond on the tool substrates during this research.

1.3. The Importance of Diamond Coatings for Machining Operations

Cutting fluids are traditionally introduced to machining processes in order to perform uninterrupted metal cutting operations, prolong tool life, improve surface finish, prevent workpiece overheating, remove chips from the cutting area, and reduce contact wear [7]. However, these benefits represent a considerable cost to production schemes in terms of disposal, recycling, healthcare premiums, and inventory, including new challenges from environmental legislation and footprint impact [8].

The estimated global market of over $1500 million in 2007 (increasing 6% annually) related to equipment used in filtration and separation of cutting fluids [9], provides an important reason to companies in seeking new strategies to reduce fluid

www.manaraa.com

consumption or remove them entirely from the machining operation. Additionally, companies are facing an increase in environmental concerns against the disposal of cutting fluid effluents in river/sewer discharges, mainly due to the toxic nature of nitrogen compounds present as emulsifiers in common cutting fluids.

Subsequently, all of the above-mentioned reasons influence the industry towards more cost effective and green manufacturing approaches, like minimum quantity lubrication (MQL), minimum quantity cooling (MQC), and dry machining cutting operations. Among these, dry machining represents the ultimate environmental goal of metal cutting [8]; however, it also faces new challenges in terms of the cutting tool integrity as a result of the high forces, high temperatures, and chemical interactions developed when going dry.

In order to overcome the detrimental effects in the cutting tool material associated to the harsh conditions developed during dry machining, the resulting tribological interface must be understood in terms of the friction and wear mechanisms at the contact region on the tool. The cutting process as a tribological system is illustrated in Figure 1.5, which is determined by the contact couple (cutting tool and workpiece), the operational parameters, and the environment medium [10]. Under these circumstances, the cutting tool represents the fundamental body in the process and constitutes the main aspect to be addressed during this research dissertation, by improving the tool performance when using diamond coatings deposited on commercial cemented carbides.

www.manaraa.com

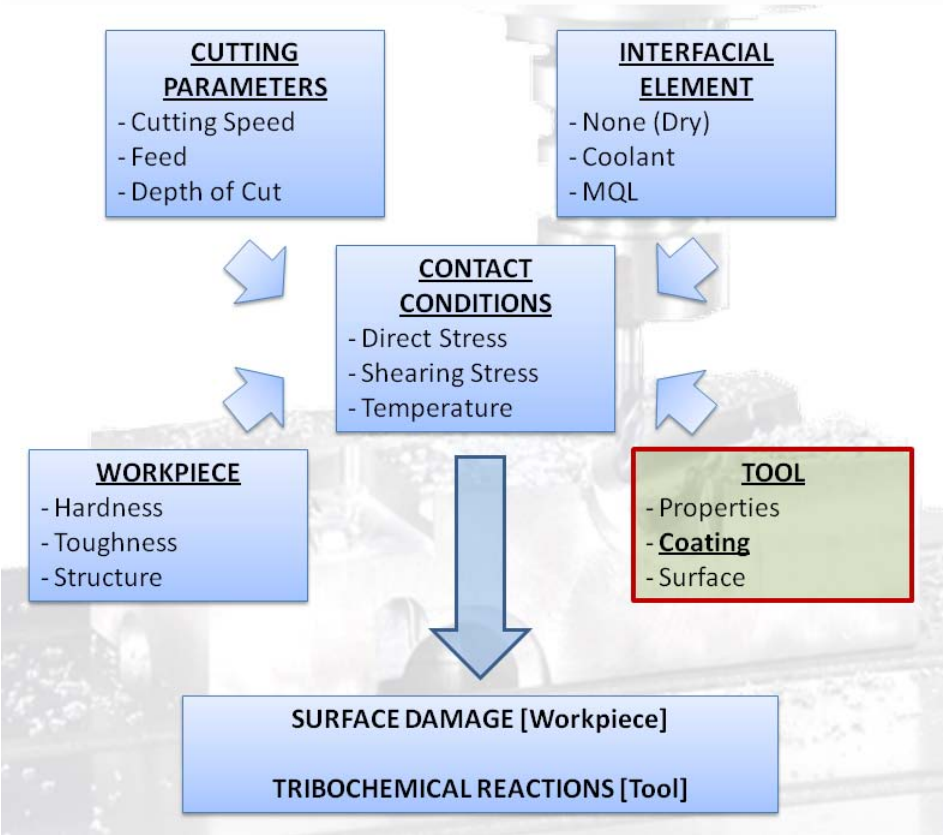

Figure 1.5. The cutting process as a tribological system. Adapted from Weinert *et al*. [11] and WorldPress [12]

Nowadays, there is an uprising trend in the dry machining of composite metals such as aluminum-silicon alloys and aluminum matrix composites as the result of the environmental impact of coolants used in traditional wet machining, disposed in the form of mist, waste, and coolant-coated chips produce a harmful effect to the environment [13].

www.manaraa.com

Diamond coatings have been proposed to enhance the performance of cemented carbide tools in the dry machining of aluminum alloys for the automobile and aerospace industries [14]. Particularly, aluminum alloys are very abrasive and extremely difficult to dry machine with conventional PVD TiN coated materials due to the formation of built-up layer (BUL) or built-up edge (BUE) over the rake surface of the tool [15]. The exceptional hardness and wear properties of CVD diamond coatings would be very suitable for this purpose [16].

However, machining performance of diamond coated tools is not yet robust due to the non-optimized adhesion between the carbide tool and the deposited diamond. An insufficient coating adhesion of the cutting tool would render it too inadequate or lead to unpredictable behavior and even possible catastrophic failure in the production. As a consequence, the development of new automated high-speed machine centers and the use of composite metal materials in the design of complex-geometry products, create a big challenge for diamond coated cutting tools under dry machining conditions. In this dissertation, a surface engineering approach is applied to WC-Co turning inserts in order to improve the diamond coating adhesion and the subsequent machining performance in the dry machining of high silicon aluminum alloys.

1.4. CVD Diamond Cutting Tools

There are two kinds of coating technologies in the market for diamond cutting tools, high pressure (HP) - high temperature (HT) polycrystalline diamond (PCD), and low pressure chemical vapor deposited (CVD) micro and nanocrystalline diamond.

www.manaraa.com

In polycrystalline diamond tools, diamond grits produced by HP-HT synthesis are compacted and sintered with cobalt as a binder to form a thick PCD tip, which is subsequently attached (brazed) to the substrate material, commonly cemented carbides like WC-Co, which have a high strength, toughness, and high hardness to be used in cutting tool applications.

In contrast, the low pressure approach produces a diamond thin-film coating (5-35μm) that is directly deposited onto the surface of the carbide by the chemical vapor deposition (CVD) technique. Thick CVD freestanding diamond wafers (150 – 1000 μm) are also produced, which the aims of these are to be laser-cut and attached to carbide substrates in a similar fashion than the PCD tips but at a higher cost when compared to conformal direct thin-film CVD synthesis.

The ability to form a conformal coating over a complex-geometry is a remarkable advantage of the CVD technology, allowing the capture of diamond in shapes not available in the industry previously. CVD diamond coated carbide tools were initially introduced to the market at the 1994 International Manufacturing Technology Show in Chicago by four tool-making companies (Crystallume, Sandvick Coromant Co, Kennametal, and Teledyne Advanced Materials-Cutting Tools), fulfilling earlier expectations about the practical use of CVD diamond cutting tools. This was also possible by the introduction of the first commercial microwave chemical vapor deposition system (MWCVD) from Applied Science and Technology Inc. (ASTeX®), capable of producing 300 SPG-422 style cutting inserts coated with 20 μm-thick diamond per day [17]. However, even though all the benefits brought by CVD diamond coated

www.manaraa.com

tools at that moment, new challenges emerged in terms of how to improve the adhesion of the diamond coating and extend the cutting tool life, and still remain today.

Initial studies tried to overcome the undesired catalytical role of Co present in the cemented carbides as the binder, which has a negative influence in the resulting diamond adhesion and the machining performance when compared with PCD tools [18]. The cobalt effect must be minimized or suppressed in order to achieve a practical adhesion between the diamond and the cemented carbide.

Multiple approaches have been evaluated in the last fifteen years, and will be discusses later as part of the surface engineered treatments evaluated in this dissertation. For the moment, visualize the diamond coating and the WC-Co substrate material as a "composite" system, where the interface between the coating and the substrate plays an important role in the tool behavior and the resulting dry machining performance. This system is shown in Figure 1.6 which depicts a microcrystalline diamond (MCD) coating deposited on a surface modified WC-Co substrate.

www.manaraa.com

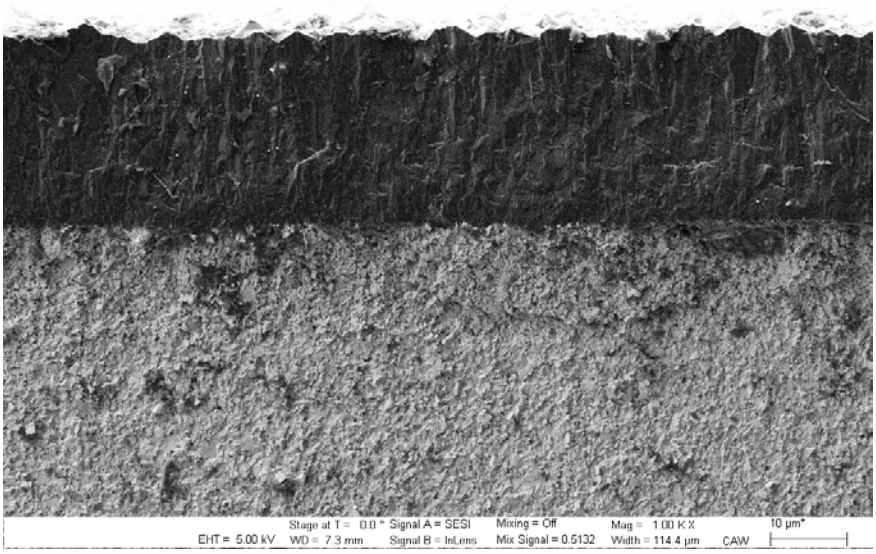

Figure 1.6. Microcrystalline diamond (MCD) coating (top) deposited in a WC-Co substrate. This image corresponds to a cross section produced by fracture

1.5. Dissertation Scope and Outline

The scope of this dissertation in terms of the activities necessary to achieve the main research objective is discussed as the sum of the following tasks:

- To understand the process variables and material properties involved in the deposition of diamond coating by chemical vapor deposition (CVD)
- To produce different engineered surfaces on commercial WC-Co cutting tool substrates, in order to promote the interlocking mechanism in the diamond coating and decrease the detrimental effects of the Co binder
- To deposit diamond coating at different processing conditions

www.manaraa.com

- To characterize the properties of diamond coatings, resulting from different interfaces, including microstructure, crystal characteristics, residual stresses, and adhesion
- To evaluate the dry machining performance of the diamond coated tools in terms of cutting forces, tool life, and wear failure mechanisms, in correlation with the different surface engineered interfaces and initial adhesion
- To provide a guideline in surface engineering techniques in order to improve the CVD diamond coated tool adhesion during dry machining operations

Chapter 2 provides a background on machining and tooling topics for cutting operations, describing the essential concepts required to explain the mechanisms and behaviors associated to the dry machining results discussed in this dissertation. This chapter discusses the key aspects related to the orthogonal cutting model in terms its fundamental concepts, the development of cutting forces and how are resolved in turning operations, a brief description about the required properties for cutting tool materials, some important tool wear and tool failure mechanisms, and a cutting tool life criteria.

Chapter 3 presents the insights about synthetic diamond growth with particular interests in diamond coatings grown by microwave chemical vapor deposition (MWCVD) and hot filament chemical vapor deposition (HFCVD) processes, the latter being the one used to deposit the MCD coatings on cutting tools evaluated in this dissertation. Important characterization techniques are discussed in this chapter with

www.manaraa.com

emphasis in the micro/nano structural aspects of diamond grown by CVD methods and their influence in the resulting diamond coating quality. Relationships between the structural properties of diamond films and their application in tool coatings will be also established.

In accordance to the categories established for surface engineering technology, this dissertation deals with the optimization of substrate surfaces in terms of adhesion, to successfully deposit diamond coatings and enabling coating technology to be applied in industrial applications. Accordingly, Chapter 4 corresponds to the discussion about the experimental work done during this research in regard to the deposition of CVD diamond coatings on cemented carbides. It begins describing details about the synthesis requirements for diamond coatings on WC-Co turning inserts, then discusses the surface conditions necessary to achieve successful adhesion between the substrate and the diamond coating, and finally presents an analysis of the significant surface features obtained by using different pretreatments on the tool substrates, which will provide the main input to the subsequent understanding about the diamond coating adhesion under dry machining conditions. This surface engineered analysis represents a key objective in terms of the wear and failure modes of diamond coatings deposited on commercial WC-Co cutting tools.

Chapter 5 discusses the characterization of diamond coatings deposited on the pretreated surfaces of WC-Co turning inserts in terms of the structural properties obtained from depositions by a HFCVD process. In addition, a comprehensive evaluation of the coating behavior under Rockwell indentation conditions is presented. This analysis

www.manaraa.com

encompasses a correlation between the structural properties of the diamond coatings, the estimated stress conditions, and the delamination analysis correlated with the initial substrate surface characteristics discussed in Chapter 4, by the use of several characterization methods.

The final dry machining behavior of the diamond coated turning inserts is presented in Chapter 6. The selection of the workpiece material and the dry machining conditions is discussed initially in this chapter. This includes the cutting forces evolution and the acoustic emission profiles from the tool during the total cutting process on the workpiece. Later, a wear and delamination failure analysis of the diamond coated cutting tools is presented in terms of the consequential tool life achieved from the initial substrate surface characteristics.

Finally, Chapter 7 provides the conclusions and closing thoughts as part of this research dissertation with the aim to correlate the experimental results from previous chapters and propose suggestions for future work on the present field.

www.manaraa.com

CHAPTER 2. MACHINING AND TOOLING BACKGROUND

2.1. Introduction to Metal Cutting

In a simple explanation, metal cutting can be understood as a category of manufacturing processes, which includes a group of cutting operations intended to remove material from the surface of a workpiece by producing chips or abrasion with the aim to fabricate a part with the desired dimensions and surface finish. Conventional machining processes consist of mechanical cutting operations at a macro scale which use a sharp cutting tool mounted in a power-driven machine known as the machine tool to produce a specific geometry out of a bulk material. These operations include turning, drilling, milling, broaching, and other cutting configurations.

A schematic representation of a turning operation where the cutting tool moves axially to the left at a certain velocity per workpiece revolution, know as *feed*, to reduce the radius of a cylinder in an amount determined by the value of a *depth of cut*, is shown in Figure 2.1. The cutting action of the tool removes a layer of material as it moves to the left producing a chip, which moves towards the top surface of the tool known as the *tool face*.

www.manaraa.com

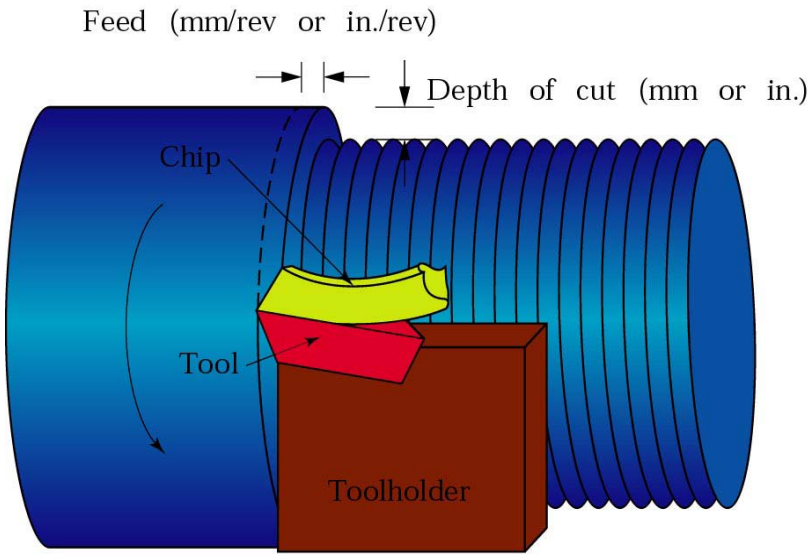

Figure 2.1. Schematic of a turning operation depicting its characteristic features [19]

Nowadays, the importance of material removal operations may be realized by the continuous advances in high technological products which demand the use of new materials and novel manufacturing techniques to produce them at competitive production levels. In this case, machining may be the only available manufacturing process to produce parts from advanced materials such as carbon fiber reinforced polymers, graphite, magnesium, titanium alloys, high silicon aluminum alloys, and other types of hybrid materials, in a net-shape condition or close to the final desired specifications. This fact has a significant influence in the development of advanced cutting tools capable of dealing with the challenging machining conditions imposed by the new product requirements and evolving metal cutting scenarios.

www.manaraa.com

Consequently, another important aspect about metal cutting operations from a material science and engineering point of view is related to the interaction between the workpiece material and the cutting tool during the cuttings, which operate as a system in terms of thermal exchange, chemical reaction, and mechanical contact, and constitute the fundamental factor in the resulting behavior of their surfaces. These interactions lead to the constant development of new cutting tool materials designed to sustain particular machining conditions, and constitute, in particular, the main scope of the present research.

In order to understand the mechanics involved in machining operations, an idealized two-dimensional model of chip formation proposed by Ernst and Merchant in the 1940s is depicted in Figure 2.2. This scheme known as the orthogonal cutting model, represents a wedge-shaped cutting tool moving to the left at a constant velocity, V, and a depth of cut, t_o, removing a layer of metal ahead of the tool in the form of a chip, by plastically deforming and shearing a plane surface extending upward from the cutting edge. In comparing Figure 2.1 and Figure 2.2, the *feed* in turning operations is equivalent to the dimension t_o, and the depth of cut is equivalent to the width of the cut, w.

www.manaraa.com

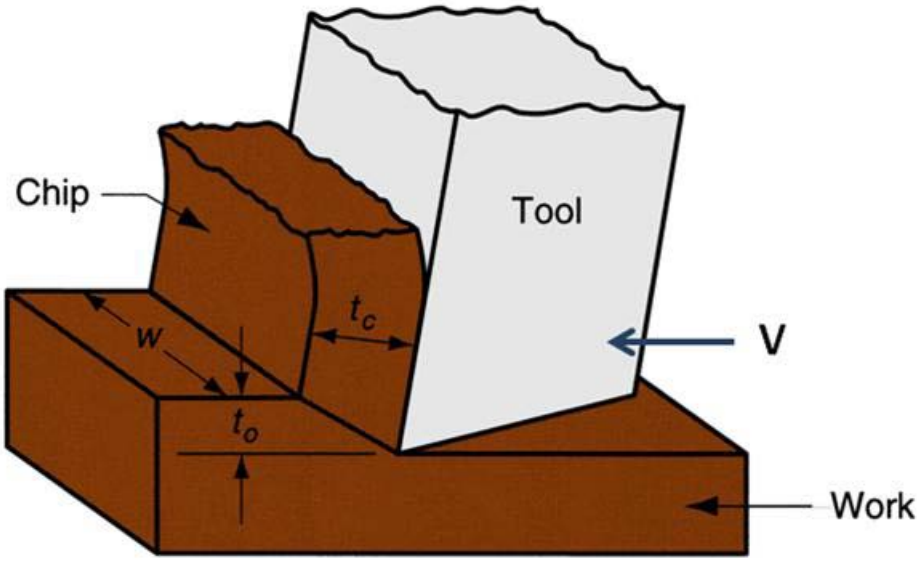

Figure 2.2. Orthogonal cutting model scheme as a three dimensional process [20]

In Figure 2.2, the tool has a *rake face,* corresponding to the surface in contact with the chip flow, and a ground back relief surface or *flank face*, which clears the workpiece machined surface. These two sets of faces define the *rake angle*, α, and the *relief* or *clearance angle* of the tool, respectively. The orthogonal cutting model also defines a shear plane or shear zone (the inclined plane in Figure 2.2) where the cutting action takes place by shearing, produced by the cutting edge of the tool (the line perpendicular to the page), and located at the contact point between the tool and the workpiece. Moreover, this two-dimensional model represents a simplified useful approach to study the resulting cutting forces and chip formation originated from a single plane of interest, rather than a three-dimensional model.

Workpiece and cutting tool materials, surface conditions, and their interactions, produce a number of factors that define the metal cutting operation, classified as

www.manaraa.com

independent variables, which influence the development of other parameters in the cutting process, known as dependent variables that affect the final result of the machining process. Figure 2.3 shows an illustration of these factors that influence the cutting and their interrelationships with the final machining performance.

Therefore, in the present research work, cutting parameters have been selected in order to minimize the experimental workpiece material consumption during cutting, when high silicon aluminum alloys are dry machined in turning operations, by using surface modified cemented carbide (WC-Co) square indexable inserts coated with a thick microcrystalline diamond film. The main objective of this dissertation is focused in analyzing the resulting dependent variables in terms of the cutting forces developed during cutting, the tool wear mechanism, and the diamond coating failure, when the previous independent factors are chosen.

The effect of the temperature will be evaluated in terms of the presence of crater wear in the tool rake face after cutting. However, this is kindly unexpected due to the exceptional thermal conduction properties of diamond. The resulting conditions and integrity of the workpiece surface after machining will not be evaluated in the present research.

www.manaraa.com

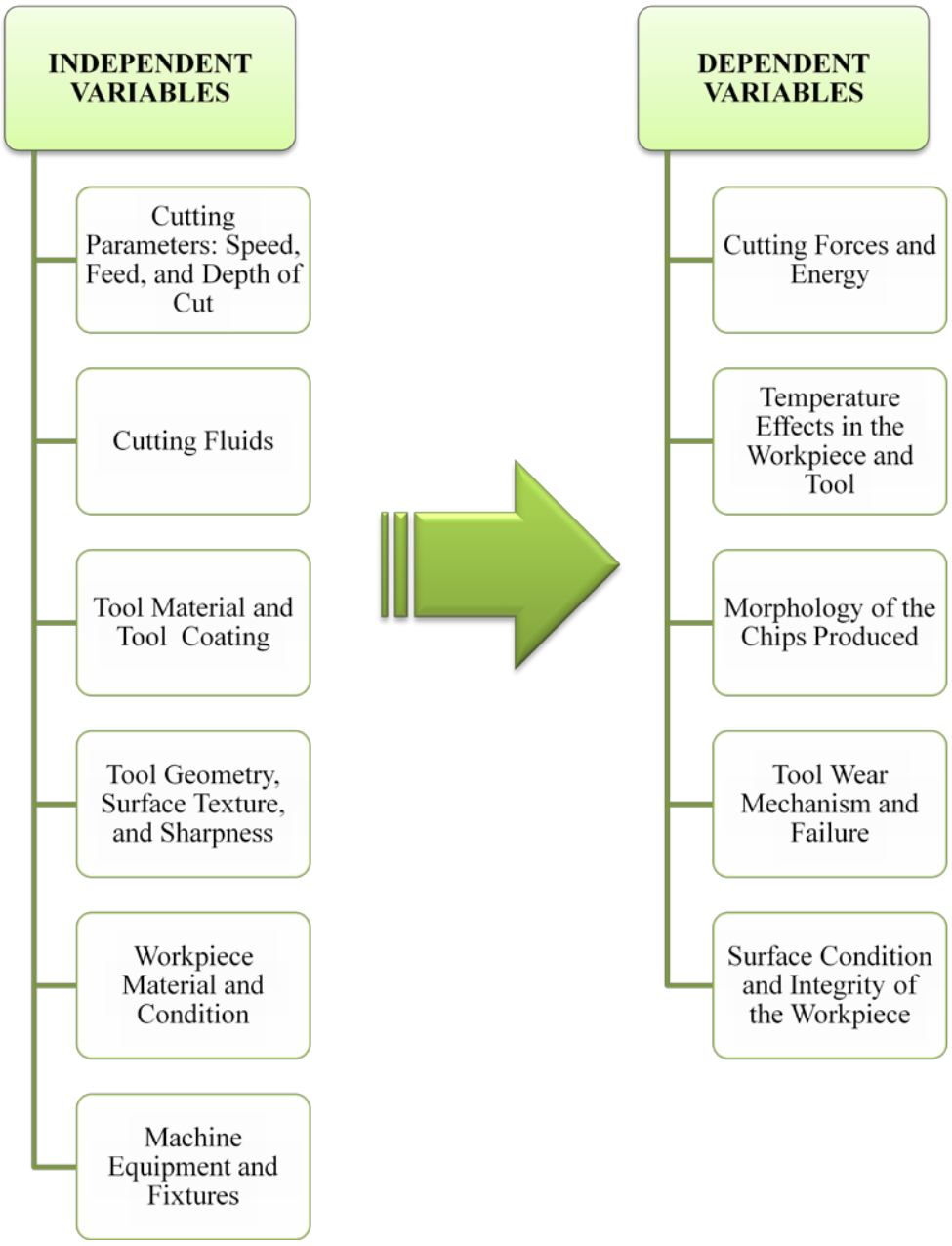

Figure 2.3. Factors that influence metal cutting operations

www.manaraa.com

2.2. Cutting Forces During Machining

As discussed, the chip formation due to the cutting action is produced by shearing localized at the zone where the tool acts in a rake angle, α. In Figure 2.4, the equilibrium free body analysis of the chip considers the action of only two equal forces defined as the force acting between the tool rake face and the chip (R'), and its opposite force (R) acting along the shear plane localized at the interface between the chip and the workpiece. These two forces can be resolved in a set of components as also shown in Figure 2.4:

- The ones resolved out of the resultant force R in the horizontal and vertical direction, F_t and F_c, known as the thrust force and cutting force, respectively. The cutting force acts in the direction of the cutting speed, V, and provides the required cutting energy. The thrust force is normal to the cutting force; it represents the force that has to be provided by the machine tool in the direction of cutting
- The ones along and perpendicular to the shear plane, Fs and Fns, known as the shear force and normal force. These forces can be expressed in terms of F_t and F_c from analytical correlations with respect to the shear angle, ϕ
- The forces along and perpendicular to the tool rake face, F and N. The ratio between these forces determines the coefficient of friction at the tool-chip interface. The angle λ is known as the friction angle

www.manaraa.com

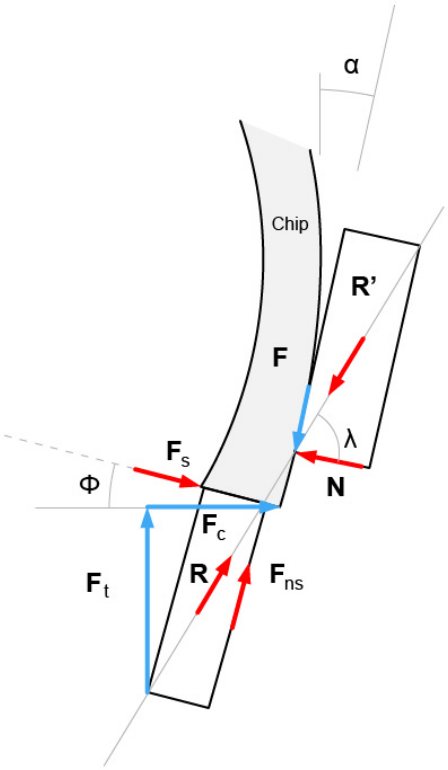

Figure 2.4. Schematic of the free body diagram depicting the resultant and resolved forces acting on the chip. Adapted from [21]

Thrust force and cutting force can be determined experimentally by using dynamometers and the rest of them by analytical correlations as mentioned. The importance in estimating the cutting forces resolved during machining is due to avoiding undesired deflections in the machine tool, minimizing distortions in the machine components, obtaining accurate dimension in the machine part, and calculating electrical power consumptions.

www.manaraa.com

In turning operations, the three principal forces developed from the cutting force, F, due to the contact of the cutting edge with the workpiece during machining are shown in Figure 2.5. The tangential cutting force F_t acting downward on the tool edge supplies the energy for cutting and accounts for more than 95% of the machining power. The axial force F_a, or feed force, is mainly due to the feed rate, pushing the tool away from the holding fixture. The radial force, F_r, is generated from the workpiece pushing action.

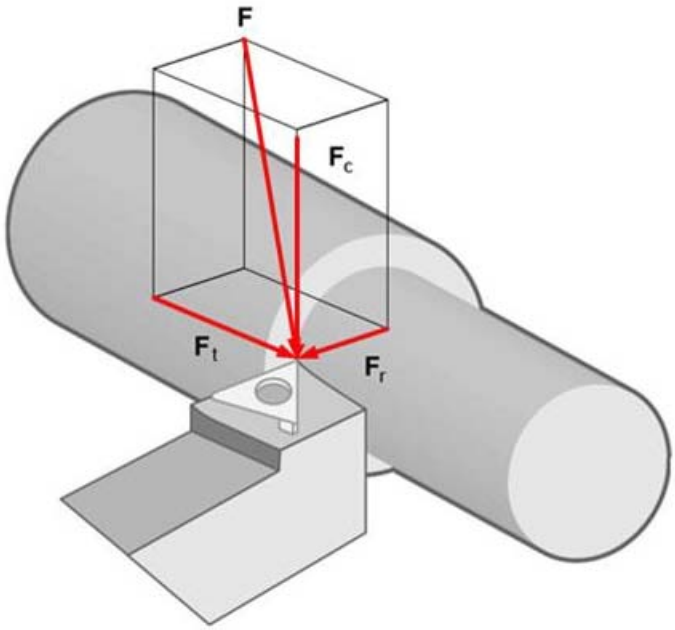

Figure 2.5. Forces acting in cutting tool during turning. Adapted from [22]

The evolution of the forces during machining provides estimation about the integrity of the tool during cutting. The machining performance of the tool can be evaluated by analyzing the variation of the forces, especially the axial and radial forces, which normally experience a sudden increase as the tool fails.

www.manaraa.com

In this research, these forces were measured with the aim to evaluate the performance of the diamond coated tools and associate the force changes with coating delamination and the subsequent tool failure. During experimental conditions, cutting forces can be measured by using piezoelectric dynamometers. These devices are built using electromechanical transducers made from crystalline materials like SiO_2 (quartz) and $BaTiO_3$ (barium titanate) which exhibit identifiable dipoles at its ends when strong electrical fields are applied. If an electrode is attached to the crystal ends, any distortion due to mechanical tension or compression will result in a change in voltage.

Establishing the appropriate locations of the surfaces in a piezoelectric crystal with respect to its axe, a shear or normal stress can be sensed by the generation of a small electrical charge correlated to the value of the input force. Figure 2.6 a) shows a three-component piezoelectric quartz dynamometer (Kistler ®) utilized in the present research to measure the three orthogonal components of the force. Additionally, a typical graph representing the output signal of the tangential, axial, and radial forces during machining is shown in Figure 2.6 b).

www.manaraa.com

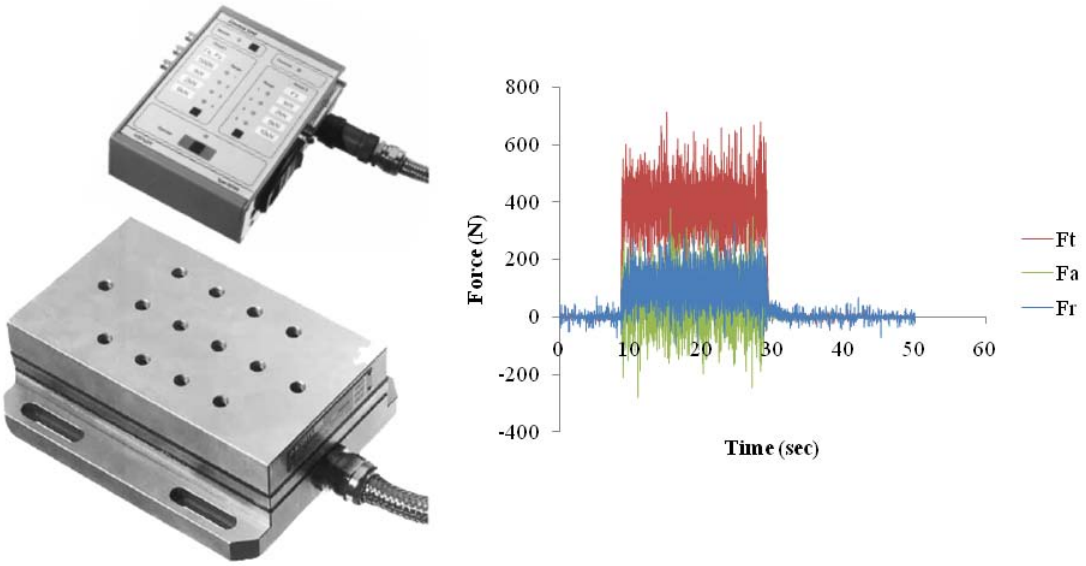

a) b)

Figure 2.6. Three-component dynamometer and its built-in charge amplifier including the output signal data representation corresponding to the three orthogonal components of the cutting force [23]. The holes in the platform plate allow accommodating tool shanks during turning operations

2.3. Tool Wear and Failure

During metal cutting operation, the tool experiences an aggressive environment as the result of the high forces leading to high localized stresses and high temperatures developed at the tip of the tool. The cutting tool must withstand the cutting forces without fracturing or deforming excessively. In addition, approximately 98% of the energy consumed in machining is converted to heat, so the cutting tool must not soften and fail due to plastic deformation and loss of its sharp edge.

www.manaraa.com

However, even if the cutting tool is able to endure these conditions, continual wearing of the tool becomes the ultimate failure mechanism causing the tool to fail at some point during cutting. In this latter case, the tool time to failure or *tool life* is determined by the selection of the independent variables listed in Figure 2.3.

All of the aforementioned tool failure mechanisms have to be controlled in order to minimize the amount of machining products out of dimensional specifications, avoid damages to the machine tool, and reduce the overall manufacturing cost. Out of the possible failure modes, gradual wear is the preferred because it produces the longest possible tool life during machining, maximizing the production rate or minimizing the cost per unit. The gradual wear of the tool is basically produced by wear mechanisms such as adhesion, abrasion, diffusion, fatigue, delamination, microchipping, fracture, and plastic deformation [24].

During machining operations, wear failures occur mainly at the top rake face (crater wear) and the flank of the tool (flank wear), shown in Figure 2.7. In this figure, the locations of both can be distinguished; the crater and flank wear with respect to the depth of cut and feed parameters during cutting, including other wear zones known as the nose radius and notch wear.

The amount of wear at the flank of the tool is measured by the average flank wear-land (VB), correlated with an increase in friction during the process due to a decrease in the relief angle on the flank face of the tool. Figure 2.8a depicts the representation of the wear bandwidth (VB) in the flank face of the tool. Figure 2.8b

www.manaraa.com

shows an optical image from the flank face of a worn diamond coated turning insert after cutting.

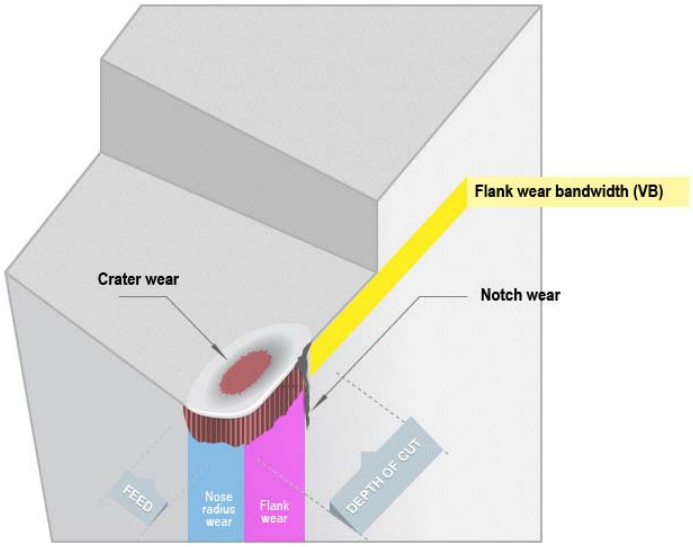

Figure 2.7. Illustration of the typical types of wear and locations in a worn cutting tool

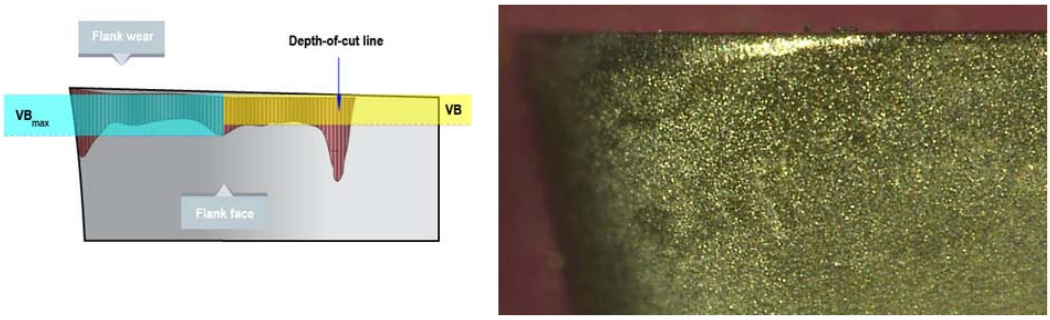

a) b)

Figure 2.8. a) Scheme of the wear-land in the flank face of a cutting tool indicating the average flank wear distance (VB) and b) optical image of the flank of a diamond coated carbide turning insert evidencing the flank wear-land after cutting

www.manaraa.com

The tool life (min) resulting from the selection of particular machining independent variables is given by a criteria adopted in terms of the amount of the VB value that avoid the final catastrophic failure of the tool. In a traditional tool wear behavior, three wear zones are evidenced when the VB value is plotted versus the cutting time.

These regions are visible in a wear growth curve as shown in Figure 2.9, characterized by a rapid initial wear rate or break in period, followed by a steady-state wear zone, finally reaching the undesired failure region where wear begins to accelerate. This behavior is mainly affected by the cutting speed, V, the workpiece material, and cutting tool material. The tool life criterion avoids using the cutting tool until the final failure point in order to maintain the quality of the production and the integrity of the machine tool. A common tool life criterion for tungsten carbide tools cutting mild steel is a value of 0.030 in (0.75 mm) for the maximum allowable wear-land value, VA. When Figure 2.9 is plotted using log-log coordinates, a tool life equation known as the Taylor tool life equation represents the wear behavior

$$VT^n = C \qquad (2.1)$$

where V is the cutting speed, T is the tool life, and C and n are constants depending on the feed, depth of cut, tool-workpiece material, and the tool life criterion used.

www.manaraa.com

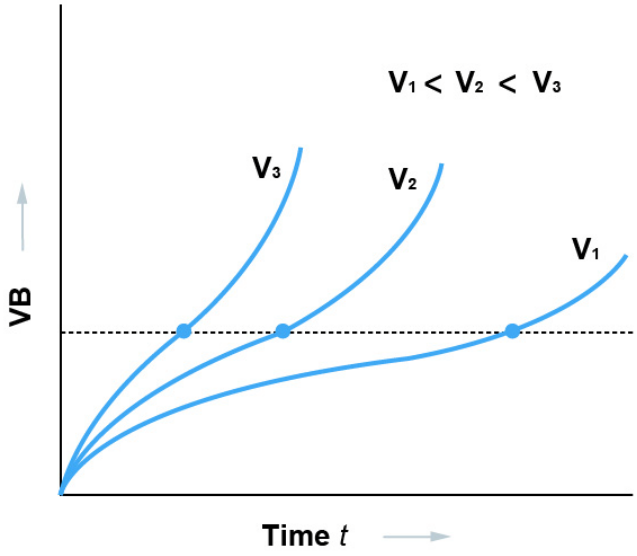

Figure 2.9. Variation of the wear-land value (VB) with time (t) for three cutting speeds (v). The dashed line indicates the tool life criterion used to avoid the sudden failure region [25]

2.4. Dry Machining Operations

As discussed in Chapter 1, dry machining is the ultimate goal of eco-friendly metal cutting. The environmental impact is due to the possibility to remove the negative effect of cutting fluids in terms of pollution of the atmosphere (or water), health, and the end-user manufacturing costs, which are higher than the labor and tools cost, accounting for 17% of total manufacturing cost in the automobile industry [26].

Traditionally, cutting fluids are important during machining operations because they help to reduce the heat generated during the operation, extend the tool life, maintain dimensional stability, wash chips away from the cutting zone, prevent the adhesion of

www.manaraa.com

material to the edge of the tool (built-up edge), and improve the surface finish of the product [27].

On the other hand, new environmental regulations established by the Occupational Safety and Health Administration (OSHA) trough its Metalworking Fluid Standards Advisory Committee (MWFSAC), are focused in reducing the amount of exposure to metalworking fluids by incorporating medical surveillance to the workers in conjunction to a monitoring systems at the workplace.

These efforts are made in response to petitions filed to OSHA by The United Auto Workers who requested a decrease in the cutting fluids exposure limits from 5.0 mg/m^3 to 0.5 mg/m^3 [28]. Consequently, dry machining constitute a metal cutting scenario with a promising future by completely removing the cutting fluids out of the manufacturing process, however, it is subjected to technical barriers that still limit its applicability.

Analyzing the orthogonal model during metal cutting, the primary shearing plane is characterized by a zone where a chip is removed from the workpiece around the tip of the cutting tool, creating a new clean and chemically active surface under the presence of high normal stresses. These conditions create an ideal scenario for the formation of solid face welding at the tool face, especially at large contact lengths with low cutting speeds, promoting a strong adhesion of work at its surface, capable to produce a secondary shear zone along the tool rake face. This mechanism contributes to the development of high temperatures at the chip-tool interface, potentially above 900 °C [7].

Therefore, the action of entirely removing the cutting fluids from the machining operations needs to be accompanied by a methodical approach to control the high

www.manaraa.com

temperatures developed in the overall process when running dry, particularly in removing the chips away from the cutting zone, which carry 85% of the heat generated from the cutting action.

In dry machining, the resulting heat from the friction between the tool and the workpiece material is higher as a consequence of the high temperatures developed, increasing the adhesive wear that promotes mechanical interlocking and diffusion between the chip and the tool, ultimately decreasing the tool life. However, there is no guarantee that introducing cutting fluids result in an improvement in the heat transfer problem by following the traditional cutting fluid application approaches. In some particular cases, the cooling action of the cutting fluid goes to regions that are not necessarily the "hot spots" during cutting. Cooling must be directed to the interaction zone between the chip and the workpiece (the heat source) and not being focused to the surrounding warm regions [29]. In some other cases during interrupted machining operations, the additions of cutting fluid may induce thermal shocks on the cutting materials.

In other cases, adding cutting fluids may produce stains on the surface of some workpiece materials and contaminate them. This is an important aspect to consider when machining biocompatible materials intended to be part of medical implants such as hip and knee ball joints. Open-faced machining operations such as turning and milling are more suitable for dry machining because the chips leave the cutting zone out of the proximity of the tool and workpiece carrying the heat away. In closed-faced machining operations such as drilling and tapping, chips cannot be flushed out of the cutting zone

www.manaraa.com

easily, so if there is no other mechanism to remove them, heat builds up, negatively affecting the tool performance during cutting. For instance, in drilling applications chips could bind in the hole increasing the roughness of the machined surfaced.

In addition, machining strategies in terms of using MQL or near-dry machining approaches in some cases, selecting new tool geometries to reduce friction, adopting new fast chip removal machine tool concepts, increasing cutting rates, and using novel air handling systems, are proposed to overcome the consequences of dry machining operations [30].

The workpiece material properties with respect to their ductility, toughness, and adhesive behavior also have an influence in deciding if dry machining is an appropriate approach to machine them. Figure 2.10 shows the common materials used in modern machining applications and its suitability for dry machining. Magnesium alloys need to be dry machined under an inert atmospheres due to potential fire hazards from the magnesium chips at high temperature in contact with oxygen [31]. Titanium and its alloys are extremely difficult to dry machine due to its low thermal conductivity, sticky behavior under cutting, and low flash point. These conditions can cause ignition of the workpiece during dry cutting if a cooling media is not supplied to during cutting.

Therefore, cutting fluids are still required to cut titanium until today. Steel materials and cast irons can be dry machined under certain operational conditions by using reduced depth of cuts, high surface speed and feed rates, and air blast systems with the aim to remove the chips away from the cutting zone [27]. However, stainless steels have difficulties associate to the formation of built-up-edge (BUE) along the cutting edge

www.manaraa.com

decreasing the surface finish quality of the workpiece. In the case of martensitic alloys, over-tempering may also occur.

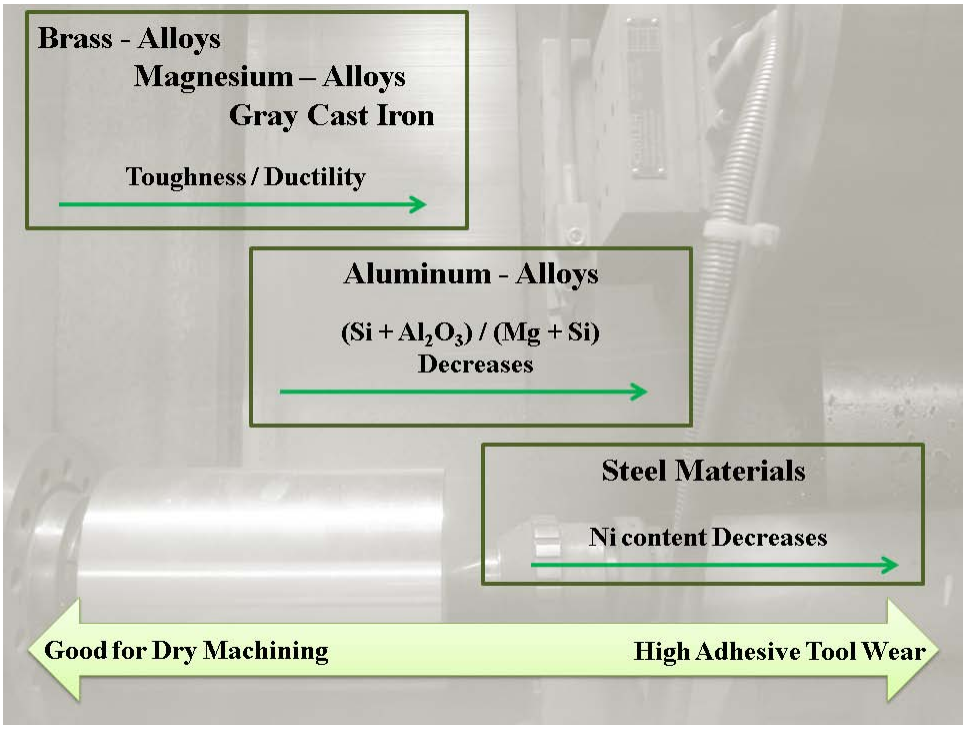

Figure 2.10. Suitability of workpiece materials for dry machining. Adapted from Weiner et al. [11]

During the last ten years, aluminum alloys represent one of the most used workpiece materials in dry machining operations. This trend is also influenced by the increase in using aluminum alloys in engines and powertrain components in the automobile industry. In general, cutting fluids are not necessary during aluminum alloys cutting processes because the temperatures are not as high as compared with steel. However, the high thermal conductivity of the aluminum may cause deformation to the workpiece due to its high thermal expansion coefficient.

www.manaraa.com

The addition of silicon in the range of 2 – 20% to the aluminum composition produces alloys with high wear resistant properties, low thermal expansion coefficient, and load-bearing capacities for reduced weight components such as pistons, engine blocks, cylinder heads, transmission cases, pump bodies, etc [32].

The aluminum-silicon phase diagram is characterized by a eutectic point at 12.6% that originates the precipitation of hard and abrasive silicon particles for compositions greater than this value. This is the case of the common A390 18% Si-aluminum alloy used in the automobile industry which is very difficult to machine using conventional machining processes and tools.

Unconventional marching processes such as water jet [33], laser-assisted [33], ultrasonic [34], electrochemical spark [35], and electro-discharge cutting [36], have been evaluated, but are limited in mass production applications due to their resulting production time, operational costs, and surface/subsurface integrity effects when compared to traditional machining approaches. Due to the necessity in achieving high cutting speeds to evacuate the chips away from the cutting zone during the dry machining of Al-Si alloys, cutting tools technology is the key factor to improve the performance of the operation.

2.5. Diamond Coatings for Dry Machining of High Silicon Aluminum Alloys

The ability to retain hardness at high temperatures (hot-harness) is a critical property for any cutting tool material in order to maintain its wear resistance and strength

www.manaraa.com

at the high temperatures encounter during dry machining operations. Moreover, toughness in cutting tool materials is essential to avoid failures produced by fracture.

There are other factors that determine the abrasion wear resistance of such as its surface finish, chemical stability, and thermal characteristics. However, hardness is the most important property needed to withstand the harsh conditions resulting from dry machining operations as the result of the abrasive action of the silicon particles present in aluminum alloys with silicon contents greater than 12%.

Also, the purpose of maintaining the hardness at high temperature is attributable to maintain the integrity of the tool cutting edge or tool nose during cutting, so the workpiece surface texture remains constant during the operation. This problem could be solved by decreasing the cutting speed; however, this may not be a good practice in dry machining due to the necessity to evacuate the chips as quick as possible from the cutting zone, worsen for the machining of heat-insulating materials.

Particularly for high silicon aluminum alloys, silicon particles can be detached during cutting, get airborne and deposited on the tool surface then diffused into the tool at high temperatures causing a continuous degradation of the tool with a detrimental effect in machining performance [37].

Traditional cutting tool materials generally do not exhibit all the previously discussed properties in a single composition. Actually, optimizing one of them may lead to a decrease in others, so chemical and structural modifications in the tool geometry have to be done in order to achieve the desired performance out of the tool. High speed steels (HSS) experience a decrease in the hot-hardness at high temperatures during dry

www.manaraa.com

machining operations and do not exhibit good abrasion resistance in machining high-silicon aluminum alloys. Cermets are limited by their non optimal fracture strength at high loads which makes them brittle when cutting dry in some cases. Cubic boron nitride (CBN) has a hardness and chemical stability close to diamond and is the cutting tool material of choice in the dry cutting of ferrous materials, a field that is unfeasible for diamond tools because the diffusion effects produced at the high temperatures during the dry machining operations. An important technological approach is related to the development of advanced protective coatings deposited by PVD and CVD techniques on the tool surface, which is the case in the present research, particularly for diamond coatings. Tool coatings technology is the optimal solution to overcome the challenging conditions encountered during the dry machining of high-silicon aluminum alloys. The main characteristic of any tool coating is to provide a heat barrier to the tool substrate as the result of their lower thermal conductivity, so the tool as a body can absorb less heat and extend its cutting life.

One of the most common coatings in dry machining applications is titanium aluminum nitride (TiAlN) coatings produced by PVD methods deposited on the tool substrates like cemented carbides, surpassing titanium nitride (TiN) coatings in high temperature uninterrupted cutting operations when high thermal stresses are present. This behavior is attributed to the formation of amorphous aluminum oxides at the tool coated surface during cutting induced by the dry machining high temperatures. Aluminum oxide can also be produced by CVD processes to coat cutting tools intended for dry machining operations. Diamond is the best candidate for dry machining operations of high-silicon aluminum alloys because it possesses most of the desired properties for a cutting tool

www.manaraa.com

when going dry. These properties are described in Table 2.1. Diamond can be used as a single crystal cutting tip, a polycrystalline diamond (PCD) tip sintered directly in the tool cutting edge, a thick CVD diamond free-standing wafer attached to the tool tip, or as a thin CVD diamond film conformally deposited to the geometry of the tool. The CVD synthesis processes can produce diamond films in a microcrystalline grain size structure (MCD), a reduced nanocrystalline grain-sized film (NCD), or a multilayered MCD/NCD coating. The advantages and disadvantages of each of them are summarized in Table 2.2. The performance of diamond coatings in the dry machining of high-silicon aluminum alloys related to the surface characteristics of cemented carbide substrates prior the diamond deposition is evaluated in Chapter 6 of the present research.

Table 2.1. Desired properties of CVD diamond for dry machining applications. Adapted from Cline and Olson (2002) [38]

CRITICAL PROPERTY	ROLE IN THE PERFORMANCE OF DRY MACHINING
HARDNESS	Diamond is the hardest known material that provides outstanding wear behavior combined with its capability to retain the hardness at elevated cutting temperatures
THERMAL EXPANSION COEFFICIENT	Diamond possesses a low thermal expansion coefficient which is critical to maintain the dimensional stability of the tool
THERMAL CONDUCTIVITY	Diamond has a highest thermal conductivity which helps to spread the heat away from the cutting edge and provide an increase in tool life
CHEMICAL STABILITY	Diamond is chemically inert in applications that do not involve its oxidation or corrosion such as high oxygen atmospheres. Diamond is the best candidate to dry machine nonferrous alloys, which do not represent chemical diffusion issues at high temperatures
MECHANICAL STRENGTH AND FRACTURE TOUGHNESS	Good for tool edge retention during cutting and comparable to advanced ceramics such as silicon nitride
COEFFICIENT OF FRICTION (COE)	Diamond COE is similar to Teflon, which minimize the adhesion during the dry machining of smooth workpiece materials, improving surface finishing, lower cutting forces, and less frictional heating

www.manaraa.com

Table 2.2. Properties of CVD diamond for dry machining applications. Adapted from Cline and Olson (2002) [38]

DIAMOND STRUCTURE	ADVANTAGES	DISADVANTAGES
Single-Crystal Diamond	High thermal and dimensional stability during cutting Superior surface finish High dimensional tolerance can be achieved Suitable for ultra precision machine tools	High production costs for complex geometries Low fracture resistance due to directional properties along the single crystal directions
Polycrystalline Diamond Compacts (PCD)	Uniform mechanical properties due to the random grain orientation High shock resistance Larger tool size Superior tool life and high productivity for nonferrous workpiece materials compared to HSS and coated carbides. It can be polished in different surface grades	High production cost when compared to cemented carbides and ceramic tools Tool geometry constrains. Small coated area Depth of cut limitations
Thick-Film CVD Diamond	High thicknesses range Lower production cost compared to PCD tools Cutting edges can be reground	Depth of cut limitations Uniformity and defect formation difficult to control
Thin Film CVD Diamond	MCD	MCD
	High diamond phase content (sp^3 bonds)	Preferential crack propagation along grains
	NCD	NCD
	Smother surface with better tribological characteristics	Presence of non diamond phases (sp^2 bonds)

www.manaraa.com

CHAPTER 3. CVD DIAMOND SYNTHESIS AND STRUCTURE

3.1. The CVD Synthesis Process

A Chemical Vapor Deposition (CVD) process – also known as vapor-phase epitaxi (VPE) – is a technique considered very suitable for the development and manufacturing of thin films coatings and fibers from different materials, including compounds like carbides, nitrides, and oxides. Also, it is very useful in the surface modification technology areas, especially in the electronic industry for the doping of semiconductors to change their electrical conductivities. This technology covers a wide spectrum of film thicknesses ranging from the nanoscale up to microns, exhibiting several differences among their characteristics in terms of the resulting properties for the desired application.

In simple terms, a CVD process is a kind of reaction in which a gaseous specie is activated and deposited on a substrate surface in a class of vapor-transfer process as the result of a deposition of atoms or molecules, or a combination of both as shown in Figure 3.1.

www.manaraa.com

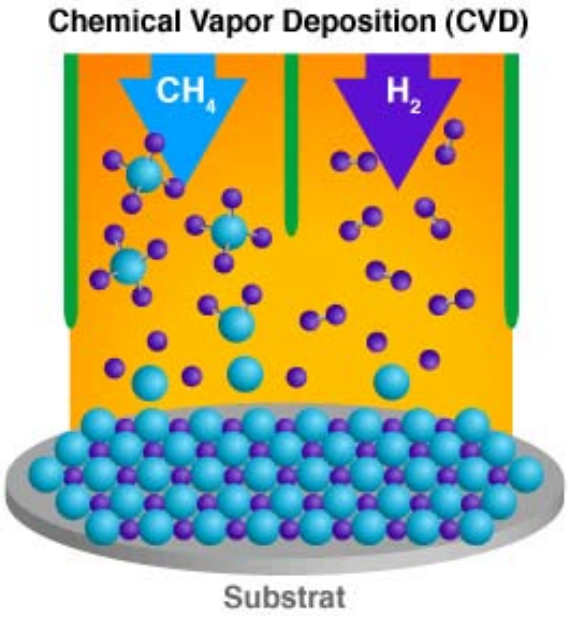

Figure 3.1. Basic principle of the chemical vapor deposition CVD synthesis. Image Credit (itech.dickinson.edu) [39]

The CVD reactions occurring during the process are governed by the thermodynamics of the reaction (driving force) that indicate its direction and the kinetics which define the transport process and the material transfer rate mechanism. In CVD synthesis, the transport of energy occurs when the gaseous compounds inside the chamber react to form the atomic/molecular deposits and the by-product gases of the reactions. A thermodynamic analysis will indicate what to expect from the reactants when they reach the surface of the substrate at the process temperature, but a mass transport analysis gives us the answer about how these gases reach the surface.

www.manaraa.com

An approximate sequence of events during a CVD process can be summarized as the following:

- A gas feedstock enters the chamber
- A diffusion process from the gases occurs inside the vacuum chamber
- A source of energy activates the gases
- Gas reactions are dissociated in atomic/molecular subspecies
- Atomic/molecular subspecies come in contact with the substrate surface and are absorbed (diffusion at the surface)
- Deposition takes place onto the surface of the substrate due to chemical reactions
- By-product gases of the reaction are diffused away from the surface

It is important to mention that another technique named physical vapor deposition (PVD) is also available for thin film depositions, such as evaporation, sputtering, molecular beam epitaxy, and ion plating processes. The distinction between CVD and PVD vacuum processes relies in the way materials are transferred onto the substrate; in CVD synthesis, the deposition occurs by a chemical reaction from the material gaseous subspecies, whereas in PVD, the deposition occurs when the solid material source (target) is vaporized, transported atom by atom across the chamber to the substrate, and condensed onto its surface. CVD synthesis is usually endothermic and PVD deposition is exothermic.

www.manaraa.com

The most important reason in using CVD technologies is to produce new kinds of material properties that are impossible to find if we try to use a homogeneous material. Today this is possible through the deposition of materials in the form of thin film coatings. These coatings create surfaces with properties that are different from the bulk and provide the opportunity to develop new product designs in different areas.

Nanostructured materials are obtained also by using CVD techniques. The CVD of nanocrystalline powders, nanowires, and nanotubes (e.g. carbon nanotubes) are some examples of the different kinds of advanced applications in the material science field. According to the type of industry, applications of CVD products could be classified such as electrical, opto-electrical, optical, mechanical and chemical. The advantages and limitations of CVD are shown in the Table 1.1.

There are two major focus research areas for CVD processes in recent years, one is focused on the semiconductor industry in the production of electronic devices, and the other one named metallurgical – coating industry focused on cutting tool coating technologies. New trends in the integration between CDV and PVD technologies have been achieved in the last few years for novel equipment designed with the concept of cluster tools which may incorporate CVD, etching, sputtering, and ion implantation in one piece of equipment. Metallo-organic CVD (MOCVD) is one of the recent process variations of CVD with the use of lower deposition temperatures that permits the use of a broader spectrum of substrates.

www.manaraa.com

Table 3.1. Advantages and limitations of CVD. Adapted from Pierson (1999) [40]

ADVANTAGES	LIMITATIONS
• Is not restricted to a "line sight" deposition which is the main requirement in sputtering systems and other PVD techniques • High flexibility to coat complex geometries and shapes • High deposition rates • Uniform films with good reproducibility • Thick coatings can also be obtained • Normally it doesn't require complex high vacuum equipments • High flexibility due to the different gas compositions used during the deposition • It has the ability to control crystal structure, surface morphology, and orientation of the deposited films by controlling the process parameters such as gas ratios, pressure, substrate temperature, and energy power	• Is most versatile at temperature above 600 ˚C • Requires chemical precursors (starter materials) with high vapor pressure which are generally hazardous • Toxic and corrosive by-products • Difficult to deposit multilayered /multicomponent materials • High cost for vacuum systems in some CVD variants

The nature of the film deposited and the rate of nucleation for the process are strongly affected by the nature of the substrate. This is called the type of epitaxi for the process. Epitaxi can be understood as the crystal growth of a film on a crystalline substrate surface. Depending on the nature of the combination between the substrate and the deposited material, the phenomena is known as homoepitaxi for the same deposit and substrate material or lattice parameter, and heteroepitaxi when is different, but epitaxial growth it is not possible for great differences [40].

www.manaraa.com

The final crystal microstructure of the resulting deposited film is a function of deposition conditions, especially temperature. The microstructure for a CVD process can be classified into three major types, columnar grains, faceted columnar grains, and equiaxed fine grains as shown in Figure 3.2.

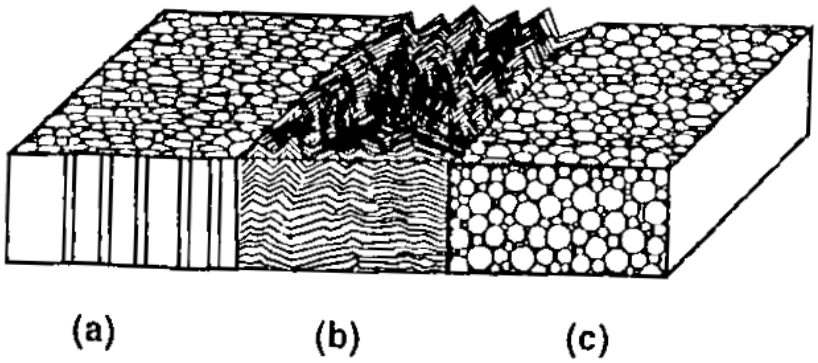

Figure 3.2. Schematic microstructures obtained by CVD: a) columnar grains, b) faceted columnar grains and c) equiaxed fine grains [40]

Furthermore, the microstructure has different characteristics depending on the type of material. Ceramics obtained by CVD (e.g. SiO_2, Al_2O_3, Si_3N_4) tend to be amorphous or with some small quantities of equiaxed fine grains, metals tend to be more crystalline displaying columnar grains. The highest mechanical properties in terms of hardness and fracture toughness can be achieved with equiaxed fine grains microstructure.

www.manaraa.com

3.2. CVD Diamond Synthesis

As discussed in Chapter 1, diamond can be grown over a substrate using deposition methods at low pressure by means of a gaseous feedstock (CH_4) in addition to energy (thermal, electrical, etc.) that dissociate the gas for the deposition. There are four commonly used CVD techniques for the synthesis of diamond to achieve the required energy for the dissociation process of the molecule from the input gases: hot – filament reactors, microwave plasma reactors, DC arcjet reactors, and combustion synthesis reactors. All of them have significant variations in their engineering aspects but they have important features in common [41]:

- Large amounts of energy (electrical or chemical) for the dissociation process of the molecular hydrogen and the hydrocarbon (CH4)
- Moderately low pressure (20 – 100 Torr) to prevent the recombination of H ions to molecular hydrogen
- High temperatures for the gas ambient in the activation zone (greater than 1700 °C) and the use of cooling systems to hold the substrate temperature at a lower temperature (~900 °C)

Differences among the reactor types involve different transport processes and growth rates:

- Microwave plasma and hot-filament CVD reactors are characterized by a diffusion process. The growth rate is a weak dependent of input gases, and flow velocity to the system. The driving force for the film deposited is the linear gradient in temperature between the highest temperature zone

www.manaraa.com

(filament or plasma) and the substrate surface, in addition to the gases concentrations

- Arc-jet and combustion CVD reactors are characterized by higher growth rates and higher temperatures reached in the substrate that may cause a significant limitation for some materials

The chemistry involved in diamond deposition is complex in comparison to other CVD synthesis processes due to the many chemical reactions originated from the different gases and the nature of each process. It is also very important to achieve deposition of sp^3 carbon in order to maintain the bonding state corresponding to diamond and the desired crystalline configuration. The typical parameters for deposition are a pressure in the range of 50 – 100 Torr, a hydrocarbon – hydrogen gas composition of 1% CH_4 in H_2, a total gas flow rate of 25 – 800 sccm, temperatures between 700 - 900 °C using microwave plasma enhanced chemical vapor deposition (MPECVD) technologies. It is important to note that under these conditions the stable form of carbon is graphite according to the phase diagram for carbon, but the kinetics of the reaction produce crystalline metastable diamond phase instead of graphite by the reaction of the hydrocarbon precursor combined with the radical formation and graphitic etching action of atomic hydrogen [42].

$$CH_4(g) \rightarrow C \text{ (diamond)} + 2H_2 \qquad (3.1)$$

The schematic reactions for convectional MPECVD are shown in Fig. 3.3.

www.manaraa.com

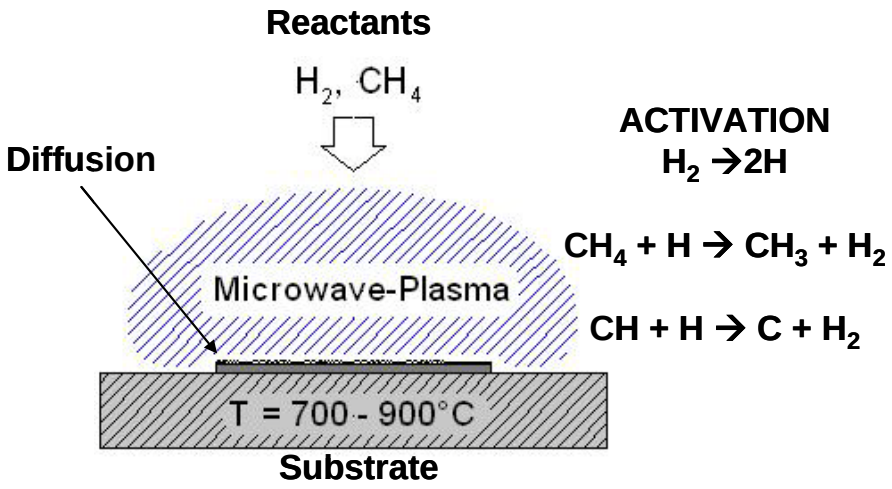

Figure 3.3. Schematic mechanism for conventional MPECVD diamond deposition and the corresponding activation reactions for the process

To achieve diamond depositions over nondiamond substrates, additional surface pretreatments are required in order to produce nucleation sites for the diamond growth and improve the adhesion of the film. These pretreatments are known as seeding processes and can be achieved by different methods, including ultrasonic scratching with diamond nanopowders in a alcohol solution [43], high methane concentration in low pressure plasma treatments [44], substrate surface scratching with diamond micropowder paste [45], or bias enhanced nucleation (BEN) [46]. Figure 3.4 depicts homogeneous diamond seeds distribution in a silicon substrate after being exposed 30 minutes in a diamond growth plasma composition with the aim to characterize the nucleation density of the seeding method.

www.manaraa.com

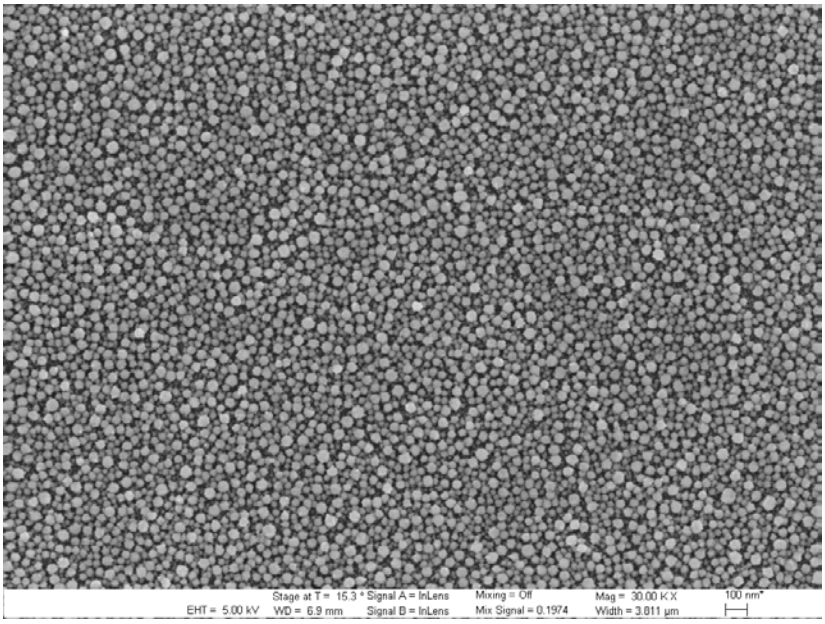

Figure 3.4. Distribution of diamond seeds deposited in a silicon substrate after exposed 30 min in a diamond growth plasma

The incubation time for nucleation depends on conditions on the substrate such as the interface bonding type, coefficient of thermal expansion, lattice parameter, diffusivity properties etc. The best surface conditions to promote good high diamond nucleation density are related to the ability of the substrate material to form carbides, which is also an essential condition to achieve a good adhesion of the film.

Transition metals and alloys of iron, nickel, and cobalt are considered to be non viable substrates for diamond deposition due to the high bulk diffusion rates of carbon in these materials, which promote a graphitization instead of a diamond phase nucleation and the homoepitaxial growth of the diamond film at the substrate surface [47,48]. Consequently, buffer layers must be used as interdiffusion barrier layers to overcome the poor nucleation density on these substrate materials.

www.manaraa.com

Diamond grain size can be controlled by manipulating the gas feedstock chemistry, gas rations, and process pressure during the synthesis where a secondary nucleation (diamond on diamond) becomes dominant in a dendrite type of growth. Other subspecies can be added to the diamond chemistry in order to modify the growth rate, surface termination, and electrical conductivity, i.e. nitrogen and boron.

Nanocrystalline diamond (NCD) films can be deposited in microwave enhanced chemical vapor deposition (MWCVD) reactors as shown in Figure 3.5 by adding Argon gas to the feedstock and following the process conditions summarized in Table 3.2. By reducing the H_2 content in the gas chemistry from 99% to 1% and consecutively replacing it with argon, the grain size of the diamond films can be reduced from several microns to a few nanometers.

Figure 3.5. Cyrannus I ® IPLAS MPECVD reactor at University of South Florida

www.manaraa.com

The transition of the grain size of diamond films from microcrystalline to nanocrystalline regime was systematically studied by depositing films at different Ar/H_2 ratios. Scanning electron microscopy images depicting the surface morphology of the diamond films grown in different argon compositions are shown in Figure 3.6. The presence of argon in the reactant gas mixture promotes the concentration of highly reactive C_2 dimers that enhance the secondary heterogeneous re-nucleation and aids the growth of NCD [49].

Table 3.2. Process conditions for the deposition of NCD and MCD films by using the MWCVD reactor at University of South Florida

Deposition conditions	**CH_4**	**Ar**	**H_2**	**Microwave Power**	**Pressure**	**Substrate Temperature**
Nanocrystalline Diamond (NCD)	0.5%	98.5%	1%	1.8 kW	135 T	750 ˚C
Microcrystalline Diamond (MCD)	1%	-	99%	1.0 KW	25 T	800 ˚C

www.manaraa.com

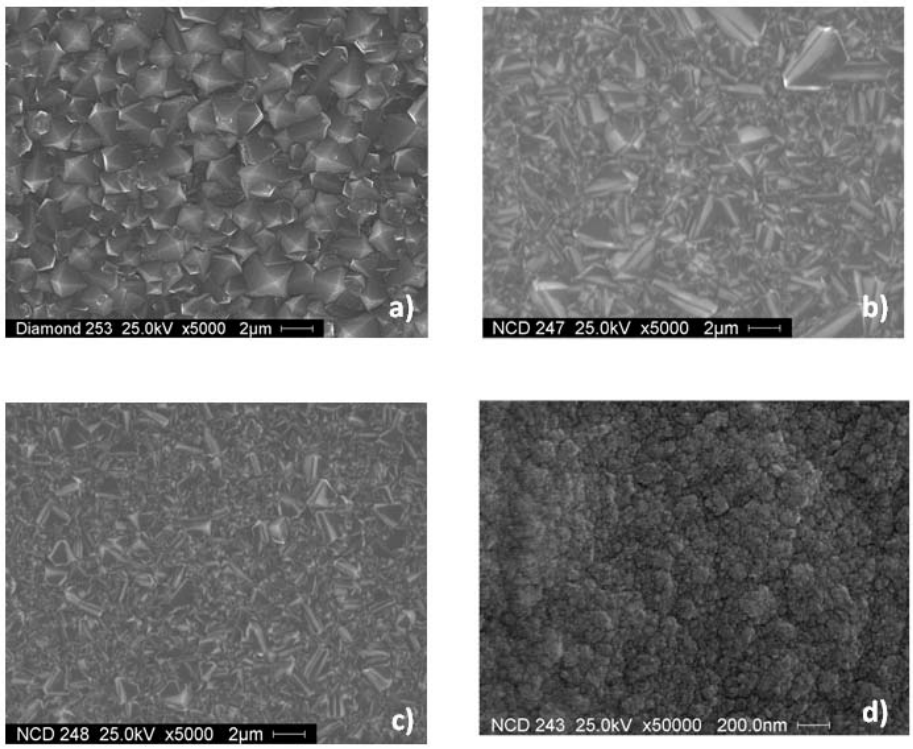

Figure 3.6. SEM images of diamond films grown with different Ar percentages: (a) 0%, (b) 50%, (c) 75% and (d) 98% [49]. © Inderscience [50]

Both NCD and MCD films can be obtained also by the hot filament chemical vapor deposition (HFCVD) synthesis process by increasing the methane concentration [51] or by decreasing the process pressure when Argon is added to the chemistry [52]. In HFCVD systems, the energy required to achieve the gas activation is provided by refractory metal filaments (i.e. tantalum or tungsten) heated to temperatures around 2000°C. The temperature in the filaments is produced by a voltage generated between a pair of electrodes and along the filaments array. This particularity confers to HFCVD synthesis great flexibility in depositing diamond coatings on complex 3D geometries. Filament arrays can be positioned close to the surface of interest and can vary in number

www.manaraa.com

and orientation depending on the substrate requirements. Figure 3.7 shows the HFCVD system at University of South Florida and a schematic of its important components. The main component is the vacuum chamber where gases are flowed inside at the desired flow rate. The substrate is placed underneath a pair of tungsten filaments by a sample retracting system, the pressure is controlled by a two pressure valves connected to the vacuum line, and voltage is generated between the electrodes by using a voltage regulator; the amount of voltage defines the deposition temperature at the filaments. Cooling water runs through a copper line wrapped around the vacuum chamber. Argon gas is used to vent the chamber to atmospheric pressure after the deposition process. The process conditions used to deposit MCD and NCD films in this system are summarized in the Table 3.3.

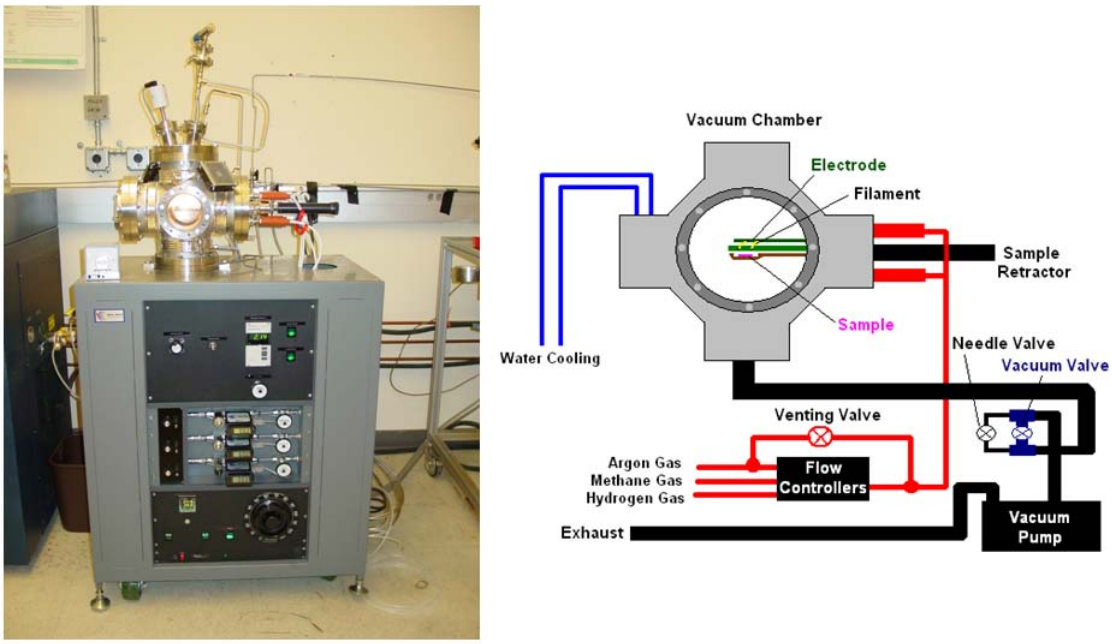

Figure 3.7. Bluewave Semiconductor ® HFCVD reactor at University of South Florida

www.manaraa.com

Table 3.3. Process conditions for the deposition of NCD and MCD films by using HFCVD reactor at University of South Florida

Deposition conditions	**CH_4**	**H_2**	**Voltage (V)**	**Pressure**
Nanocrystalline Diamond (NCD)	9%	91%	80	20 T
Microcrystalline Diamond (MCD)	3%	97%	90	20 T

3.3. CVD Diamond Structure

There are many techniques for the characterization of diamond properties in accordance with the field of interest. Also, there are specific characterization methods for CVD diamond films in order to ensure the development of the growth morphology (MCD or NCD), the microstructure condition, the grain orientation, the chemical compounds present, the type defects developed during the growth, the surface texture and morphology, and the amount of carbon bonding (sp^2 or sp^3).

3.3.1. Scanning Electron Microscopy (SEM)

The principle of scanning electron microscopy (SEM) is the detection and visualization of secondary and backscattering electrons coming from the interaction between an electron beam and the sample surface. Conventional light microscopes use a

www.manaraa.com

series of glass lenses to bend light waves and create a magnified image. When a focused electron beam strikes the sample surface, different types of signals are generated from the sample as shown in Figure 3.8.

The focused beam scans the surface of the sample and the signals are detected by different sensors depending on the type of analysis. Secondary electrons (low energy) indicate information about the surface of the specimen. Backscattering electrons come from a deeper interaction zone of interest and provides information about the chemistry distribution (atomic number) of the sample. X-rays are used for chemical analysis due to the dependence of the magnitude of an x-ray signal and the atoms which produce it.

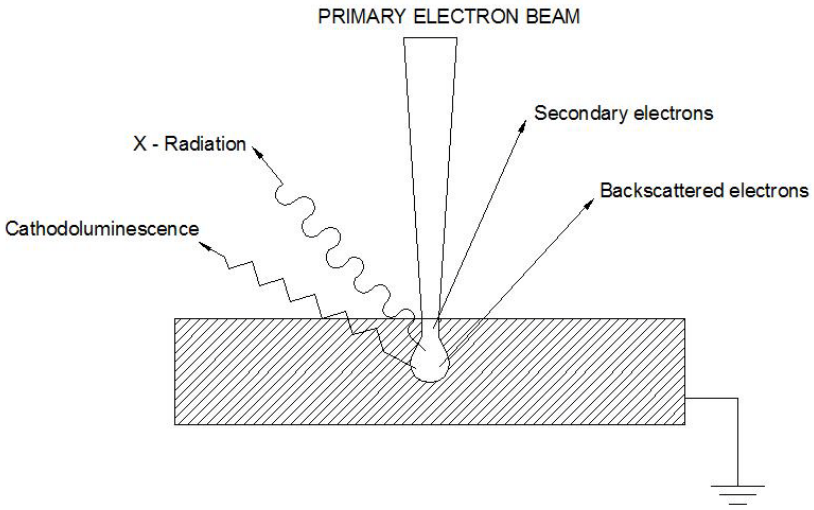

Figure 3.8. Schematic representation of emission events generated in the scanning electron microscope [53]

www.manaraa.com

The final image is built up from the number of electrons emitted from the sample at much higher magnifications than a light microscope. SEM is an invaluable tool for the observation of CVD diamond films in terms of surface morphology and growth patterns. Figure 3.9 corresponds to a group of SEM micrographs that depict the reduction in the diamond films grain size deposited by HFCVD synthesis at different methane concentrations. Larger faceted diamond grains are observed for low methane concentrations whereas more equiaxed ball-agglomerates grains are present at higher concentration.

www.manaraa.com

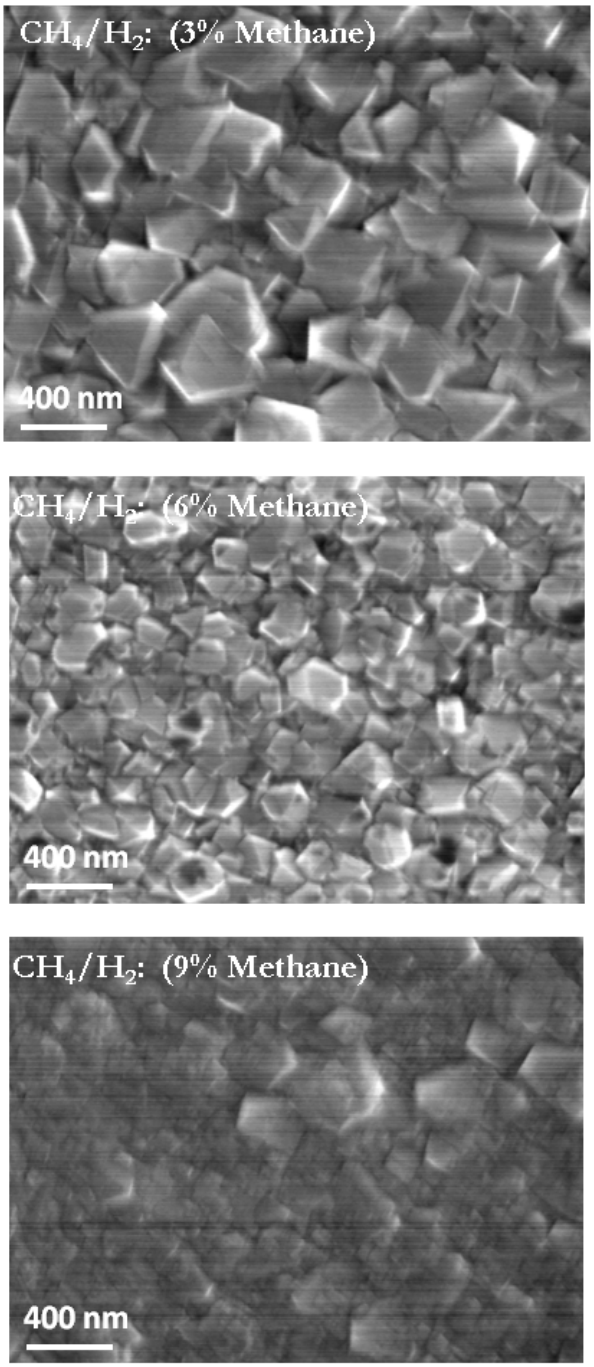

Figure 3.9. SEM micrographs corresponding to the deposition of diamond films at different methane concentrations by HFCVD synthesis

www.manaraa.com

3.3.2. Transmission Electron Microscopy (TEM)

TEM works similar to the SEM principle except that it transmits a beam of electrons through the specimen rather than raster the beam across the sample. The transmitted beam is then projected onto the viewing screen, forming an enlarged image of the sample. TEM has a high spatial resolution (~ 0.2 nm) in imaging, so it is possible to achieve a good characterization in the nanometric scale to identify a large number of defects which cannot be detected by other techniques.

Information about crystal symmetry, specimen thickness, and lattice distortion can also be obtained by special methods, such as the convergent-beam electron diffraction. In nanocrystalline diamond (NCD) applications, various types of planar defects can be observed like twining, boundaries and stacking faults as the result of different substrate materials, surface pretreatment methods, and growth parameters.

Figure 3.10 shows the high-resolution TEM (HRTEM) image of a NCD film. It was estimated that the grain size of diamond crystals was ~ 10 to 15 nm and the grain boundary width between 0.2 and 0.4 nm. The inset shows a sharp ring pattern corresponding to (111), (220), and (311) planes of the diamond crystal indicating the polycrystalline nature of the film. There were no reflections due to graphite or amorphous carbon observed showing the phase purity of the diamond. From HRTEM image, the inter-planar spacing between the (111) planes was found to be ~ 0.205 nm. From this characterization analysis, it was found that the diamond films grown by the current technique resulted in high quality and preserved the outstanding properties as of those deposited form hydrogen rich plasma.

www.manaraa.com

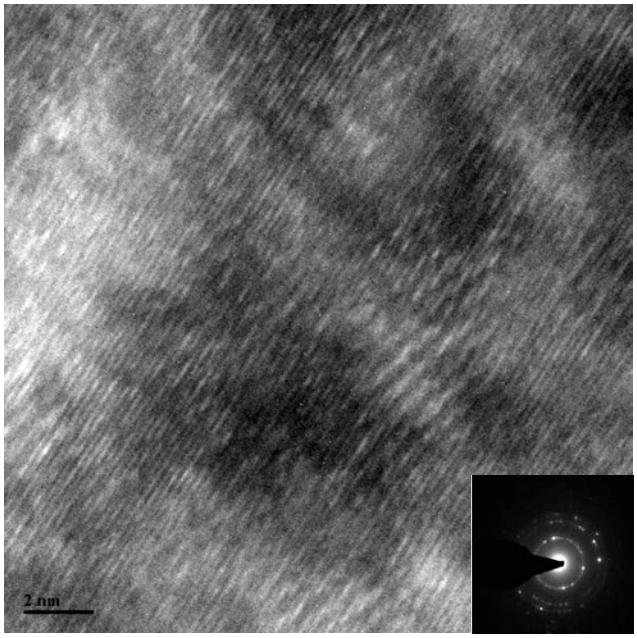

Figure 3.10. HRTEM image of an Ar/1%H_2/1% CH_4 NCD film. The inset image shows a SAED pattern image. © Inderscience [50]

3.3.3. X-Ray Diffraction

X-ray diffraction (XRD) is a characterization technique used to determine the crystal structure arrangement of materials. Diffraction occurs when a wave encounters a series of regularly spaced obstacles that are capable of scattering the wave and to have spacings that are comparable in magnitude to the wavelength. The x-ray beams (electromagnetic radiation) strike the surface of a solid material and a portion of the beam scatters in a direction associated with the type of atom or ion across the beam path. The diffraction is based on the Bragg's law that considers the relationship among x-ray wavelength, the interatomic spacing, and the angle of diffraction during the exposure. Common diffraction techniques employ powder or polycrystalline samples with fine randomly oriented particles to ensure the required orientation for all possible

www.manaraa.com

crystallographic planes diffraction. XRD is sensitive to the presence of crystalline carbons such as diamond, so it is very useful to characterize CVD diamond films. In MCD and NCD diamond films, XRD diffraction is used to determine the growth orientation and the final texture of the film. Figure 3.11 shows the (111), (220) and (311) peaks corresponding to the ring patterns shown in Figure 3.10.

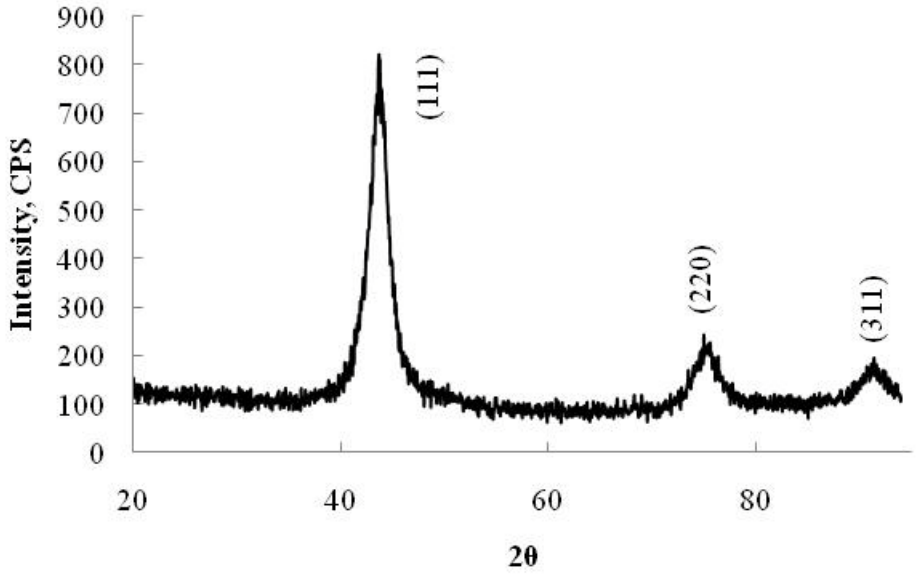

Figure 3.11. X-ray diffraction spectra corresponding to NCD films grown on a silicon substrate by MWCVD synthesis depicting the (111), (220), and the (311) reflexions. The peak corresponding to the Si single crystal substrate orientation has been removed from the spectra

www.manaraa.com

3.3.4. Raman Spectroscopy and NEXAFS

Raman spectroscopy (RS) is one of the most important tools for the chemical characterization of diamond thin films. With RS it is possible to achieve real time characterization of compounds in a non – contact mode. The sample is illuminated with a laser which produces a scattering light that can be used to identify functional groups in a molecule without the contamination or damage of the sample. The name of this technique is associated with the Raman Effect, a phenomenon resulting from the interaction of light and matter due to the vibrational and/or rotational motions of molecules with the electromagnetic radiation.

This characterization technique utilizes the singular response that different materials exhibit when exposed to a monochromatic light source, such as a laser. As a consequence of the atomic structure of its compositional material, the sample vibrational energy causes some of the incident photons from the laser to be inelastically scattered. The Raman spectrometer detects and measures this inelastic scattering, known as the Raman shift. When the resulting Raman shift is represented graphically, a characterization curve is obtained, which is unique to the subject material. Raman spectroscopy provides several key advantages for the investigation of diamond films deposited with CVD techniques.

As diamond films have both sp^3 and sp^2 bonded carbons, it is very important to precisely estimate their fraction. Raman spectroscopy is primarily used to qualitatively determine the sp^2-graphitic allotrope and the sp^3-diamond allotrope. Figure 3.12 shows the micro Raman spectra of MCD and NCD films grown on Si substrates by using a

www.manaraa.com

visible green argon laser (514.5 nm) to probe the density of optical photon states in the bulk material, yielding an indirect measurement of the predominant chemical bonding In MCD films, a sharp peak is observed at 1332 cm^{-1} representing the strong sp^3 characteristics. With the addition of argon, the intensity of the diamond peak at 1332 cm^{-1} becomes indistinct due to selective Raman scattering of sp^2 vs. sp^3 bonded carbon.

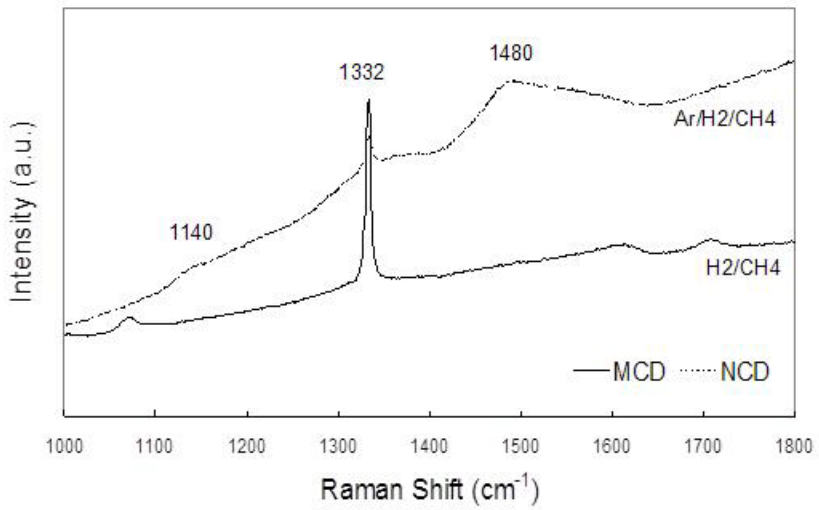

Figure 3.12. Raman spectra of H_2/CH_4 and $Ar/H_2/CH_4$ diamond films grown on Si substrates, MCD and NCD, respectively. © Inderscience [50]

Figure 3.13 shows the Raman spectra of diamond films grown on a Si substrate by HFCVD synthesis under two different methane concentrations. The increase of the methane content in the feedstock composition promotes a decrease in the diamond grain size as discussed previously, decreasing the amount of sp^3 diamond bonds due to the excess of carbon in the surface. This can be observed by the decrease of the 1332 cm^{-1} diamond peak with respect to the graphitic phase present at 1473 cm^{-1} and the increase of

www.manaraa.com

the trans-polyacetylene (TPA) state at 1130 cm^{-1} [54,55], which confirms the higher sensitivity of Raman spectroscopy to sp^2 graphitic bond scattering modes.

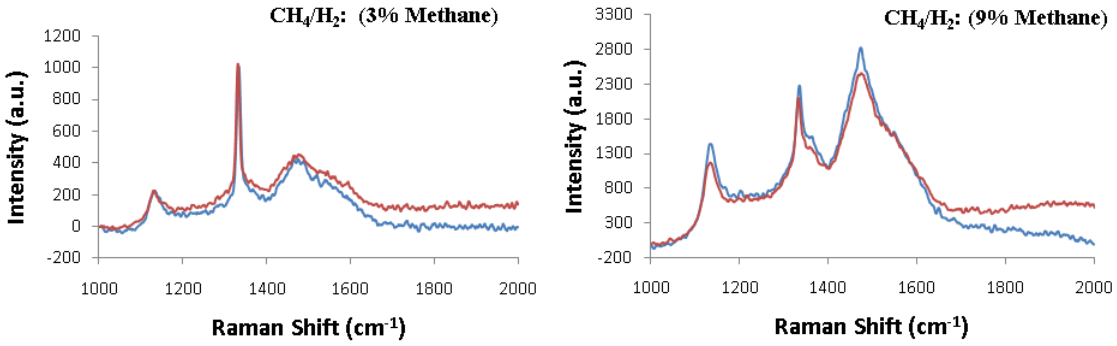

Figure 3.13. Raman spectra of CH_4/H_2 diamond films grown on a Si substrate by HFCVD displaying the structural characteristics with respect to the methane concentration

Due to the dependence on the long edge order of the material, it is difficult to distinguish a material with 96% sp^3 bonding from a material with 85% sp^3 bonding using the visible Raman spectrometry. These limitations can be surpassed by near-edge x-ray absorption fine structure (NEXAFS) technique. Figure 3.14 shows the total electron yield (TEY) C (1s) photo-absorption data of MCD and NCD films. After analyzing the data by using analytical calculations from the information derived from the Figure 3.14 and the TEY corresponding to a highly ordered pyrolytic graphite (HOPG) reference substrate [56,57], it was estimated that ~ 8 % of the total carbon in the NCD films was sp^2 bonded carbon; while the MCD films contain ~ 5 % sp^2 bonded carbon. The slight increase in the sp^2 bonded carbon in NCD films is due to increased amount of grain boundaries which host the sp^2 carbon.

www.manaraa.com

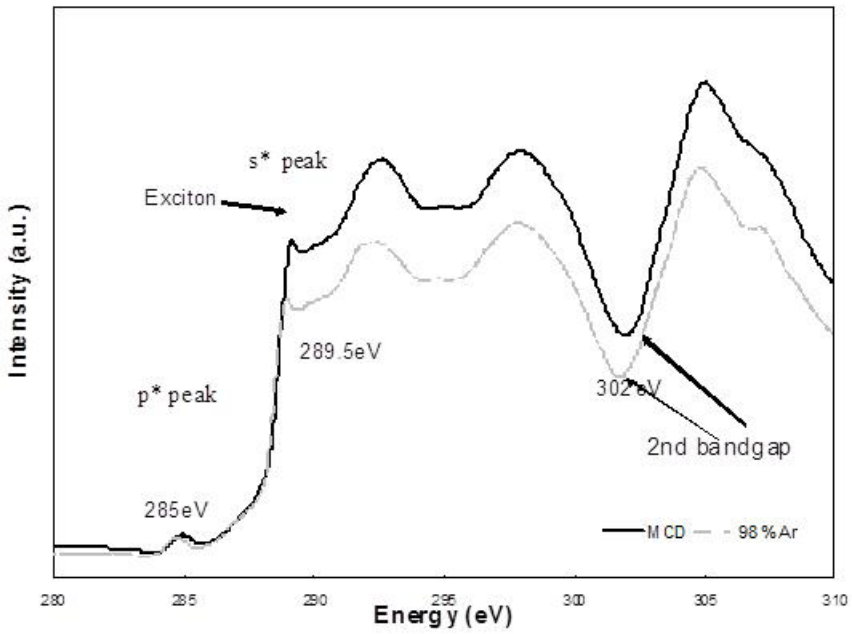

Figure 3.14. TEY NEXAFS spectra of diamond films deposited with and without Argon. © Inderscience [50]

3.3.5. Atomic Force Microscopy

The Atomic Force Microscope (AFM) principle is similar to a phonograph or profilometer on a much smaller scale. A very sharp cantilever tip is dragged across a sample surface and the change in the vertical position reflects the topography of the surface. By the collection of data from successive line measurements, it is possible to form a two-dimensional image of the surface roughness. The different heights sensed by the cantilever are used to form a complete map of the surface.

Figure 3.15 shows the surface morphologies obtained by AFM measurements corresponding to two different diamond films grown on Si substrates by HFCVD synthesis at two different methane concentrations.

www.manaraa.com

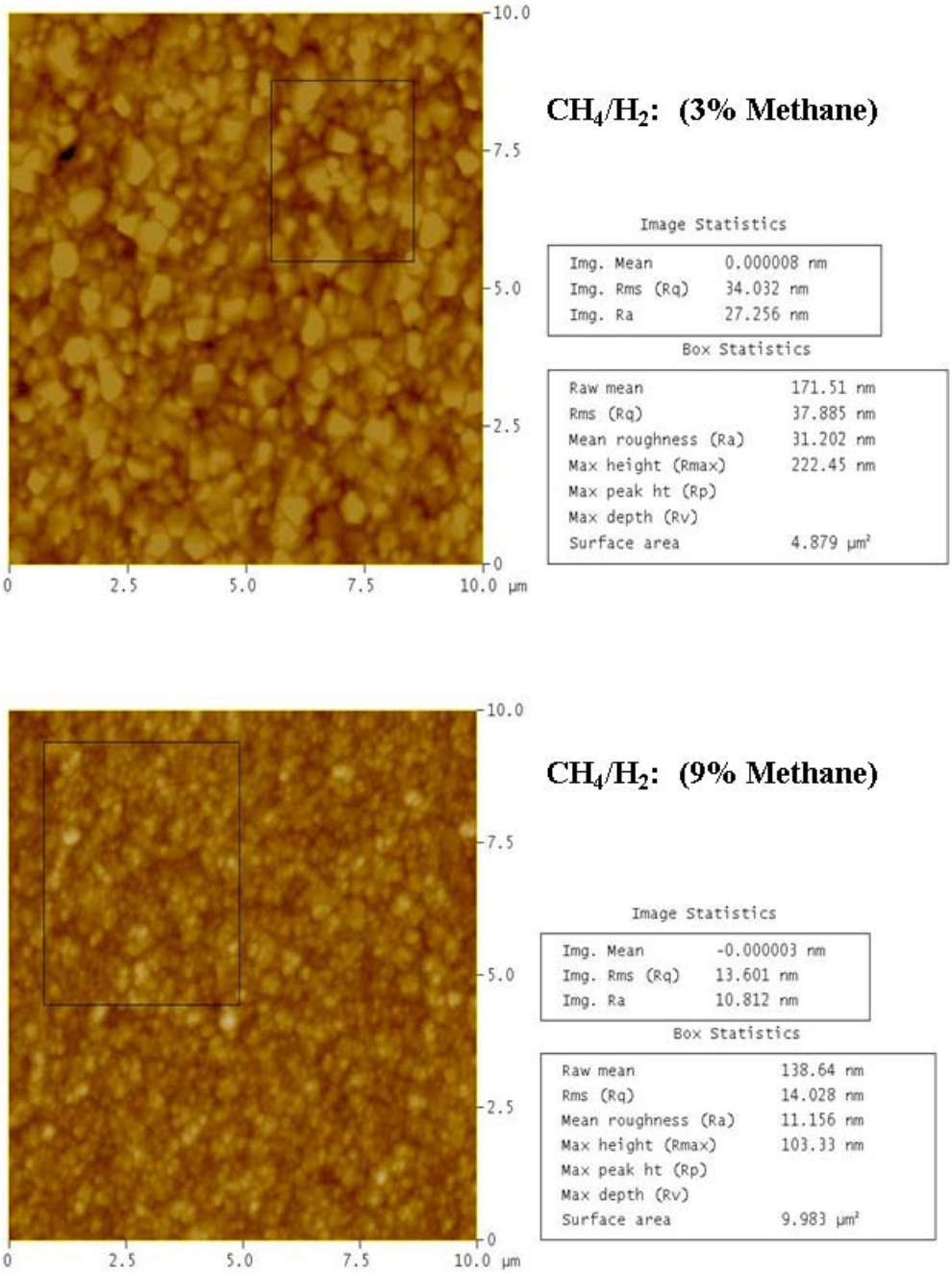

Figure 3.15. AFM images corresponding to the surface characteristics of two diamond films grown on Si substrates by HFCVD synthesis at different methane concentrations. Insets include the surface profile values R_q, R_a, R_{max}, R_p, and R_v for the area of analysis and the values of R_a and R_q for a particular box selected area

www.manaraa.com

One of the most important aspects to achieve a practical diamond thin film adhesion in cutting applications is the roughness profile of the tool surface which is strongly related with the wear rate. High surface roughness for microcrystalline diamond result in high friction and severe wear losses. However, there is a big opportunity to enhance the wear performance of diamond thin films with the growth of NCD with a low coefficient of friction associated. Basically, the fine finish of the sample surface (20 – 40 nm) is enough to guarantee a very good surface smoothness for the enhancement of the wear behavior.

3.4. The Synthesis of Diamond Films on Cutting Tools Substrates

As discussed in Chapter 1, when diamond is deposited in cemented carbide materials such as WC-Co substrates, the cobalt will play a detrimental catalytic role in the final diamond film adhesion. Any proposed solution must suppress the detrimental effect of cobalt and increase the mechanical interlocking between the film and the substrate in order to enhance the film interfacial toughness.

Different surface pretreatments have been proposed in the literature for WC-Co substrates with the aim to modify the surface roughness and halt the effect of the cobalt, so interface engineering techniques can be specifically aimed to improve the diamond coating adhesion. Since an increased surface roughness has been found to enhance the diamond nucleation density and promote a film interlocking behavior [58], surface pretreatment efforts can be tailored accordingly. The diamond-substrate interface requires the formation of strong interfacial chemical bonds between the diamond crystallites

www.manaraa.com

nucleated at the surface and the atoms of the substrate. Several interface engineering approaches have been reported in the last 15 years with the aim to reduce the undesired catalytic effect of cobalt on diamond adhesion.

The most widely successful techniques discussed in the literature are related to the cobalt removal in depths ranging in about 3 – 10 μm from the substrate surface by etching the cobalt out of the surface [59-61], halting the cobalt effect on the surface by depositing interdiffusion barrier layers that also diminish the thermal stresses caused during the diamond growth [62-68], and depleting the cobalt at the surface by selective thermal treatment methods [69-71].

The use of chemical etchings in the surface of WC-Co substrates represent the most cited pretreatment method in the literature. This method has the purpose to produce a selective etching of the cobalt binder by using a two step chemical process composed by an initial wet treatment in a Murakami solution with the aim of reconstruct and rough the surface by attacking the WC grains and exposing the Co binder, then, a second wet etching in an acid solution to reduce the exposed cobalt at a certain depth determined by the etching time. Other methods have been proposed the use of $CuSO_4$ solutions to produce a Cu cementation reaction to dissolve the cobalt at the substrate surface [72].

Interlayer materials used to avoid the cobalt-diamond interdiffusion are normally deposited by PVD methods. In order to choose the proper interlayer, the selected material must remain stable during the diamond deposition, provide a diffusion barrier between carbon and cobalt, have a low thermal expansion coefficient to minimize internal stresses, and provide a carbide formation surface to improve diamond nucleation [73,74]. These

www.manaraa.com

conditions are normally improved by using nanometer sized metal thin layers like Cr, SiC, and Ti at the top or bottom in a multilayer architecture. Typical hard coating materials used as interlayer for the adhesion improvement of diamond coatings include CrN, TiN, TiC, SiC, and Si_3N_4. Additional diamond particles may be peened at the top of the interlayer surface to provide additional diamond nucleation sites and serve as anchors to the final diamond coating.

Perhaps the extensive amount of information found in the literature in regard to improving the adhesion of diamond coatings on cemented carbide substrates by numerous pretreatment combinations and diamond growth parameters, very few correlate the surface characteristics of the substrate with respect to the dry machining performance of the diamond coating during cutting operations. A comprehensive list that summarizes a literature review of diamond coatings dry machining performance during the last ten years is shown in Table 3.4.

The criteria established to develop the review contained in Table 3.4 is based on considering experimental works that use commercial cutting tool materials as substrates, propose particular surface pretreatment methods to enhance the diamond adhesion, discuss the surface characteristics resulting from the pretreatments, evaluate the diamond structural properties with respect to the synthesis CVD method used, measure the adhesion of the diamond film by any practical experimental technique, provide information of the dry machining performance of the coated tool, and finally discuss the resulting failure mechanism of the diamond coating.

www.manaraa.com

Table 3.4. List of experimental research works conducted to enhance diamond coated tools adhesion in dry machining applications

Substrate Characteristics		Substrate Pretreatment (Surface Features)	Diamond Coating Characteristics			Initial Adhesion Evaluation	Machining Evaluation		Failure Mode	Ref.
Material	**Geometry**		**Synthesis**	**Structure**	**Thickness (μm)**		**Workpiece Material**	**Regime**		
WC-Co ISO K10,8–10 wt% Co	Twist drill bits	Etching (N/A)	HFCVD	NCD	1.5-14	N/A	Blocks of WC-5.5 wt% Co	Dry Drilling	N/A	[75]
Fine-grained carbide with 6% Co	2-flute twist drills	Etching and Electro-chemical Etching (N/A)	MWCVD	NCD	10.0	Indentation	A390 alloy	Dry Drilling	Diamond peeling	[76]
WC–6% Co	10 mm × 10 mm × 3 mm	Etching (N/A)	HFCVD	MCD	10.0	Indentation and Friction Test (ball-on-plate)	GFRP	Dry Turning	Flank Wear	[77]
WC–6% Co	Inserts	Etching	HFCVD	N/A	6.0	N/A	Al-12% Si alloy	Dry Turning	Coating flaking in both rake and flank surface	[14]
cemented carbide	Turning Insert with a tool nose radius of 0.4	N/A	N/A	“rough” monolayer, smooth monolayer, and both combined	6.0	N/A	SiC-Al (MMC)	Dry Turning	High wear rate and breakage of coating	[78]

www.manaraa.com

Table 3.4. (Continued)

(WC) with 6 wt.% cobalt	Square-shaped inserts (SPG422)	N/A (N/A)	MWCVD	NCD	25-30	N/A	A359/SiC-20p	Dry Turning	Low wear rate followed by an abrupt increase in flank wear (coating flaking)	[79]
WC 6–8% cobalt	300 μm diameter, two-flute end mills	Etching (N/A)	HFCVD	Fine Grain Dispersed (FGD) and NCD	0.5-1.0 and 0.2-0.3	N/A	6061-T6 aluminum	Dry Micro Milling	Coating flaking (NCD) and tool fracture (FGD)	[80]
WC 6% cobalt	Turning inserts of geometry SPUN 120308, ISO K10 grade	Etching and substrate (Surface Roughness comparison)	HFCVD-bias enhanced	MCD	N/A	Indentation	Rolled aluminum	Dry Turning	Flaking of the coating	[81]
WC–6 wt.% Co	Turning inserts SPGN120308	Etching (N/A)	MWCVD	NCD and MCD	35 (both)	Indentation	A390 (18wt% Si)	Dry Turning	Gradual flank wear	[82]
Si_3N_4	Round (RNMN1003 M0FN) and triangle (TNMN160308 FN) inserts	None (N/A)	HFCVD	NCD and MCD	22 ± 2 (both)	N/A	High quality EDM graphite	Dry Turning	Crater depth wear and flank wear	[83]
WC–6% Co	Drills have a 37-mm total length with a diameter of 3 mm	Etching (removal of grinding marks)	DC arc plasma CVD	NCD	~ 5.0-6.0	N/A	SiC particles reinforced aluminum matrix composite	Dry Drilling	Abrasion and no peeling	[84]

www.manaraa.com

Table 3.4. (Continued)

Si_3N_4	Insert with cylindrical shape with 10 mm of diameter and 3 mm of thickness	None (N/A)	HFCVD	MCD	15	N/A	Pearlitic grey cast iron GG25 DIN 1691	HS dry Turning	Abrasion, diffusion, adhesion wear and diamond coating graphitizatio n	[85]
WC–6%Co	Triangular inserts (TPGN 11 03 04)	Etching and SiC interlayer of 0.5 µm (SEM surface structure)	HFCVD	MCD	5.0-6.0	N/A	Graphite rods	Dry Turning	Notch formation on the relief face	[86]
WC–6%Co	Square-shape inserts (SPG422)	N/A (N/A)	MWCVD	NCD	30	N/A	A 390 alloy (18 wt.% Si)	Dry Turning	Coating flaking	[87]
WC 6–8% cobalt	300 µm diameter, two-flute end mills	Etching (Changes in tool geometry)	HFCVD	Fine Grain Dispersed (FGD)	0.5-1 and 0.2-0.3	N/A	6061-T6 aluminum	Dry Micro Milling	N/A due to Aluminum BUE	[88]
WC–6%Co	Tool inserts (TPG 110304)	Etching (N/A)	HFCVD and TMCVD	MCD	5.0 ± 0.3	N/A	ISO88 graphite	Dry Turning	Flank wear, crater wear, and notching	[89]
WC-6 wt.% Co	Cutting inserts (TPGN 160308)	Heat treatment and etching	HFCVD and TMCVD	MCD	23-25 ± 2 (HFCVD) and 5.0 (TMCVD)	N/A	Al–10% Al_2O_3-MMC (HFCVD) and graphite (ISO 88) (TMCVD)	Dry Turning	Flank wear	[90]

www.manaraa.com

Table 3.4. (Continued)

Hard-metal grades (K10 and M10–30 types, 6% Co)	N/A	Heat treatment and etching (Cutting edge surface)	HFCVD	MCD, NCD, and Multi Layer	6.0-25	N/A	(CFP) and Al-Si-alloys with low Si-content.	Turning	Flank wear	[16]
WC-6wt.%Co	Triangle inserts	Chemical etching, microwave plasma-etching (N/A)	HFCVD	Rough and soft diamond coatings	10-15	Indentation	SiC reinforced aluminum base composite	Turning	Flank wear and coating peeling	[91]
WC–Co	K10 drills	Microwave oxidation and etching (SEM surface structure)	HFCVD	MCD and NCD	N/A	N/A	SiC particles reinforced aluminum matrix composite	Dry Drilling	Flank wear Normal mechanical abrasion and no peeling	[92]
WC-6wt.%Co	Triangular (TPGN 160308) inserts	Heat treatment and etching (SEM Surface structure)	HFCVD	MCD	27±3 μm	N/A	Al-20%SiC	Dry Turning	Flank wear	[93]

www.manaraa.com

After analyzing the information contained in Table 3.4, the following facts in regard to the correlation between the substrate characteristics, surface pretreatments, diamond synthesis, diamond adhesion, dry machining performance, and wear failure can be stated:

- The most common substrate materials used are cemented carbides (WC-Co) with cobalt contents of 6%. Another substrate material evaluated is Si_3N_4, which does not require additional surface pretreatments to enhance diamond adhesion and no surface characteristics are reported besides the seeding process required for the diamond deposition
- Different tool geometries have been used during the dry machining operations; however, most of them correspond to square shaped cutting inserts and drills
- Chemical etching is the surface pretreatment used in the majority of the experimental works. Only SiC interlayers have been evaluated in the adhesion improvement and dry machining performance of diamond coated tools. Heat treatments have also been used as a cobalt suppression mechanism on the tool surface
- Hot filament chemical vapor deposition (HFCVD) is the synthesis method used in most of the experimental processes to deposit the diamond coatings
- Nanocrystalline diamond coatings have been the structural film characteristic mostly deposited during the last four years. Previously, most of the depositions correspond to microcrystalline diamond characteristics

www.manaraa.com

- Different diamond film thicknesses have been evaluated with respect to the diamond coating performance during dry machining operations. Only one systematic experimental study has been conducted in order to analyze this effect with respect to the dry machining performance
- Despite the many diamond film adhesion evaluation techniques discussed in the literature, only indentation and friction (ball-on-plate) tests have been directly compared with the dry machining performance results of the diamond coated tools by four of the experimental works
- Diverse workpiece materials have been dry machined with the diamond coated tools including: Al-Si alloys, glass fiber reinforced polymers (GFRP), SiC-Al metal matrix composites (MMC), electric discharge machining (EDM) grade graphite, graphite, Al_2O_3-Al MMC, and carbon fiber reinforced polymers (CFRP). Pearlitic gray cast iron workpiece material has been also evaluated with poor machining behavior of the diamond coated tool
- Dry drilling and dry turning have been the most evaluated cutting operations
- Flank wear is the most common failure mechanism present at the diamond coated tools during the dry machining, however, other diamond coating failures have been identified such as film peeling, film breakage, coating delamination, crater depth wear (present in Si_3N_4 substrates), abrasion, diffusion and graphitization (present in pearlitic gray cast iron), and notch formation

www.manaraa.com

CHAPTER 4. SURFACE PRETREATMENTS ANALYSIS ON CEMENTED CARBIDE CUTTING TOOLS

4.1. Introduction

The action of any surface pretreatment technique over a substrate material will produce a characteristic trace on both its superficial layer and subsurface integrity, which substantially differ from the bulk in terms of structural properties such as mechanical, thermal, electrical, and physical, energy condition, and adsorption activity [94].

The diamond coating surface roughness and the suppression of the cobalt migration in WC-Co pretreated substrates have been established as the main aspects to influence the cutting performance of CVD diamond coated tools in the machining of SiC reinforced aluminum base composites [91].

In addition to the synthesis growth requirements, the surface textures and subsurface characteristics have a direct impact on the subsequent diamond adhesive behavior [95]; hence, the final diamond coating performance strongly depends on the technological surface layers produced by the selected surface pretreatments and their consequential effects in the substrate surface/subsurface integrity, which ultimately represent the interfacial characteristics of the substrate-coating composite system.

www.manaraa.com

Besides suppressing or halting the undesired catalytic effect of cobalt on the diamond growth, a mechanical interlocking effect between the substrate surface and the diamond film is fundamental to achieve an optimal adhesion of the coating. The interlocking mechanism is mainly due to the formation of embedded nucleation sites inside the surface grain interruptions at the microscopic level. Depending on their size, distribution, and orientation, the adhesion of the diamond film coating will be determined by the substrate mechanical strength, the resulting substrate-coating chemical bonding and frictional forces [96].

However, the characteristics of the aforementioned interruptions in terms of their dimensional magnitude, orientation, and consequential subsurface modifications on the substrate material have not been studied with respect to the dry machining performance of diamond coated tools as a manufacturing chain.

The final roughness of the diamond coating deposited by HFCVD synthesis methods depends substantially on the original roughness of the pretreated substrate material [97]. This fact is even more critical when considering commercial cutting tools in their as-ground state as substrates for diamond deposition.

The amount of surface/subsurface damage present in commercial tools in terms of grind lines, fragmented WC grains, and a Co binder phase redistributed at the surface [38], creates particular considerations to take into account during the understanding of any surface pretreatment method.

www.manaraa.com

Additionally, the amount of cobalt removed out of the substrate when using chemical etching pretreatments, is characterized by a depletion band beginning at the surface toward the center in the bulk; normally, its thickness depends on the etching time. This condition creates uncertainties for chemically etched cemented carbides to be CVD diamond coated. One case is due to the possibility of cobalt flowing from the bulk to the surface during the diamond CVD synthesis process if the depletion band is not thick enough. The other case, considers an expected decrease in the fracture toughness of the carbide tool if this band is too thick.

Moreover, the surface/subsurface characteristics of the interface vary substantially when considering an inter-diffusion and stress relaxation interlayer architectures deposited in the substrate to enhance the diamond adhesion. The interaction between the bottom layers with the substrate surface and the interaction between the top layers with the diamond coatings creates two distinct interfaces with particular behaviors depending on the substrate surface texture characteristics and the conditions for the diamond growth, respectively.

With the aim to correlate the substrate surface/subsurface modifications in WC-Co turning inserts as the result of chemical etchings and the deposition of a CrN/Cr interlayer as pretreatment methods, different aspects are evaluated during this chapter in terms of the resulting features at the substrate surface/subsurface and interfacial characteristics.

www.manaraa.com

4.2. Experimental Conditions

Commercial tungsten carbide - 6 wt% cobalt square positive angle turning inserts (WC-6%Co/SPG-422) were used as tool substrates for further microcrystalline diamond (MCD) coating depositions. Different surface pretreatments were selected in order to evaluate the two most commonly reported technical approaches to overcome the detrimental effect from the cobalt binder, including the cobalt surface removal by surface chemical etchings and the suppression of cobalt-carbon solubility effect by the pre-deposition of an inter-diffusion barrier layer.

4.2.1. Chemical Etchings

Chemical etching methods involve the use of chemical agents during a specific amount of time in order to roughen the surface and suppress its cobalt binder effect [90,98,99]. The WC-Co inserts were first cleaned in an acetone ultrasonic bath for 10 minutes, followed by 5 minutes in an ultrasonic rinse in methanol with the aim to remove any contamination from previous grinding processes. After that, samples were ultrasonically treated with Murakami's solution (1:1:10 KOH + $K_3[Fe(CN)_6]$ + H_2O) for 10 minutes and then rinsed with deionized water. In Method E-1, the Murakami's step was followed by the immersion of the samples in an ultrasonic bath containing 10% HNO_3 + 90% H_2O_2 for 60 seconds. Method E-2 corresponds to the same Murakami initial etching and further immersion in an ultrasonic bath containing 3 ml of H_2SO_4 and 88 ml of H_2O_2 for 60 seconds. After all chemical etchings, samples were ultrasonically rinsed with deionized water and dried with nitrogen gas.

www.manaraa.com

4.2.2. The CrN/Cr Cobalt Inter-Diffusion Barrier Interlayer

As discussed previously, the deposition of a physical barrier layer prevents the inter-diffusion of carbon into the underlying cobalt binder phase and may also act as a stress relaxation layer reducing the thermal expansion coefficient mismatch between the diamond and the substrate material.

In this research, as received WC-Co (6%) inserts were coated with an initial layer of CrN (1.5μm) followed by a top layer of Cr (1.5μm) using a commercial cathodic-arc Physical Vapor Deposition (PVD) system. Additional treatments after the interlayer deposition were applied to the PVD coated tool surfaces in order to improve the diamond film nucleation and interlocking with the substrate by creating a rougher surface.

Method I-1 corresponds to an additional media blasting to the top Cr surface for 1 minute using diamond particles (50μm) at a pressure of 40 psi. Method I-2 corresponds to an additional surface scratching process to the chromed surface during 60 minutes in an ultrasonic bath containing a solution of 2.4g diamond powders (50μm) dispersed in 50ml of methanol.

4.3. Initial Surface Pretreatment Effects

Initially, the effects of the surface pretreatments were evaluated in general in order to establish their overall effects in terms of the substrate surface modification and propose possible optimization methods. The surface/subsurface modification will be

www.manaraa.com

evaluated later on in this chapter based upon the results of the initial pretreatment characteristics.

The substrates surface roughness and morphology before and after each surface pretreatment were measured by a Vecco Wyko-NT9100 white-light interferometer and a Hitachi S-800 Scanning Electron Microscope. Cross sectioning of the substrates before and after each treatment was performed by dicing the inserts with a refrigerated diamond saw followed by metallographic preparation of the resulting surfaces mounted on conductive epoxy resin, grinded and polished using an automatic preparation Struers Prepmatic-2 system.

Supplementary SEM analysis was conducted on metallographically-prepared samples to characterize the effect of each pretreatment in the WC-Co microstructure by immersing the cross sectioned samples during five minutes in a solution of Murakami reagent (10g $K_3Fe(CN)_6$ + 10g NaOH in 100mL H_2O) in order to reveal the modified cemented carbide microstructure. All abovementioned surface pretreatments are summarized in Table 4.1.

www.manaraa.com

Table 4.1. Surface modification pretreatments applied to the WC-Co(6%) turning inserts

Surface Denomination	Treatment Characteristics
As-received (AG)	Ultrasound cleaning in acetone and methanol
Murakami (M)	Ultrasound bath in (1:1:10 KOH + $K_3[Fe(CN)_6]$ + H_2O)
Method E-1	Murakami + ultrasound bath in 10% HNO_3 + 90% H_2O_2
Method E-2	Murakami + ultrasound bath in a solution of 3 ml of H_2SO_4 and 88 ml of H_2O_2
PVD coated (I-AG)	Deposition of 1.5µm of CrN and 1.5µm of Cr (top)
Method I-1	PVD coated + shoot peening with 50 µm grain size diamond powder
Method I-2	PVD coated + wet scratching in a 50 µm grain size diamond slurry

Figure 4.1 depicts the surface maps and roughness parameters obtained by white-light interferometer, and corresponding to the surface of as received WC-Co (6%) commercial turning inserts (AG), the surface after Murakami treatment (M), methods E-1, E-2, I-1 and I-2 respectively.

Roughness parameters values such as R_z, R_t, R_p, and R_a were recorded and averaged from six measurements on different top surface points. The scan size is determined by the optical magnification of the system (50 X) in a resulting surface area of 126 x 94µm and containing 640 x 480 data points. These values were kept constant for all roughness measurements in order to decrease the systematic error in the resulting roughness parameter values [100].

www.manaraa.com

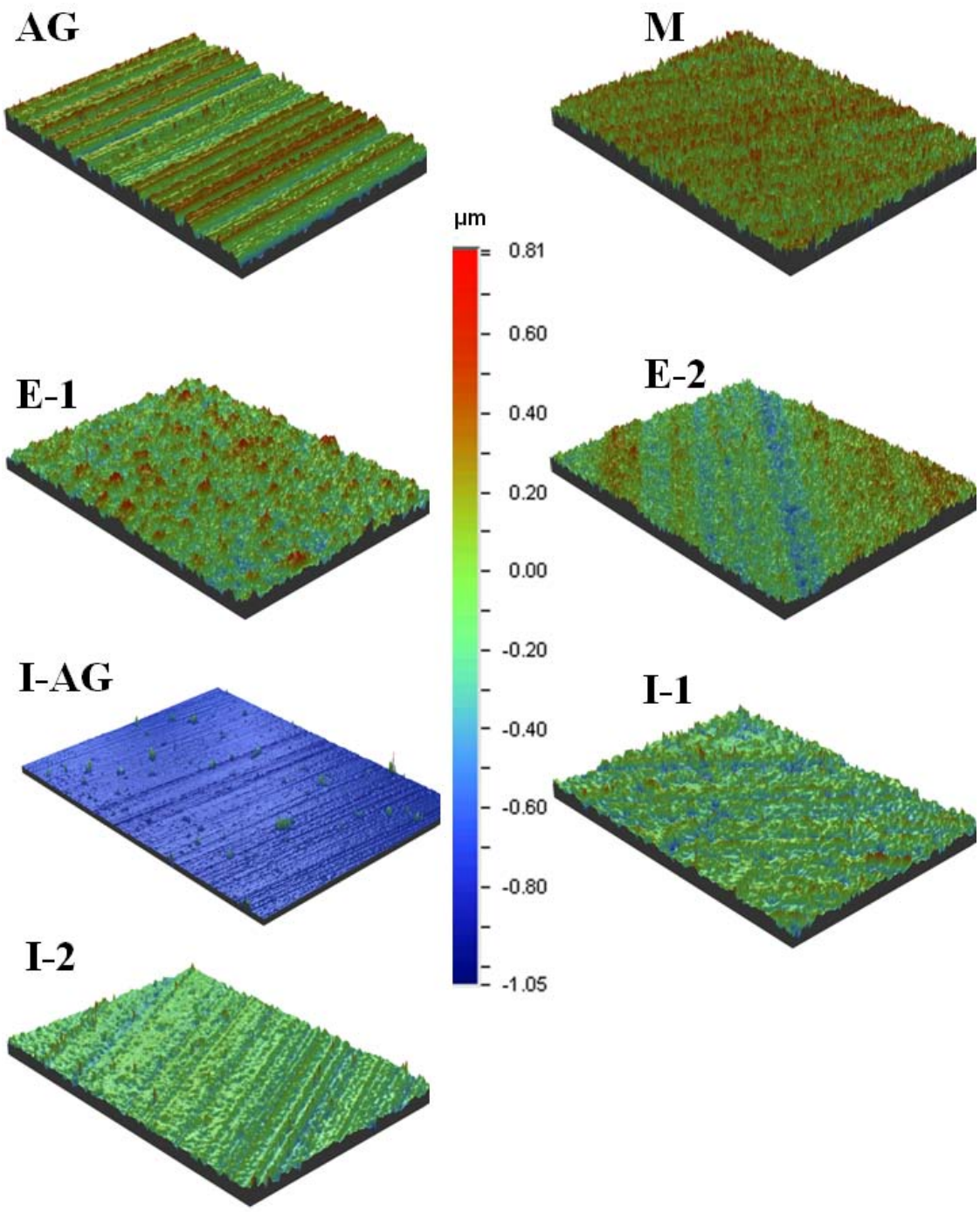

Figure 4.1. Surface maps obtained by white-light interferometry corresponding to as-received WC-Co (6%) turning insert topography (AG), Murakami treated surface (M), and surface textures after treatment method E-1, method E-2, original PVD coated substrate (I-AG), method I-1, and method I-2, respectively

www.manaraa.com

Surface map AG represents the as-ground original surface depicting the directional marks (feed marks) left by the grinding process on the surface of the tool. These feed marks confer to the surface an average roughness (R_a) of 0.16µm measured perpendicular to the feed marks across a length of 126 µm. Murakami (M) treated surfaces displayed an increased surface roughness parameter R_a of 0.24 µm with a partial removal of feed marks.

Surface topography after treatment method E-1 reveals a uniform surface with a R_a value of 0.51µm, with a complete removal of feed marks. The resulting surface characteristics of Method E-2 show a partial removal of feed marks with a corresponding R_a value of 0.45µm.

The effect of the top chromium media blasting and diamond scratching methods after the deposition of the initial PVD CrN/Cr interlayer are also characterized in Figure 4.1. The initial PVD deposition process (I-AG) produced a surface that still displays features with a preferential direction resulting from the conformal PVD coating over the initial feed marks in the as-ground surface. Furthermore, other features resulting from the cathodic-arc PVD process (microdroplets), which will be discussed later, were observed. Consequently, the roughness value for the PVD top chromium interferometry surface map are considerably affected by the combined effect of these features, and are not suitable for a quantitative pretreatment comparison purpose.

Method I-1 produced a uniform surface roughness with an R_a parameter of 0.28µm, few visible feed marks (at a bigger surface area scale of 250 x 190 µm) and completely removes the microdroplets in a microscale, however, Method I-2 generates a

www.manaraa.com

surface with an R_a value of 0.11µm, with less Cr microdroplets compared to the original PVD coating, and did not completely modify the top surface in terms of the initial as-ground feed marks, with resulting roughness parameter values close to the original as ground surface characteristics as shown in Figure 4.2, which summarizes all surface roughness parameters for each surface denomination, including the maximum and minimum values with respect to the average.

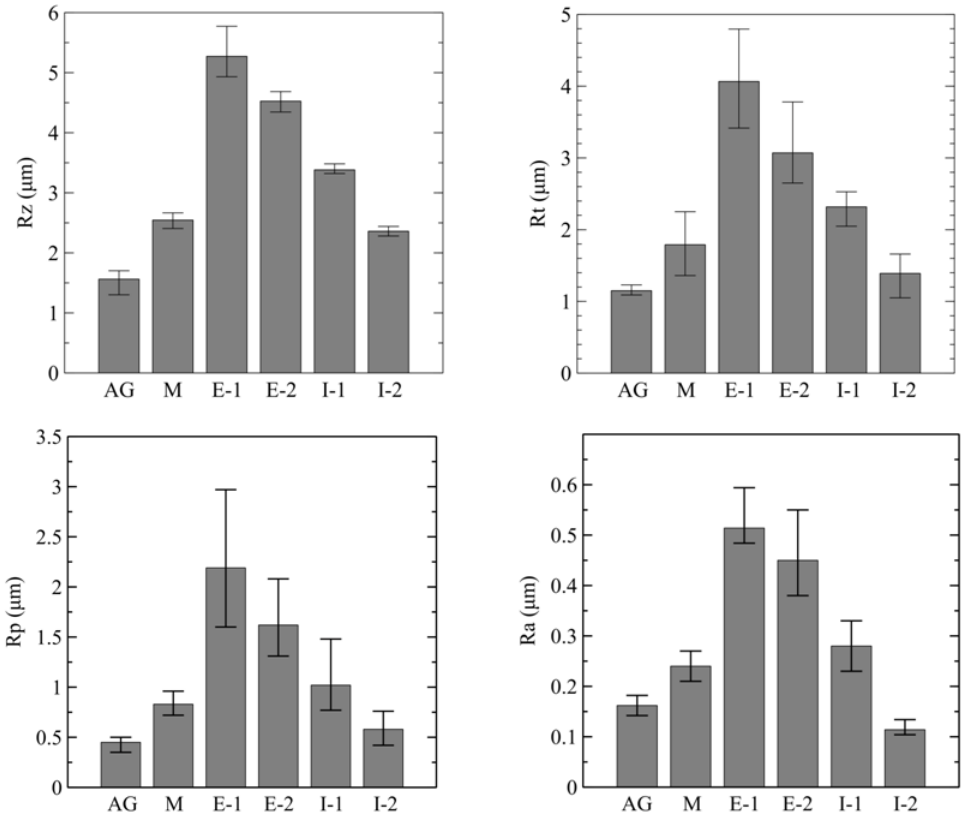

Figure 4.2. Roughness characteristics for each surface designation represented by the ten-point height (R_z), maximum peak-to-valley height (R_t), highest peak (R_p), and arithmetical mean deviation (R_a) texture roughness parameters

www.manaraa.com

Figures 4.3(a)-(d) are SEM micrographs of the substrate top surfaces and their cross sections after metallographic preparation. In Figure 4.3a, the feed marks on the surface of the tool are depicted and the microstructure (insert) of the cemented carbide corresponds to the WC grains with a diameter of 1.4µm in average embedded in a Co matrix. Figure 4.3b shows the surface modification after pretreatment E-1 with a Co removal depth of approximately 9.5µm along the cross section of the tool. The surface modification after pretreatment E-2 is shown in Figure 4.3c, which shows the cobalt binder depletion zone of ~ 8.0µm down into the cross section. It can be seen that both pretreatments, method E-1 and method E-2, modify the surface at the micro-scale in terms of eliminating the directional features from the as-received sample, which are detrimental to the final adhesion of the diamond coating due the resulting debonding of the film along the preferential direction of the feed marks.

The microstructure morphology of chemical etched samples depicts the resulting cobalt binder removal, which produces isolated WC grains in the cross section of the tool at different Co removal rates. This effect corresponds to the initial effect of Murakami's reagent, which attacks the WC grains, thus modifying the initial surface, and the final etching of the acid (for both etching methods), which oxidizes the cobalt binder to soluble Co^{2+} compounds, consequently washed out during the ultrasonication [101].

The CrN/Cr interlayer surface deposited on the top of the as received WC-Co inserts, including its cross section, is shown in Figure 4.3d, which depicts a uniform coating with the presence of Cr particles (microdroplets) entrained at the surface, this is typical for a cathodic arc-PVD process with heights ranging from 1.2 to 4.5 µm

www.manaraa.com

(interferometer measurement) and diameters between 1.5 and 3.0 µm, approximately. The cross section (inset) shows the conformal deposition and morphology of both, CrN and Cr interlayers on the top of the WC-Co substrate.

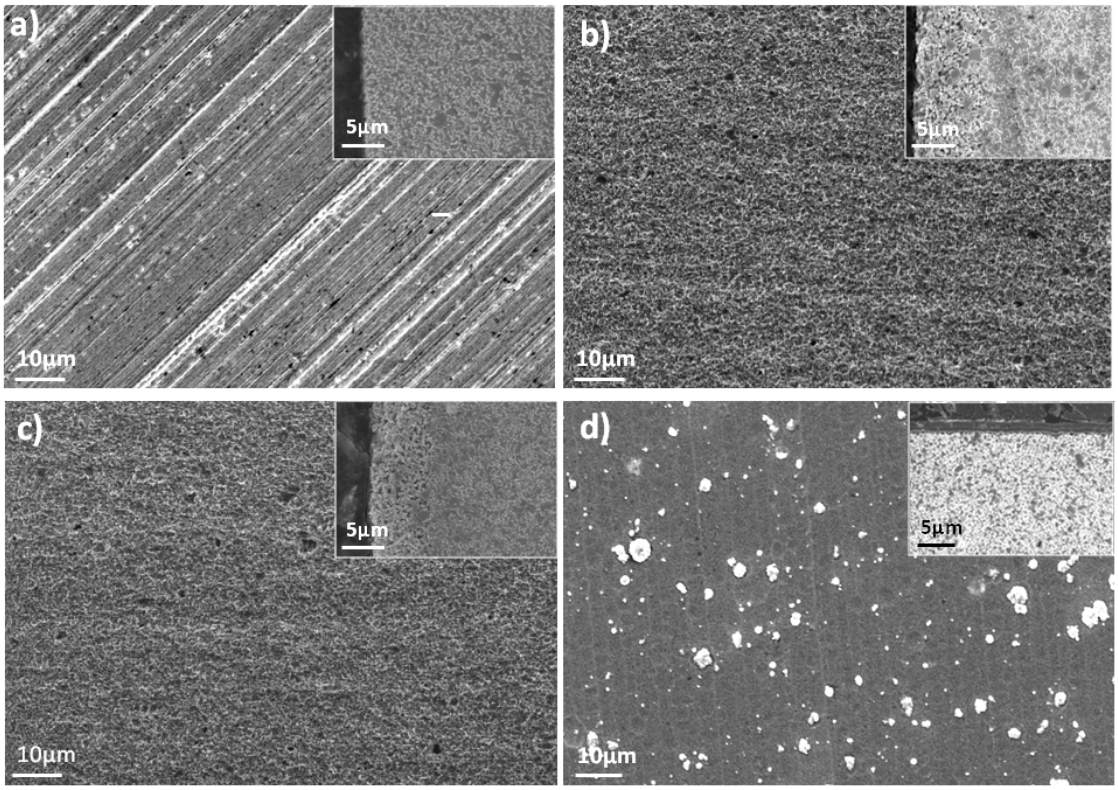

Figure 4.3. (a) SEM micrograph showing the finishing feed-marks at the surface of WC-Co (6%) as received turning inserts and the WC grains distribution (inset) in the Co binder. (b) SEM micrograph at the surface of substrates after E-1 pretreatment including the Co depletion layer (inset) in the cross section. (c) SEM micrograph at the surface of substrates after E-2 pretreatment including the Co depletion layer (inset) in the cross section. (d) SEM micrograph at the surface of substrates after the CrN/Cr PVD deposition and the cross section (inset) showing the layer interfaces and morphology

www.manaraa.com

4.4. Surface and Subsurface Integrity of Modified Surface Pretreatments

After analyzing the initial surface pretreatment effects on the surface characteristics of pretreated WC-Co turning inserts, new substrate pretreatments listed in Table 4.2 were conducted in order to obtain systematically modified surface textures and ultimately correlate them with the adhesion and dry machining performance of diamond coated tools, analyzed in Chapter 5 and Chapter 6, respectively.

The new sets of chemical pretreatments described in Table 4.2 are aimed to produce different subsurface characteristics in terms of the effect of the initial Murakami treatment on the resulting tool surface texture, and producing different thicknesses in the cobalt depletion band, both by changing their immersion time in their respective chemical solutions.

It has been reported that the effect of the Murakami reagent is to attack the WC grains present at the substrate surface, consequently roughing the surface and exposing the cobalt binder [90]. The modified surface pretreatments M1 to M4 were tailored to analyze the effect of the Murakami reagent in the reduction of the surface damage present in the as ground (AG) by increasing the reaction time.

www.manaraa.com

Table 4.2. Modified surface pretreatments applied to the WC-Co (6%) turning inserts

Surface Denomination	Pretreatment Characteristics
Method - M1	Ultrasound bath in Murakami reagent(1:1:10 KOH + $K_3[Fe(CN)_6]$ + H_2O) for 5 min
Method - M2	Ultrasound bath in Murakami reagent (1:1:10 KOH + $K_3[Fe(CN)_6]$ + H_2O) for 10 min
Method - M3	Ultrasound bath in Murakami reagent (1:1:10 KOH + $K_3[Fe(CN)_6]$ + H_2O) for 20 min
Method - M4	Ultrasound bath in Murakami reagent (1:1:10 KOH + $K_3[Fe(CN)_6]$ + H_2O) for 30 min
Method – E-1-1	Murakami ultrasound bath for 10 minutes + immersion in 10% HNO_3 + ultrasound bath in 90% H_2O_2 for 15 seconds
Method – E-1-2	Murakami ultrasound bath 10 minutes + ultrasound bath in 10% HNO_3 + 90% H_2O_2 for 30 seconds
Method – E-1-3	Murakami ultrasound bath for 10 minutes + ultrasound bath in 10% HNO_3 + 90% H_2O_2 for 60 seconds
Method – E-1-4	Murakami ultrasound bath for 10 minutes + ultrasound bath in 10% HNO_3 + 90% H_2O_2 for 120 seconds
Method – E-2-1	Murakami ultrasound bath for 10 minutes + ultrasound bath in a solution of 3 ml of H_2SO_4 and 88 ml of H_2O_2 for 15 seconds
Method – E-2-2	Murakami ultrasound bath for 10 minutes + ultrasound bath in a solution of 3 ml of H_2SO_4 and 88 ml of H_2O_2 for 30 seconds
Method – E-2-3	Murakami ultrasound bath for 10 minutes + ultrasound bath in a solution of 3 ml of H_2SO_4 and 88 ml of H_2O_2 for 60 seconds
Method – E-2-1	Murakami ultrasound bath for 10 minutes + ultrasound bath in a solution of 3 ml of H_2SO_4 and 88 ml of H_2O_2 for 120 seconds

www.manaraa.com

In methods E-1-1 to E-1-4 and E-2-1 to E-2-4, the variations are characterized by changing the chemical nature and reaction time necessary to oxidize the exposed cobalt binder at the surface, consequently producing different subsurface characteristics in terms of the cobalt depletion zone and WC grain distribution.

4.4.1. The As-Ground WC-Co Tool Surface

As mentioned earlier, the surface of the WC-Co (6%) turning inserts (AG sample) used during the present research is characterized by the presence of feed marks resulting from the final grinding manufacturing process to achieve the desired geometry. This amount of surface damage needs to be minimized in order to produce a homogeneous surface free of preferential features which may have a detrimental effect on the diamond adhesion.

Figures 4.4(a)-(c) display SEM micrographs containing additional information about the features of surface AG. Figure 4.4(a) depicts the direction of the feed marks with respect to the edge of the cutting tip of the insert. Figure 4.4(b) corresponds to the detail of the amount of surface damage in the sample of AG represented by the smearing of the cobalt binder (white areas) at the surface and its detachment at some points, creating voids and craters aligned with the direction of the feed marks. This superficial texture differed in some cases from one sample batch to another, suggesting that even when the tool insert geometry reference remains the same (SPG 422), the surface texture can be different as seen in Figure 4.4(c), which is an excessive grinding damage effect at

www.manaraa.com

the surface, that definitely has to be minimized by the surface treatments prior to the diamond deposition.

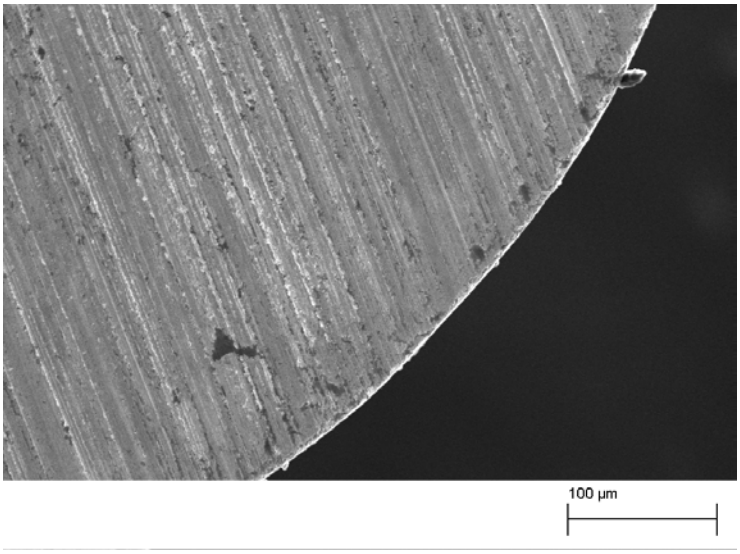

(a)

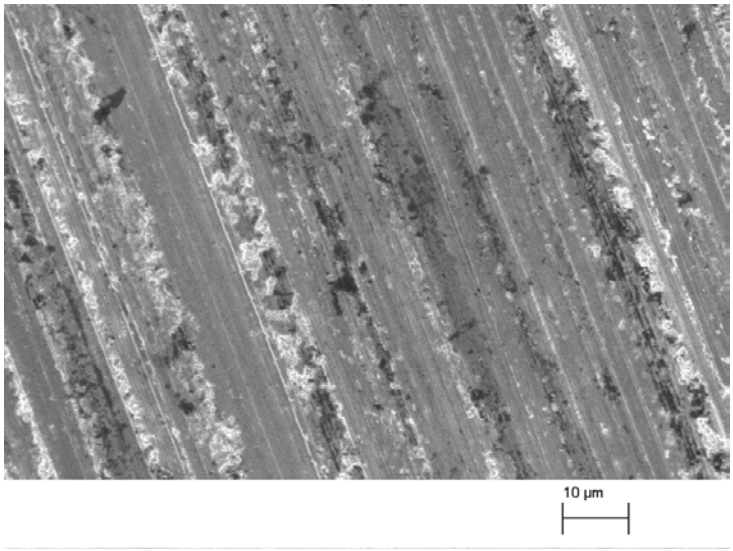

(b)

Figure 4.4. SEM micrograph corresponding to the surface of the as-ground WC-Co (6%) commercial inserts depicting: a) the orientation with respect to the cutting tip of the tool, b) the amount of surface damage and redistribution of the Co binder phase, and c) an excessive surface damage present in some batches, which need to be minimized before the diamond deposition to maximize the coating adhesion

www.manaraa.com

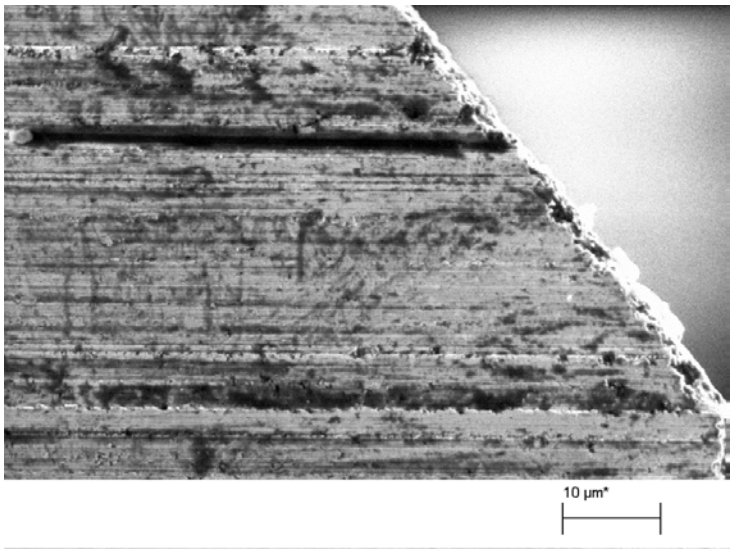

(c)

Figure 4.4. (Continued)

The surface texture characteristics of the sample AG were characterized by white light optical interferometry, and the corresponding results are shown in Figure 4.5(a) and 4.5(b). The feed marks confer to the surface an average roughness (R_a) of 0.128 µm measured perpendicular to the feed marks in a surface area of 140 by 105 µm as shown in Figure 4.5(a). From a surface profile analysis, as shown in Figure 4.5(b), it can be estimated that the features have an average maximum peak to valley R_t value of 1.19 µm.

www.manaraa.com

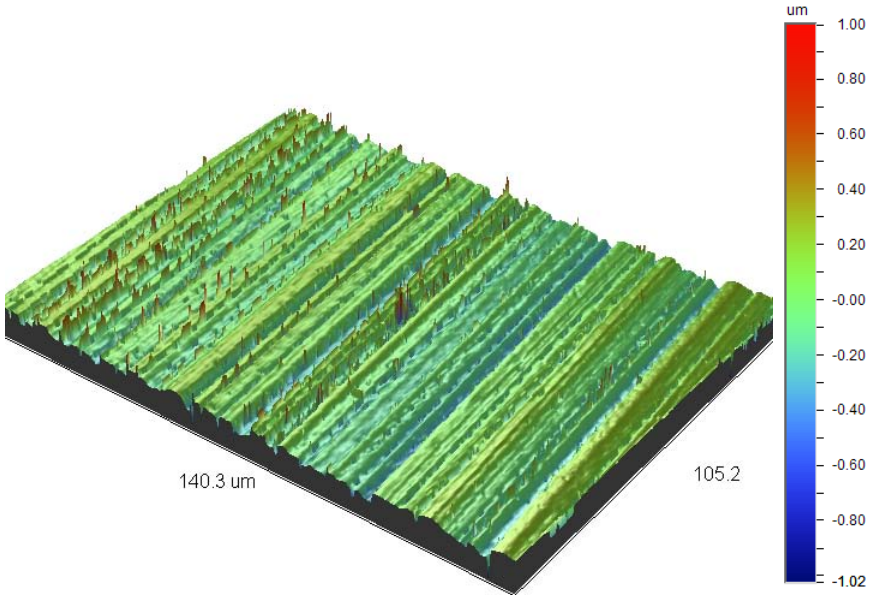

(a)

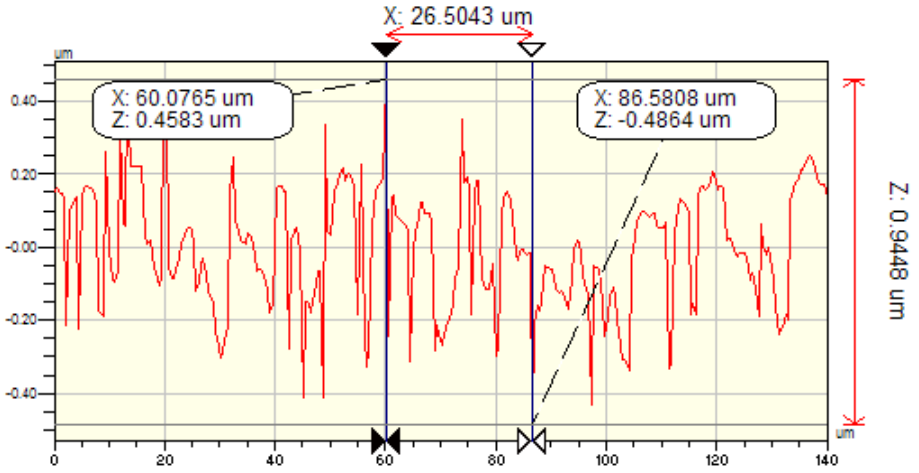

(b)

Figure 4.5. (a) The surface texture of sample AG detailing the overall surface representation and the area of analysis. The surface texture parameters were measured and averaged at three different analysis areas. (b) An example of a surface profile used to determine the roughness parameter values

www.manaraa.com

An additional interferometry analysis done in sample surface AG by using a bigger surface area corresponding to 1.4 x 1.0 mm (5x objective lens) and shown in Figure 4.6, reveals the more spaced features observed in the SEM micrographs on Figure 4.5(a)-(c), corresponding to a separation of 231.02 µm in and a maximum peak to valley R_t value of 1.45 µm.

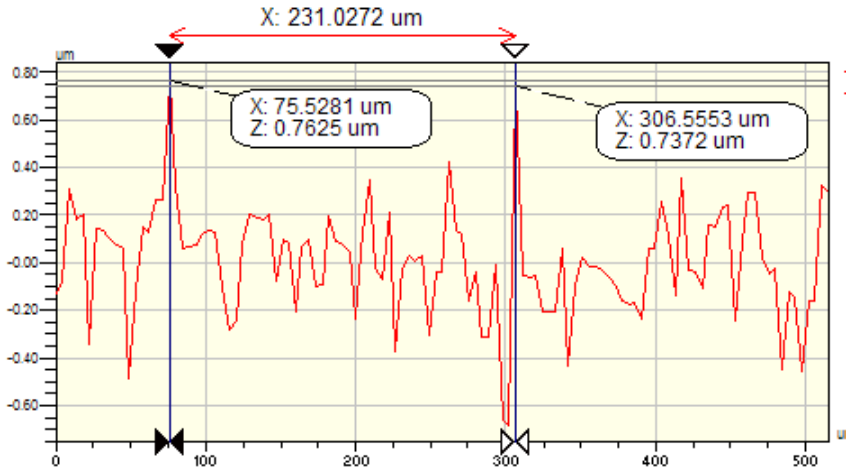

Figure 4.6. Surface profile of sample AG analyzed in a surface area of 1.4 x 1.0 mm

4.4.2. The Effect of the Murakami Treatment on the Tool Surface

After characterizing the surface texture present in the as ground samples, the surface pretreatment methods described in Table 4.2 as M1, M2, M3, and M4 were applied. Separate inserts were independently immersed in 20 ml of the Murakami solution and then agitated in an ultrasonic bath during the corresponding period of time for each method.

www.manaraa.com

Figures 4.7(a)-(d) correspond to SEM images of the insert surface after each Murakami pretreatment. The transition from a preferential surface texture to a more uniform surface texture can be seen as the result of a decrease in the height of the feed mark peaks. However, this reduction is accompanied by the exposure of surface void defects aligned in the direction of the feed marks, possibly caused by the detachment of WC grains out of the cobalt matrix due to the etching action of the Murakami reagent. This hypothesis was confirmed by the presence of WC powder precipitated at the bottom of the reaction container, which increased in weight along with the etching time. A detailed SEM image of these voids on the surface of sample M4 is shown in Figure 4.8. The alignment of the voids in the same direction of the feed marks suggest that the mechanism involved in the decreasing of the peaks heights is attributed to a detachment of weakly bonded WC grains affected by the finishing grinding action of the inserts in a non uniform cobalt binder which has been smeared on the surface.

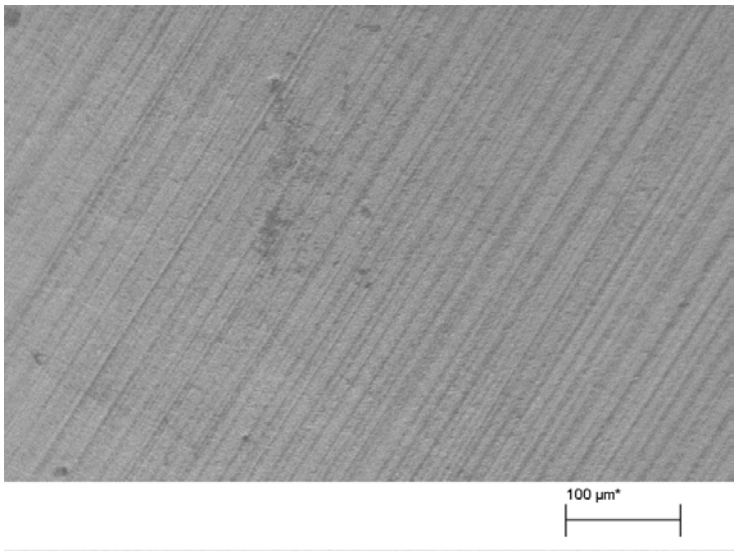

(a)

Figure 4.7. SEM images corresponding to the surface of tool substrates after pretreated in method (a) M1, (b) M2, (c) M3, and (d) M4

www.manaraa.com

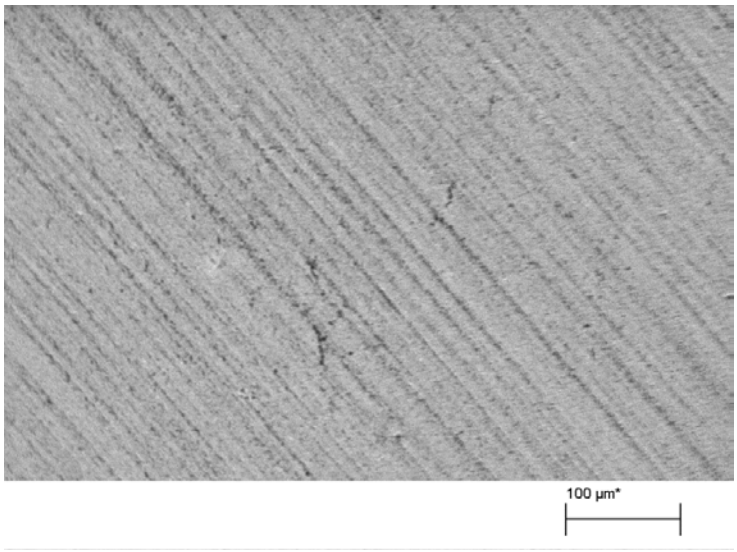

(b)

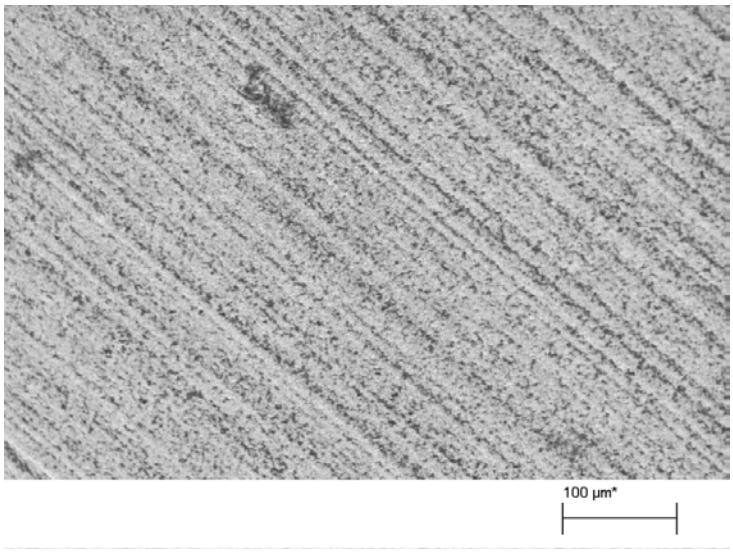

(c)

Figure 4.7. (Continued)

www.manaraa.com

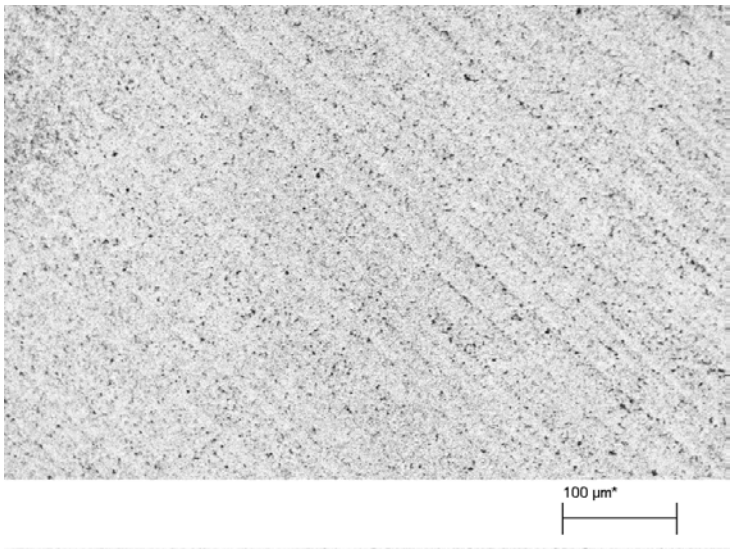

(d)

Figure 4.7. (Continued)

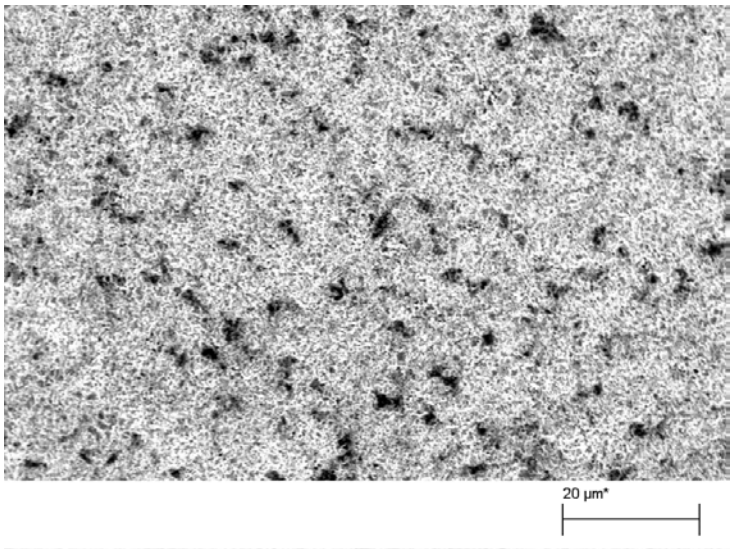

Figure 4.8. SEM images corresponding to the surface of tool of sample M4 depicting the voids at the surface corresponding to a cluster of WC grains detached from the WC-Co surface by the etching action of the chemical

www.manaraa.com

Surface texture maps of samples M1, M2, M3, and M4 are shown in Figure 4.9 and a summary of their corresponding roughness parameter values is included in Figure 4.10.

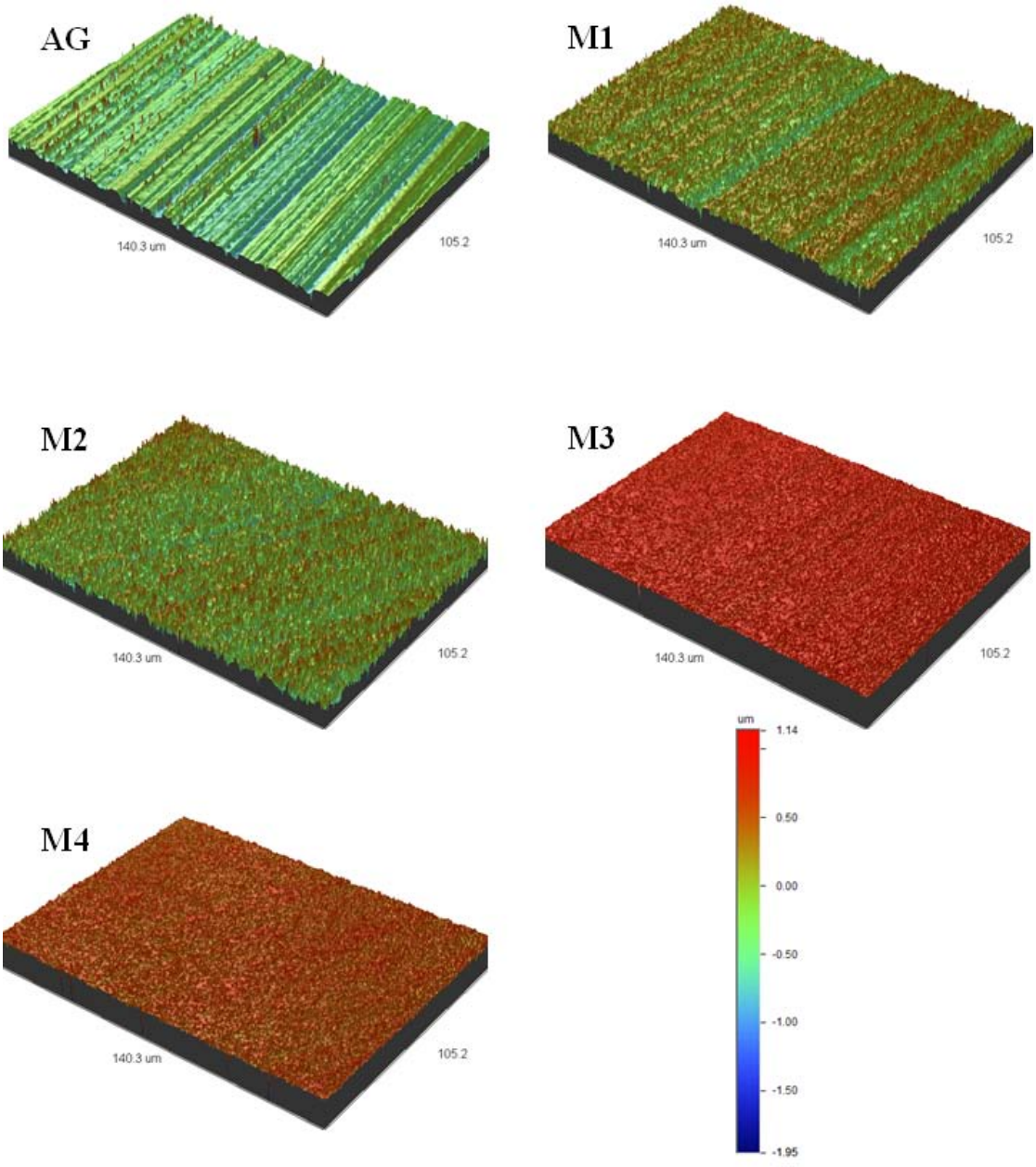

Figure 4.9. Surface textures of different Murakami surface pretreatments compared with the initial as-ground surface. The Z scale bar for all tests is included

www.manaraa.com

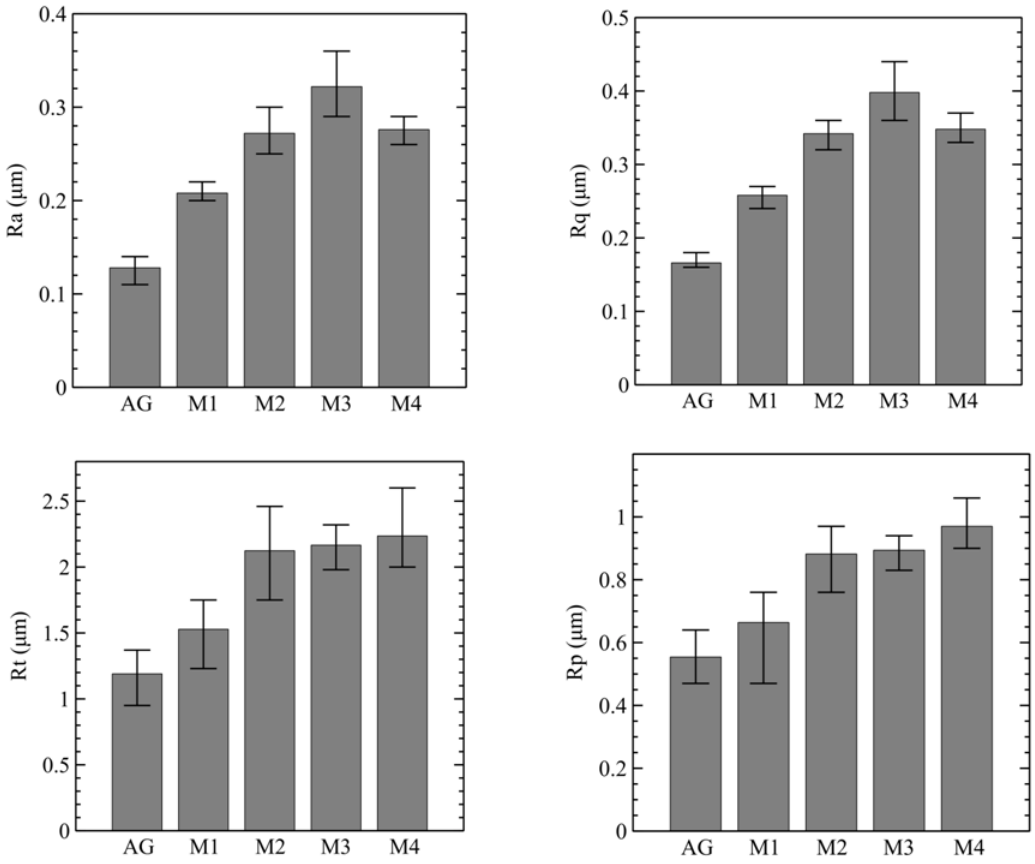

Figure 4.10. Roughness characteristics of different Murakami surface pretreatments represented by the arithmetical mean deviation (R_a), root-mean-square (rms) roughness (R_q), maximum peak-to-valley height (R_t), and highest peak (R_p), texture roughness parameters

As found from an analysis of the abovementioned data, the preferential surface texture of the as ground sample is reduced by the Murakami pretreatments by an increase in the surface roughness until method M3. The surface corresponding to method M4 is characterized by a smoother surface in both the surface texture and roughness values; however, the degree of roughness present at surface M4 is greater than the surface AG, so the decrease in the roughness parameters R_a and R_q values in sample M4 are mainly due to the reduction of the higher preferential features, however, directional features still

www.manaraa.com

appeared at higher surface areas as shown in Figure 4.7(d). The R_t and R_p values remain almost constant for surfaces M2, M3, and M4, in accordance to the chemical etching action (not mechanical polishing) in all surface interruptions, including the valleys.

4.4.3. The Effect of the Cobalt Removal from the Surface

The WC-Co turning inserts were pretreated with two types of chemicals during four different periods of time in order to remove the cobalt exposed at their surface, after being roughed with the Murakami reagent, as shown in Table 4.2. The time established for the initial Murakami pretreatment in this particular analysis corresponds to Method M2, established as the average contribution of the experimental levels from M1 to M4 to characterize the effect of the second etching step without having the smoother surface, or the one with the highest roughness value.

The effect of the Co removal pretreatments is analyzed with respect to the surface and subsurface integrity of the tools in terms of the surface textures produced and their corresponding cobalt depletion layer. The surface texture integrity is evaluated following the same experimental conditions during the Murakami pretreatment analysis. The subsurface modification was analyzed by a characterization of the tool substrate cross sections using metallographic preparation and SEM imaging. Surface texture maps of samples E-1-1, E-1-2, E-1-3, E-1-4, and their initial surface M2 are shown in Figure 4.11 and similarly for samples E-2-1, E-2-2, E-2-3, and E-2-4 in Figure 4.12. The summary of all surface roughness parameters for all variations in E-1 and E-2 method is shown in Figure 4.13.

www.manaraa.com

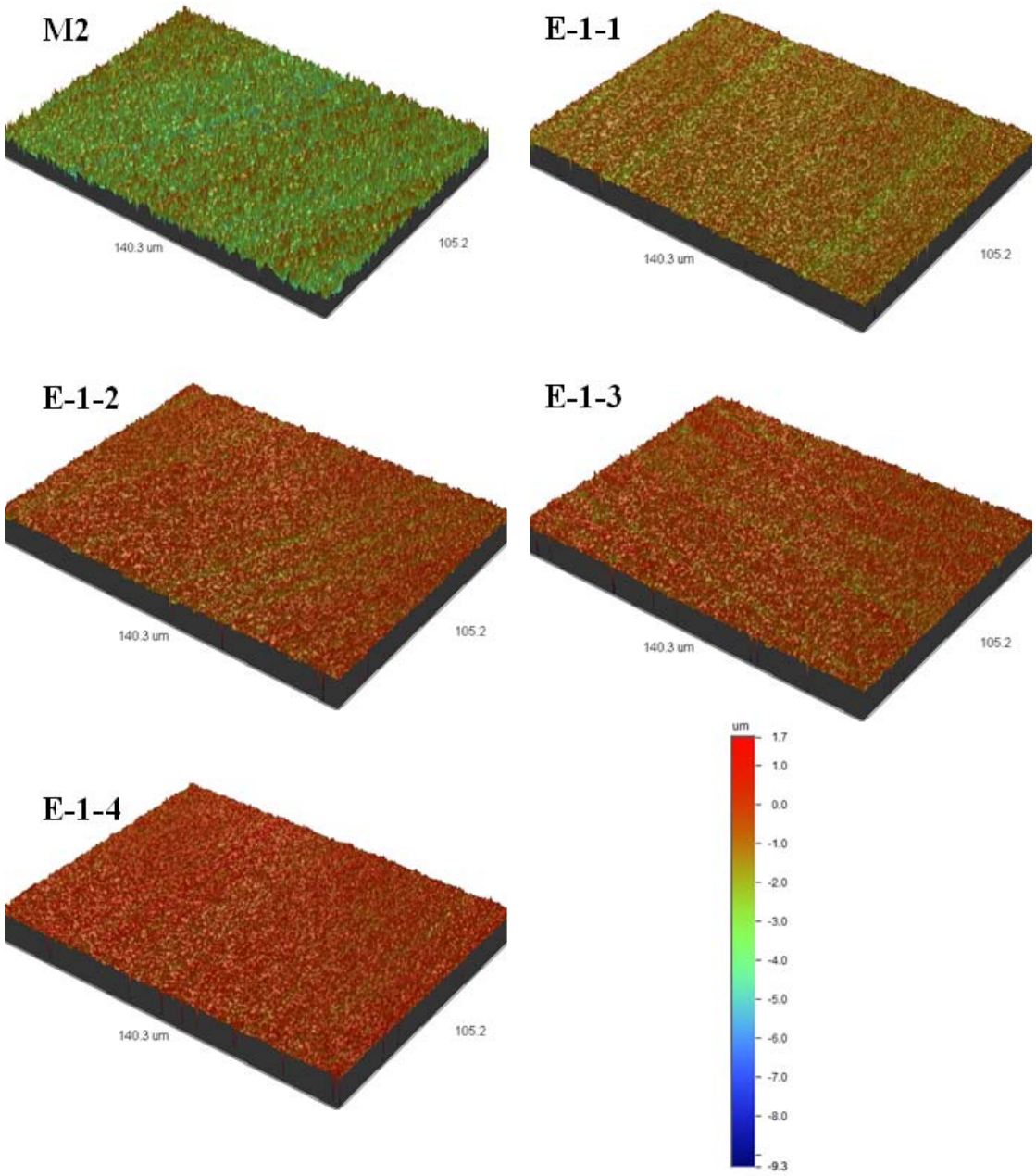

Figure 4.11. Surface textures corresponding to pretreatments E-1-1, E-1-2, E-1-3, and E-1-4, and compared with their initial surface corresponding to the method M2. The Z scale bar for all tests is included

www.manaraa.com

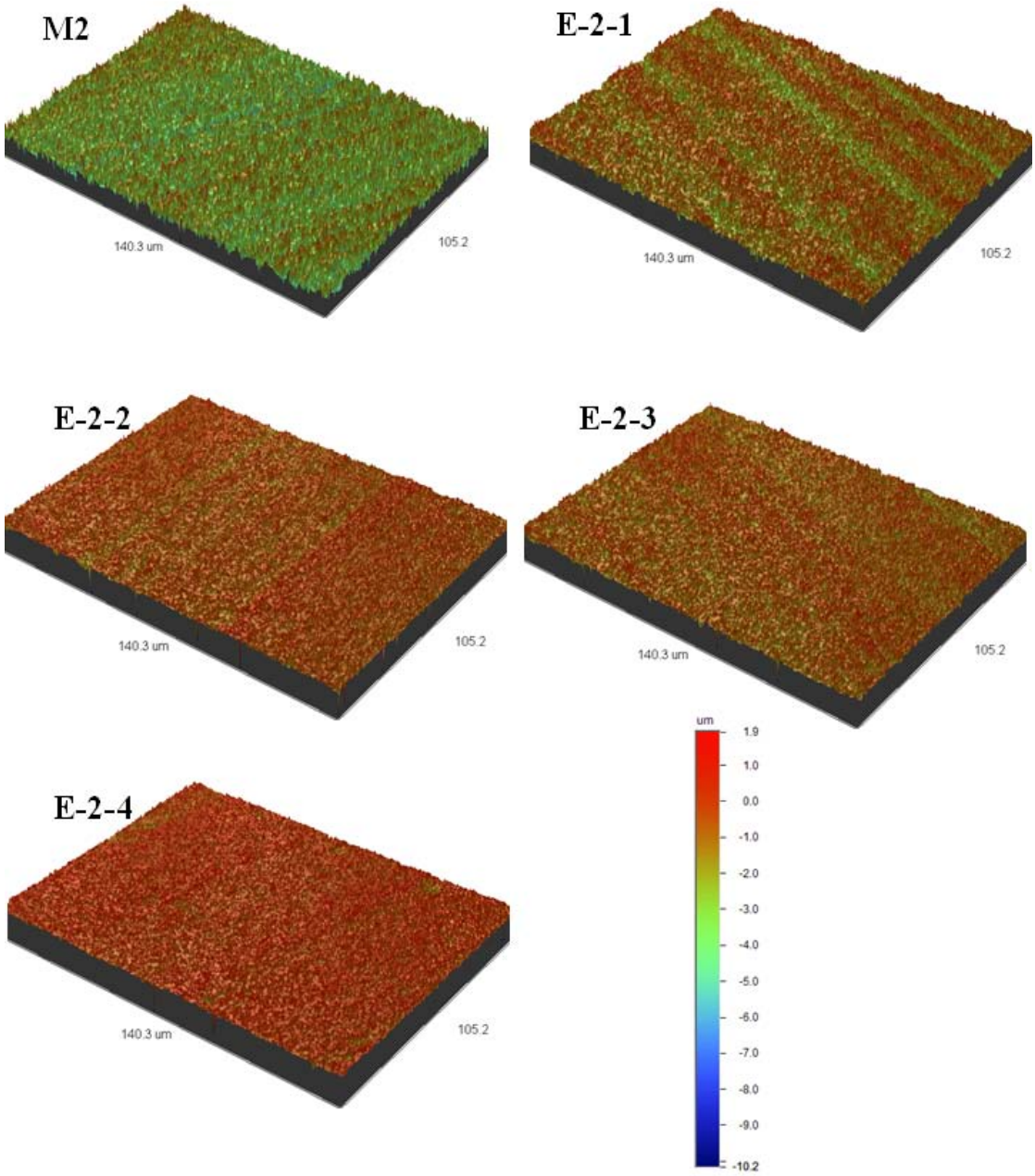

Figure 4.12. Surface textures corresponding to pretreatments E-2-1, E-2-2, E-2-3, and E-2-4, and compared with their initial surface corresponding to the method M2. The Z scale bar for all tests is included

www.manaraa.com

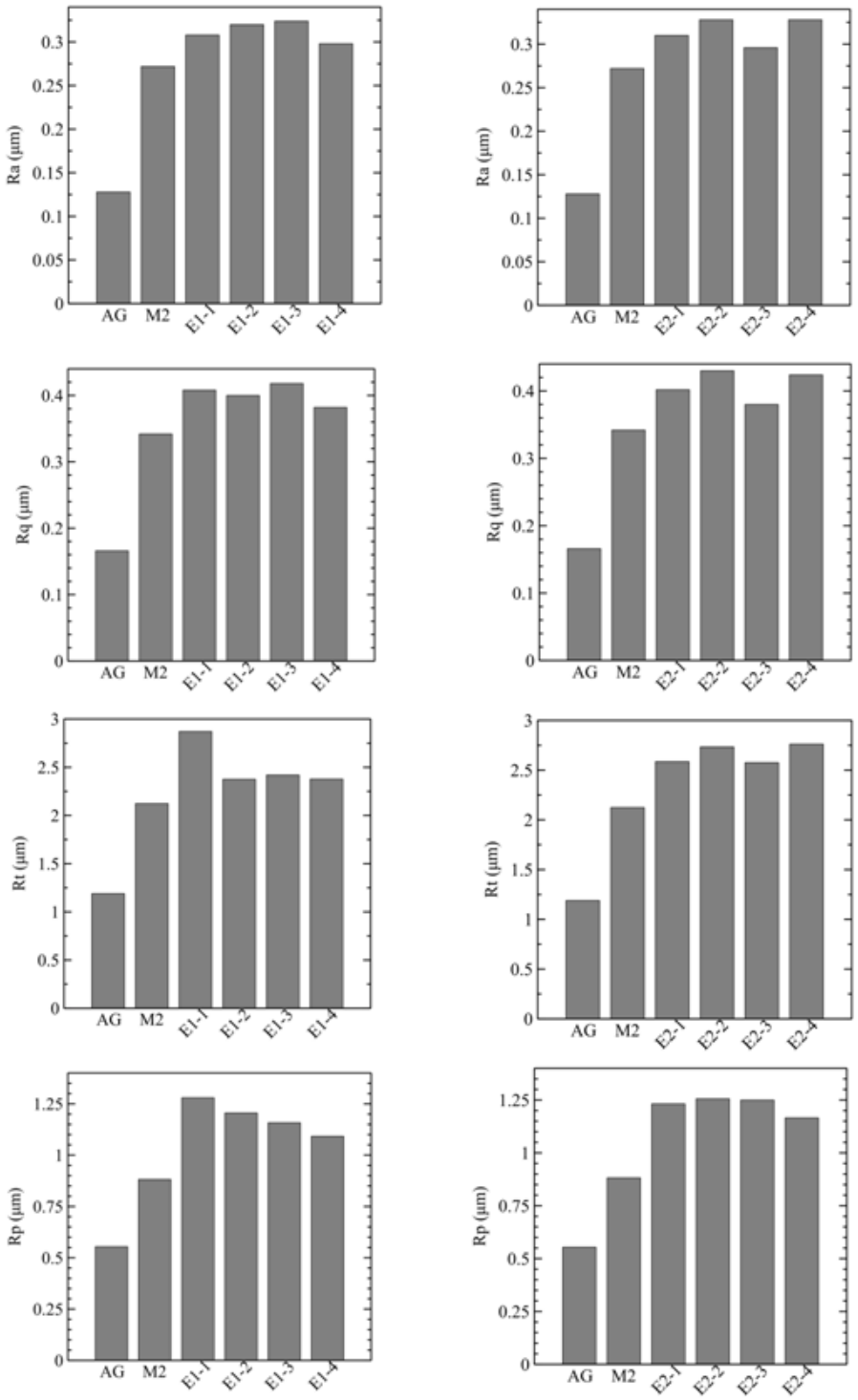

Figure 4.13. Average roughness characteristics of different variations in methods E-1 and E-2 by the arithmetical mean deviation (R_a), root-mean-square (rms) roughness (R_q), maximum peak-to-valley height (R_t), and highest peak (R_p), texture roughness parameters

www.manaraa.com

It can be seen from Figures 4.11 and Figure 4.12 that after the initial Murakami pretreatment M2, both chemical surface pretreatments E-1 and E-2 provide an additional surface texture reconstruction to the substrate, however, the amount of reconstruction differs from the reaction time on each chemical, being more notorious after 30 seconds of etching in method E-1 and sixty seconds of etching in method E-2.

There is an additional increase in all the substrate surface roughness parameters after the Murakami treatment for both methods during short etching immersion times and no significant change of R_a and R_q after 15 seconds of etching, as seen in Figure 4.13. Method E-1 displays a slight decrease in the roughness parameters R_t and R_p after fifteen seconds of etching; no major changes were observed in these parameters for method E-2.

The subsurface characteristics of the WC-Co turning inserts were evaluated in terms of their integrity resulting after both methods E-1 and E-2 by measuring the cobalt depletion band after methalographic preparation of the substrate modified cross sections.

Figures 4.14 (a)-(d) are SEM micrographs of the substrate cross sections after metallographic preparation and corresponding to methods E-1-2, E-1-4, E-2-2, and E-2-4, respectively. The effect of the second etching step in the cobalt binder removal is clearly depicted by the formation of the depletion band from the surface. It was found that the thickness of the band is relatively the same for both surface pretreatment methods with a value of approximately 10 μm for methods E-1-2 and E-2-2 in Figures 4.14(a) and 4.14(c), respectively, and a value of approximately 14μm for methods E-1-4 and E-2-4 in Figures 4.14(b) and 4.14(d), respectively. These values demonstrated that the cobalt depletion band corresponding to a period of 120 seconds is not double the value

www.manaraa.com

corresponding to sixty seconds; however, it was found a lesser amount of cobalt binder remaining over the WC grains in method E-2-4 than in method E-1-4 when compared to Figures 4.14(d) with Figure 4.14(b), respectively. This can be visualized in detail at the interface between the cobalt depletion zone and the original cemented carbide structure as depicted in Figure 4.15(a) and 4.15(b) corresponding to methods E-1-4 and E-2-4, respectively.

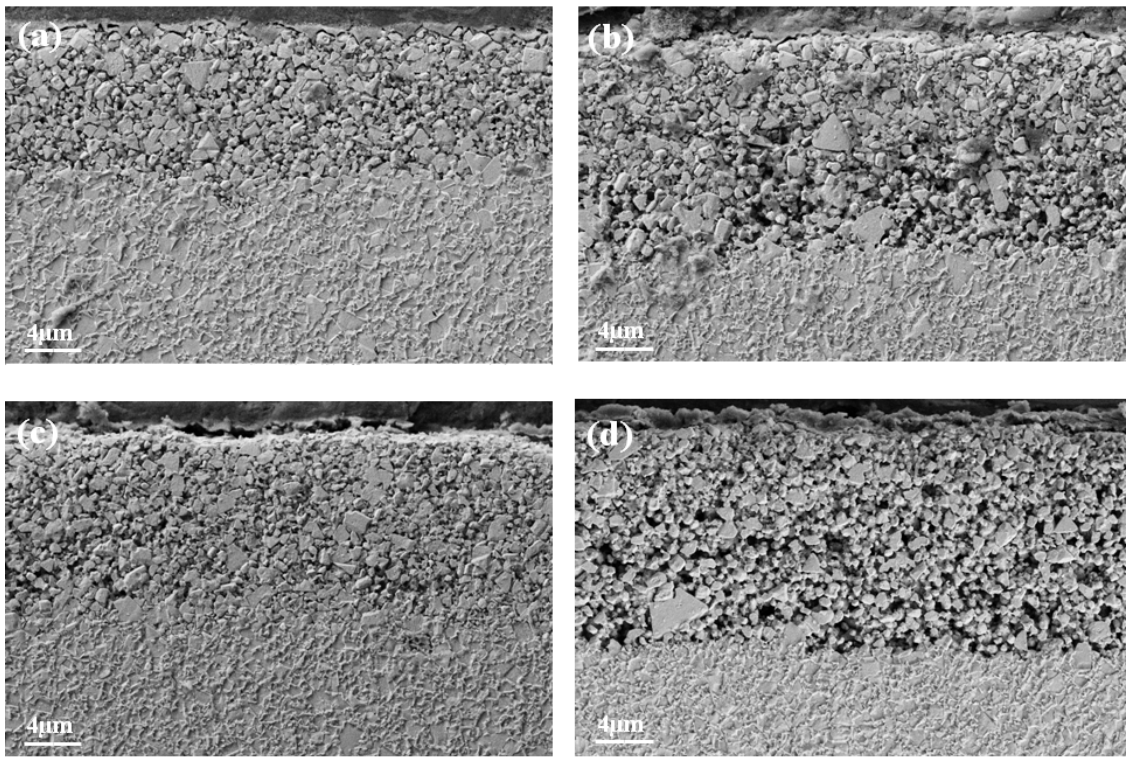

Figure 4.14. SEM micrographs corresponding to the subsurface integrity after the pretreatment methods (a) E-1-2, (b) E-1-4, (c) E-2-2, and (d) E-2-4 on the M treated sample, where the corresponding thickness of the cobalt depletion band can be distinguished

www.manaraa.com

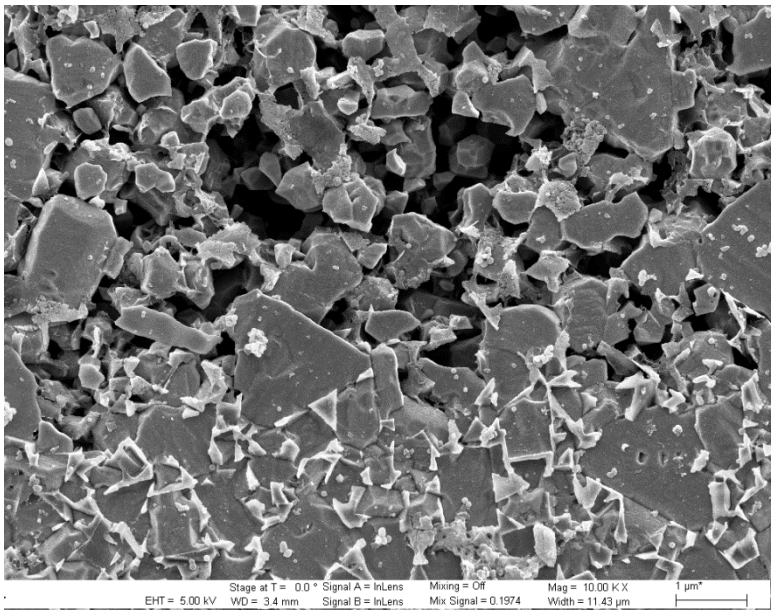

(a)

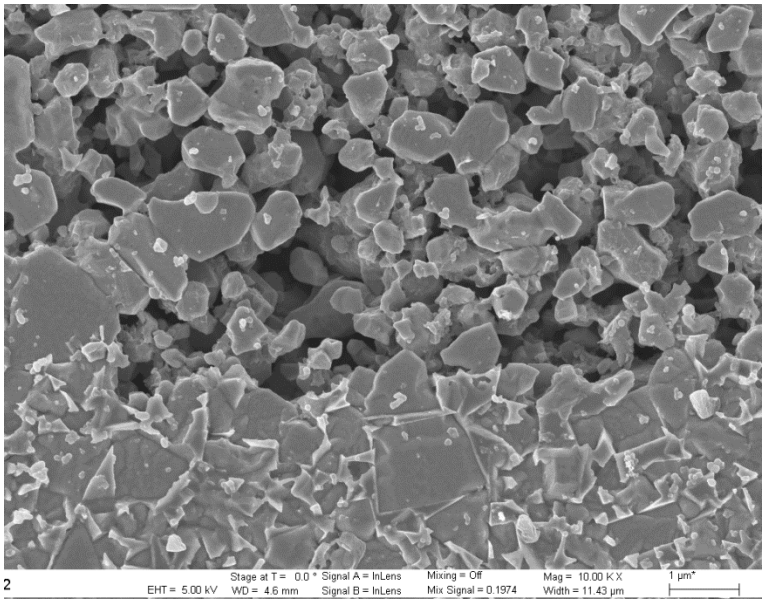

(b)

Figure 4.15. SEM micrographs corresponding to the subsurface integrity after the pretreatment methods (a) E-1-4 and (b) E-2-4 on the as-ground WC-Co samples, depicting the interface between the cobalt depletion band and the non etched cemented carbide structure

www.manaraa.com

A detailed analysis of the surfaces resulting from SEM images of methods E-1 and E-2 at different etching immersion times revealed no differences for the same method and different etching times and small superficial differences between methods E-1 and E-2 as shown in Figure 4.16. A less uniform surface texture at a smaller area and a higher amount of pits at the surface is noted for method E-2. The latter aggresses with the observations at the subsurface damage characterized by a larger amount of voids in between the WC grains.

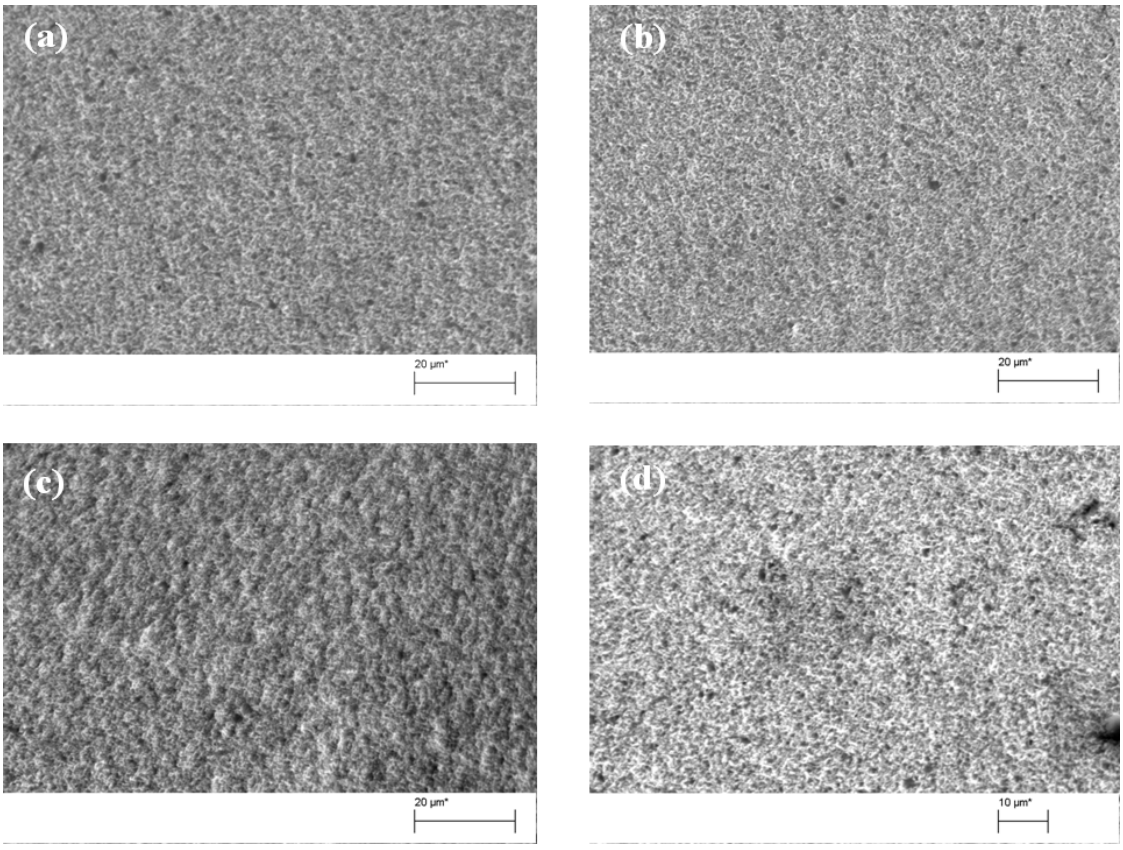

Figure 4.16. SEM micrographs corresponding to the surface morphology after the pretreatment methods (a) E-1-2, (b) E-1-4, (c) E-2-2, and (d) E-2-4 on the M treated sample, where a small difference in surface roughness can be distinguished between both pretreatment methods

www.manaraa.com

4.4.4. The Interface Between the CrN/Cr Interlayer and the WC-Co Substrate

The predeposition of the CrN/Cr interlayer prior the CVD diamond synthesis creates an additional interface with the substrate material, which is related to the surface condition of the substrate. In this research, the PVD-CrN/Cr was deposited on the WC-Co turning inserts without any additional surface pretreatment corresponding to the characteristics of the sample AG.

A cross section of a sample I-AG, according to Table 4.1, was prepared for metallographic analysis using the same conditions than the chemical etched cross sections. Figures 14.17(a) and 14.17(b) show the resulting characteristics of the interface between the CrN/Cr interlayer and the as-ground WC-Co turning insert. Figure 4.17(a) depicts the interface between the interlayer and the carbide surface, where a non complete contact between the bottom CrN layer and the substrate is observed. The CrN layer sits on the top of the substrate surface irregularities, producing a conformal coating to these, as shown in the texture map corresponding to the sample surface I-AG in Figure 4.1. Additionally, it was found that the thickness of the interlayer is not uniform, ranging from 2 – 3 μm in total.

A detailed morphology of the interface between the CrN layer and the WC-Co substrate is shown in Figure 4.17(b), depicting the WC grains and the Co binder at the substrate, and the non contact regions between the interlayer and the as-ground surface.

www.manaraa.com

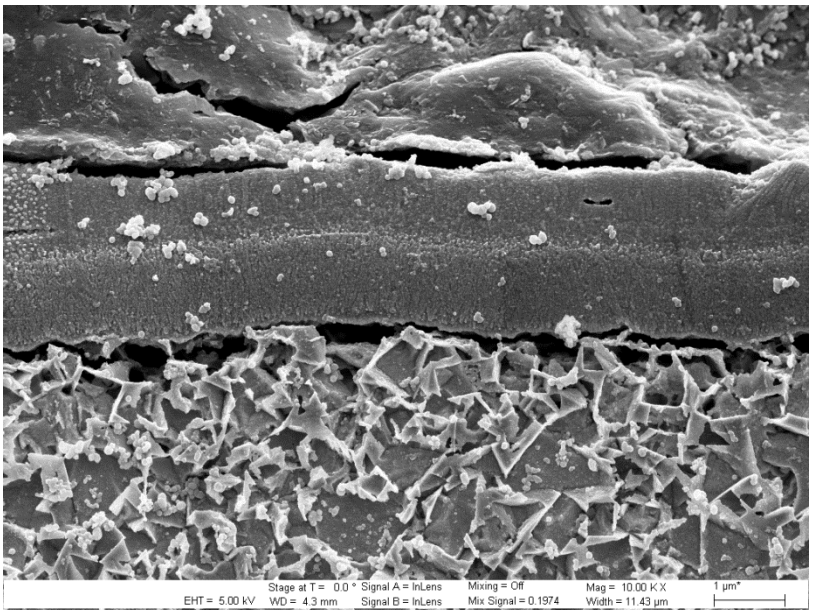

(a)

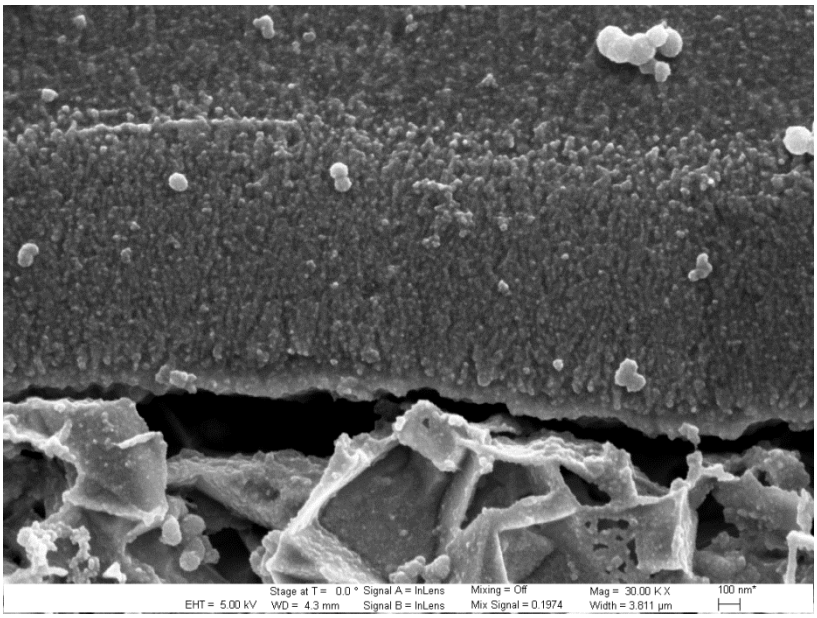

(b)

Figure 4.17. SEM micrographs corresponding to the subsurface integrity after the deposition of the CrN/Cr interlayer on the WC-Co as-ground samples

www.manaraa.com

CHAPTER 5. DIAMOND DEPOSITION AND CHARACTERIZATION OF PRETREATED WC-CO SUBSTRATES

5.1. Introduction

In this chapter, diamond coatings were deposited on the pretreated surfaces from the methods listed previously in Table 4.1 and Table 4.2. It is expected that the differences in the surface texture features obtained from the surface pretreatment methods provide different structural and morphology characteristics to the deposited diamond coatings. These differences will certainly have an impact on the fundamental adhesion of the coating and the resulting machining performance during the dry machining operations.

The results presented in this chapter will evaluate the properties of the diamond films deposited on the pretreated WC-Co turning inserts in terms of the adhesion of the coating and lately will provide an estimation of the resulting machining performance of the coated tools, discussed in Chapter 6. Additionally, the effects produced by the surface and subsurface integrity present at different variations of chemical pretreatment methods will be evaluated as well.

One of the big uncertainties is related in the use of Rockwell indentations as an adhesion evaluation technique in diamond coatings ranging from 25 to 30 μm, and if the failure mechanism can be extended to the wear failure mechanism experienced by CVD

www.manaraa.com

diamond coated cutting tools under dry machining conditions. There are several studies including contradictory results in terms of the most appropriate method to determine the diamond adhesion properties when deposited on cemented carbide tools. This research will provide a new insight in determining a practical correlation between a classical indentation technique method and the wear failure under dry machining conditions for a particular manufacturing chain featured by high silicon aluminum alloy workpiece materials.

Besides traditional scratch test and indentation methods [102-104], diamond adhesion has been evaluated by other laboratory methods that promote the coating wear by:

- A pin-on-disc tribometer friction device composed with a WC pin coated by a diamond layer acting against a XC30 steel disc [105]
- An erosion wear test carried out by using a high velocity air-sand flow (340 ms-1) at an impact angle of 90° for the impingement of diamond coatings deposited in a WC substrate [106]
- Loading a projected diamond coating on the edge of WC-Co substrates as the result of a grinding a lapping process on the insert that produces a diamond film projection on the edge due to the differences in hardness between the coating and the substrate [107]
- A cavitation erosion equipment produced by modifying an ultrasonic device according to ASTM G32-92 composed by a high frequency

www.manaraa.com

sonotrode that cause a cavitation bubble field on the top of the coating in evaluation [108-110]

- A sand abrasion wear device composed by a rotating rubber wheel, which is fed with a constant flow of sand particles that are introduced in between the wheel and the surface of the sample in order to abrade the sample diamond coating when a force is applied to the sample holder against the wheel [111]

In this research, we have used a combination of Rockwell indentations and Raman spectroscopy to evaluate the adhesion and stress field of the diamond coatings deposited on the pretreated substrates. Rockwell indentations are useful in determining the diamond adhesion by evaluating the effects of the interface between the coating and the substrate. The large loads produced by the indenter will be enough to promote the growth of both interfacial and cohesive crack in the substrate/coating system that can be associated with the surface/subsurface integrity present in the substrate.

The determination of a critical load is also possible when doing successive loads at different levels that can be correlated with the delamination characteristics of the coating. However, Rockwell indentation is not a test that can be applied for repetitive quality control measurements due to the degradation of the diamond indenter tip after a number of tests and the possibility of a substrate rupture if the test is conducted near the cutting edge of the tool [109].

Raman spectroscopy can be useful in determining the structural characteristics of thin diamond coatings deposited on surface modified substrates when techniques such as

www.manaraa.com

the radius of curvature method in conjunction with the Stoney equation [112] and x-ray diffraction grazing angle [113], are not possible to use due to the difficulties in obtaining reliable values from thick diamond coatings deposited on geometrically complex substrates. Furthermore, the scratch test method is limited by the geometry of the scratching indenter in relation to the diamond coating thickness, which is more appropriate to use in thin diamond films.

5.2. Experimental Conditions

Commercial diamond films were synthesized by a sp^3 M650 Hot Filament CVD system using hydrogen and methane as gas precursors at a pressure of ~ 40 Torr, a substrate temperature of ~ 850°C, and forming a continuous microcrystalline diamond film of approximately 25μm deposited on the pretreated turning inserts. The diamond surface characteristics were measured by white-light interferometer and SEM analysis.

X-ray diffraction (XRD) patterns were recorded before and after the diamond deposition by a Bruker-AXS D8 Discover diffractometer operated at 40 kV and 40 mA. Data were collected at 2θ between 25° - 85°, using an integration time of 7 seconds per step and a step size 2θ of 0.01°.

Raman spectroscopy of diamond coated-pretreated tools was performed using a Renishaw 1000 Raman spectrometer with an Argon laser at a wavelength of 514.5 nm, and a laser spot size of 1 μm at a power of 25 mW.

www.manaraa.com

Rockwell C indentations were conducted by a Wilson/Rockwell Hardness Tester (Series 500) to evaluate the diamond coating adhesion at different load levels. Resulting diamond delaminations from the center of the indentation zone were measured in all samples by using a Keyence VHX-500 digital microscope and fracture patterns were analyzed by SEM.

Film compositions in the indentation zone were determined by electron probe microanalysis (EPMA) with a Cameca Instruments Model SX100 Electron Probe. Electron beam conditions were typically 15 kV and 40 nA during the analysis.

5.3. The Diamond Coated Surfaces after the Initial Surface Pretreatments

Diamond has been deposited on the different surface modified substrates after the initial surface pretreatments according to Table 4.1 with a coating thickness of approximately 25 μm. It was observed that diamond coatings on the samples corresponding to method I-2 delaminated from the substrate right after the deposition. No after-growth diamond delamination was observed for samples E-1, E-2, and I-1, and their surface characteristics in SEM micrographs are depicted in Figure 5.1. Diamond surface corresponding to pretreatment method E-1 shows a continuous diamond film with well defined polyedrical crystal facets due to the <100>{111} texture surface, grains of ~ 2 – 4 μm in size with many distributed small diamond crystallites, and averaged roughness parameters R_a of 0.50μm measured by optical interferometry. The surface characteristics of the diamond coatings on substrates from method E-2 reveal a smaller

www.manaraa.com

diamond grain size ~ 1 – 2 μm, sub-micron facetted crystals, and an increase of non-diamond carbon phases, with resulting roughness parameter R_a of 0.38 μm.

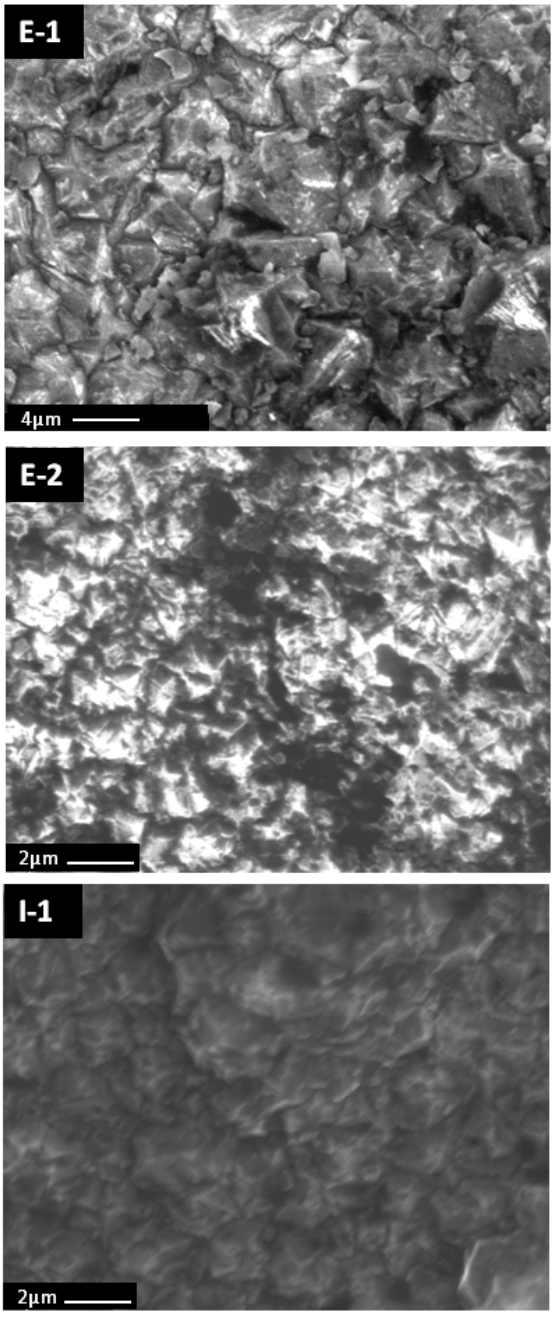

Figure 5.1. Morphology (SEM) of HFCVD grown diamond coatings deposited on surfaces pretreated samples corresponding to methods E-1, E-2, and I-1

www.manaraa.com

Diamond coatings on samples I-1 consist of a combination of small crystal facets in ball-like agglomerated deposits, a crystal size of ~ 1 μm, and roughness parameter value R_a of 0.31 μm.

A comparison between the surface morphology and roughness parameters of coated samples from methods E-1, E-2 and I-1 confirms that the final roughness and morphology of the diamond coating are correlated to the initial roughness and characteristics of the substrate. The higher R_z value (aerial surface data corresponding to the average absolute value of the five highest peaks and the five lowest valleys) obtained in coated samples E-2 and I-1 with respect to sample E-1, confirms that diamond coatings deposited in pretreated surfaces under methods E-2 and I-1contain partial surface features related to the original feed marks of the as-ground (AG) sample, and also visible in the interferometry results of diamond coated surface texture maps.

Figure 5.2 shows the XRD patterns of as-ground WC-Co (6%) samples (AG) prior to diamond deposition, diamond coated sample after method E-1, diamond coated sample after method E-2, PVD CrN/Cr coated sample (I-AG), and diamond coated sample after method I-1.

These XRD patterns present the significant peak contribution of the WC (hexagonal) {101} reflection with a characteristic high intensity peak at 2θ – 48.2° which overlaps with the α-cobalt (hexagonal) peak normally present at ~ 2θ – 47.0°, ({101} reflection as well) due to the scattering efficiency of W compared to that of cobalt for a 6% composition [31]. However, Co peaks corresponding to the {111} and {101} reflections can be distinguished at 2θ – 44.4° and 2θ – 76.9°, respectively.

www.manaraa.com

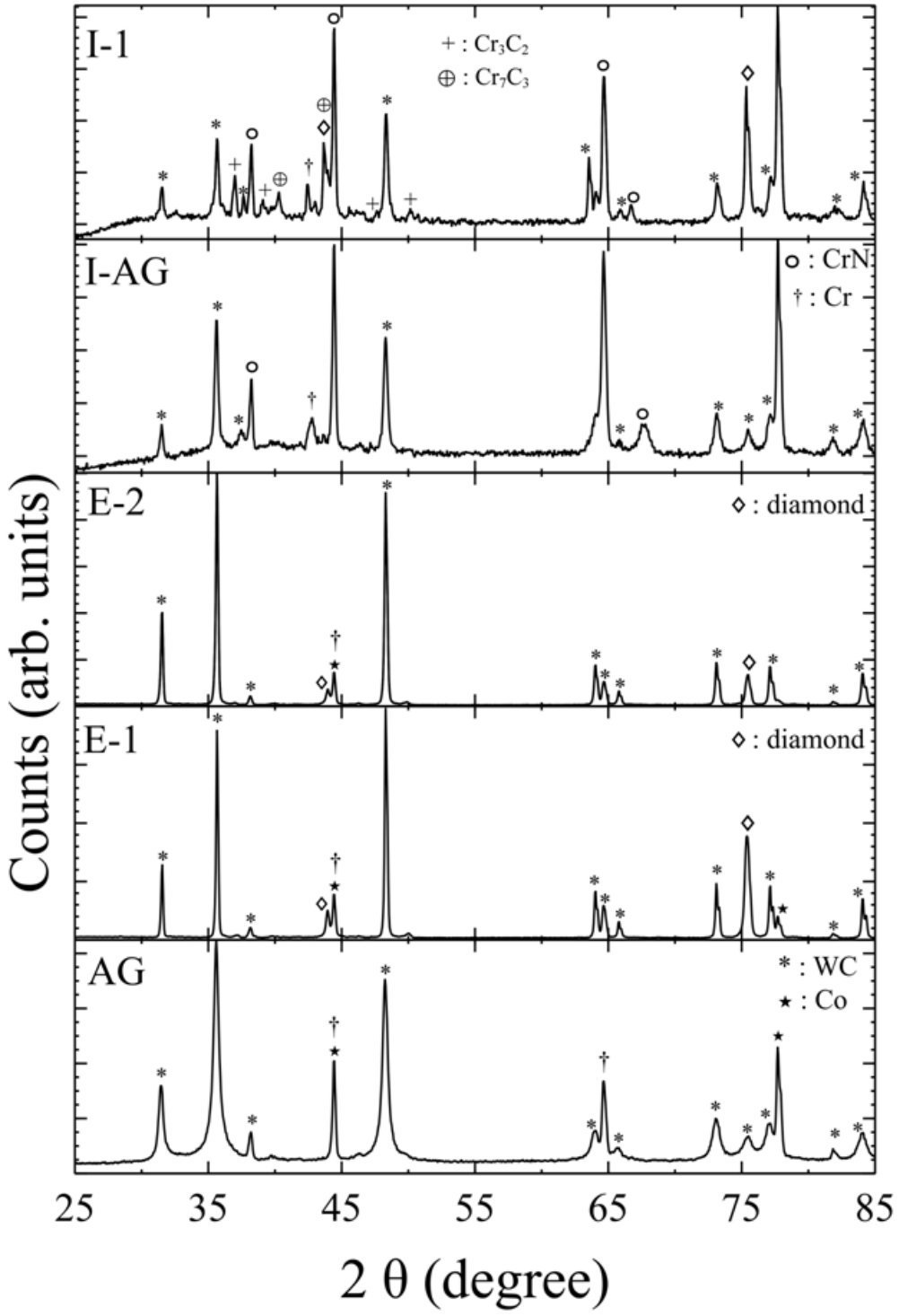

Figure 5.2. XRD patterns of as-ground WC-Co (6%) samples (AG) prior to diamond deposition, diamond coated sample after method E-1, diamond coated sample after method E-2, PVD CrN/Cr coated sample (I-AG), and diamond coated sample after method I-1

www.manaraa.com

After the deposition on samples E-1 and E-2, a diamond peak corresponding to a {111} reflection is present at 2θ – 43.85° and the {220} diamond crystallization is present at 2θ – 75.35°, which might overlap with the WC peak at 2θ – 75.2° distinguished in sample AG. The XRD spectrum of sample I-AG shows broad peaks attributable to chromium nitride at 2θ – 38.2°, 44.4°, 64.65°, 77.65°, and 2θ – 42.65° corresponding to the chromium. Diamond coated samples after pretreatment method I-1 show XRD patterns with additional peaks representing Cr_3C_2 and Cr_7C_3, suggesting that intermediate chromium carbide compounds are formed during the diamond deposition.

Raman spectra of diamond films deposited onto the three aforementioned pretreated samples are shown in Figure 5.3. The Raman spectrum of MCD samples E-1, E-2, and I-1 show sharp diamond peaks centered at 1335.1, 1336.6, and 1333.5 cm^{-1}, respectively, and shifted of about 2.7 cm^{-1}, 4.2 cm^{-1}, and 1.1 cm^{-1} with respect to natural diamond (1332.4 cm^{-1} at atmospheric pressure and 25°C), which correspond to biaxial residual compressive stresses of 2.91, 4.53, and 1.19 GPa, respectively [114]. Thermal stresses are expected to be the same due to the uniform diamond deposition temperature by the use of a substrate heater and a constant relative position of the samples with respect to the filaments during the HFCVD deposition batch; hence the residual stresses present in the samples may be solely attributed to the intrinsic stresses induced during the growth phase, which are correlated to the final morphology of the diamond coating as shown in the SEM micrographs in Figure 5.1. Furthermore, the stress relief effect of the CrN/Cr interlayer can be observed from the biaxial compressive stress values.

www.manaraa.com

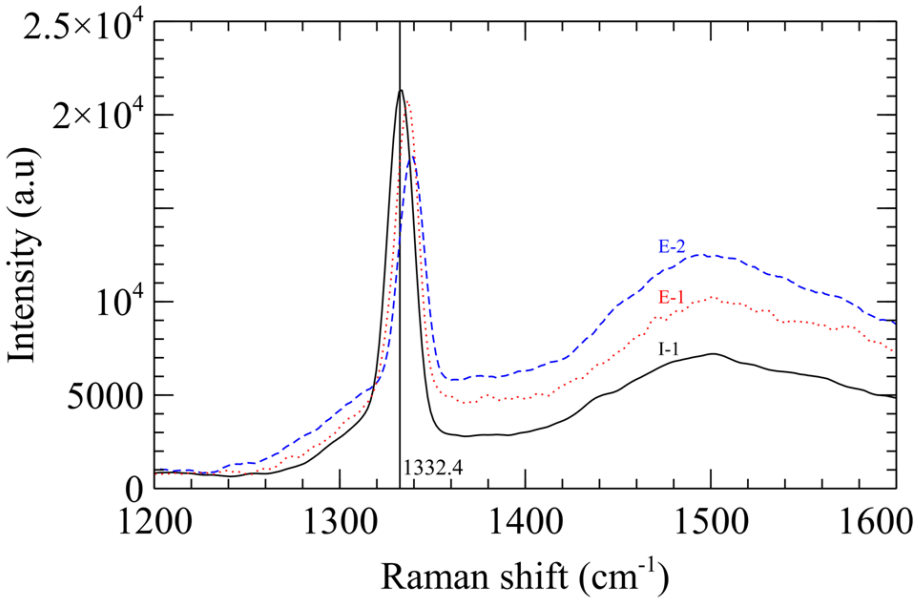

Figure 5.3. The Raman spectrum of samples E-1, E-2, and I-1 after diamond deposition

Diamond coating adhesions were evaluated in terms of the lateral crack lengths resulting from discrete indentations levels at 45, 60, 100, and 150 Kg. Three indentations were performed at each level to ensure a delamination in the films, and ten crack length measurements per indentation were recorded for the analysis. When the indentation force is sufficiently high, lateral cracks are initiated and propagate between the coatings and the substrate. Figure 5.4 shows the average lateral crack lengths versus the indentation load for diamond coated samples after pretreatment methods E-1, E-2, and I-1. It can be seen that crack lengths are higher for sample E-1; however no diamond delamination and no white marks surrounding the indentation spots were observed at load levels of 45 and 60 Kg.

www.manaraa.com

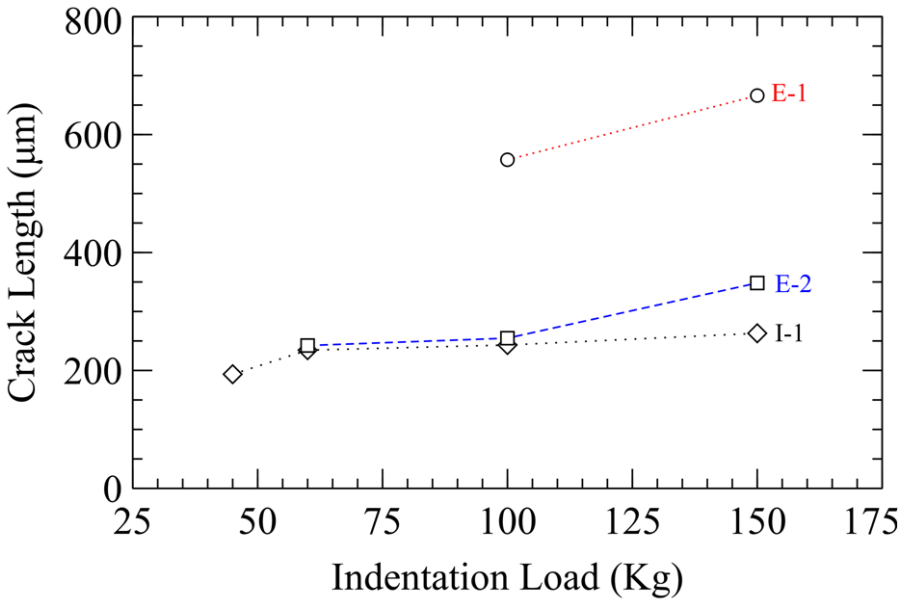

Figure 5.4. The lateral crack lengths present in diamond coated samples E-1, E-2, and I-1, resulting from discrete indentations levels at 45, 60, 100, and 150 Kg

Likewise, no delamination was observed for sample E-2 at 45 Kg. In contrast, delamination was observed at all indentation load levels for sample I-1, which displays similar crack length values with respect to sample E-2 at 60 and 100 Kg. The relative error (with respect to the average) is different for all samples at each discrete indentation force, i.e ~10% for sample E-1 at 150 Kg, 7% for sample E-2 at 60 Kg, and 15% for sample I-1 at 45 Kg. Moreover, no fracture or delamination was observed at some indentation loads for all samples when white circular marks appear at the diamond surface, which suggest that the coating was still not adherent, and the crack energy was not sufficient enough to promote a complete delamination; so care must be taken at the moment of measuring the delamination crack lengths in order to consider the previous aspects. Under these circumstances, resulting from different surface pretreatments effects,

www.manaraa.com

it may not be appropriate to make a numerical comparison of the interfacial toughness of the diamond coatings based upon the slope obtained from the plots in Figure 5.4, which is considered proportional to 1/Gc, where Gc is the critical strain energy release rate for crack propagation. Figure 5.5 shows the backscattering SEM micrographs (left column) of samples E-1, E-2, and I-1, depicting the white spallation area of the diamond coatings and the lateral cracks when an indentation load of 100 Kg was applied to all samples. The spallation area was analyzed by EPMA, and W and C Ka x-ray mappings which are shown in Figure 5.5 for samples E-1 and E-2, whereas Cr and C maps are depicted for sample I-1 at the center and right columns, respectively.

Diamond coating features can be distinguished from the C maps, where ball-like agglomerates are present in sample I-1, feed marks in sample E-2, and a uniform diamond surface in sample E-1. It can also be observed that the diamond delamination for samples E-1 and E-2 occurred from the Co free WC substrate whereas the diamond delamination for sample I-1 occurred at the diamond/interlayer, which suggest that the adhesion of the interlayer and the substrate is stronger than the adhesion of the interlayer and the diamond coating during the indentation. The semi-quantitative composition analysis on the peeled surface in sample I-1displays 77 wt% of Cr with less than 1% of W and Co. This suggests that the flaking of the diamond coating may have occurred mainly at the diamond/CrN interface. Some exposed WC-Co areas after delamination are observed in sample I-1 (blue area) surrounding the indentation where the level of stress is higher.

www.manaraa.com

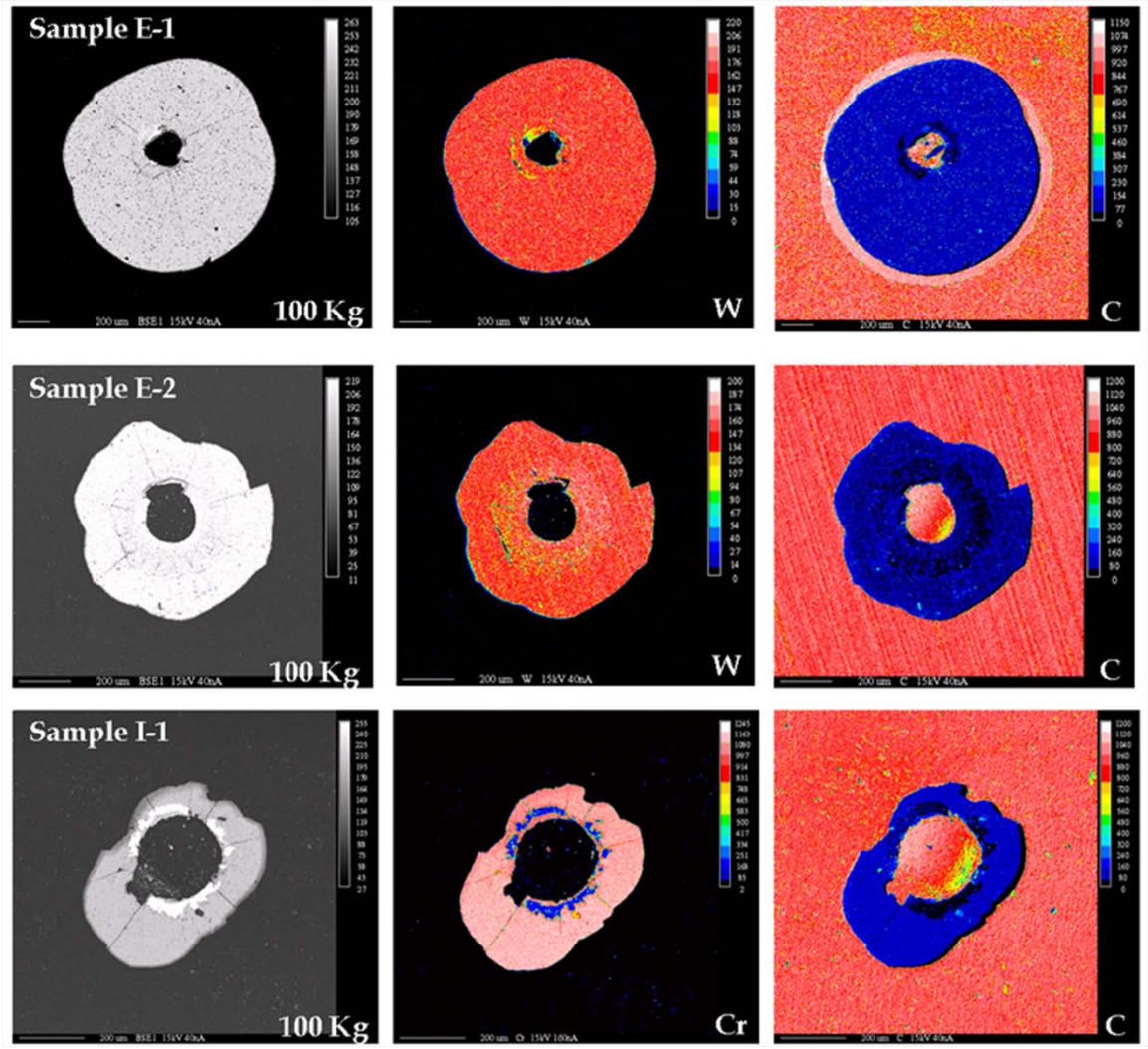

Figure 5.5. Backscattering SEM micrographs (left column) and W, Cr, and C Ka x-ray mappings (center and right columns) for samples E-1, E-2, and I-1

www.manaraa.com

5.4. The Diamond Coated Surfaces after the Modified Surface Pretreatments

Diamond coatings with a coating thickness of approximately 30 µm have been deposited on the different surface modified substrates after the initial surface pretreatments E-1-1, E-1-2, E-1-3, E-1-4, E-2-1, E-2-2, E-2-3, and E-2-4 according to Table 4.2.

The surface roughness values R_a and R_q after the diamond deposition from all samples are summarized in Table 5.1. These values correspond to aerial roughness values measured in a surface area of 140 x 105 µm, and averaged from four different interferometry measurements at each sample surface. The aerial values were used for comparison due to a predominant homogeneous surface present at the top of the diamond coatings differing from the preferential features observed in some surface textures of the pretreated surfaces after the diamond deposition.

Table 5.1. Average roughness parameters R_a and R_q for diamond coated samples on surface pretreated methods E-1 and E-2 with respect to the chemical etching time

Roughness Parameter	**Method E-1**				**Method E-2**			
	E-1-1	**E-1-2**	**E-1-3**	**E-1-4**	**E-2-1**	**E-2-2**	**E-2-3**	**E-2-4**
R_a (µm)	0.61	0.63	0.64	0.63	0.44	0.46	0.46	0.47
R_q (µm)	0.78	0.80	0.83	0.82	0.58	0.62	0.60	0.61

It can be seen in Table 5.1 that there is no significant statistical difference in the roughness parameter values with respect to the etching time for one single method.

www.manaraa.com

However, Method E-1 produces a rougher diamond surface than method E-2, with an approximately a 200 nm increase in both R_a and R_q values. This difference between method E-1 and E-2 can be seen in the texture maps in Figure 5.6 may be attributed to a higher diamond nucleation density in method E-2 as the result of a rougher pretreated surface at the submicron scale due to a higher amount of pits at the surface, as discussed in Chapter 4. At this point, method E-2 produces a smoother diamond surface than method E-1, but with the presence of higher preferential texture features at the interface for short etching immersion periods.

A new set of adhesion evaluation tests were conducted in the diamond coatings deposited on the modified surface pretreatment methods by successive indentations at the same previous loads but differing in the way of quantifying the diamond peeling failure. In this latter case, attention was focused mostly in characterizing the delamination mechanism for each load in terms of the crack morphology and propagation.

www.manaraa.com

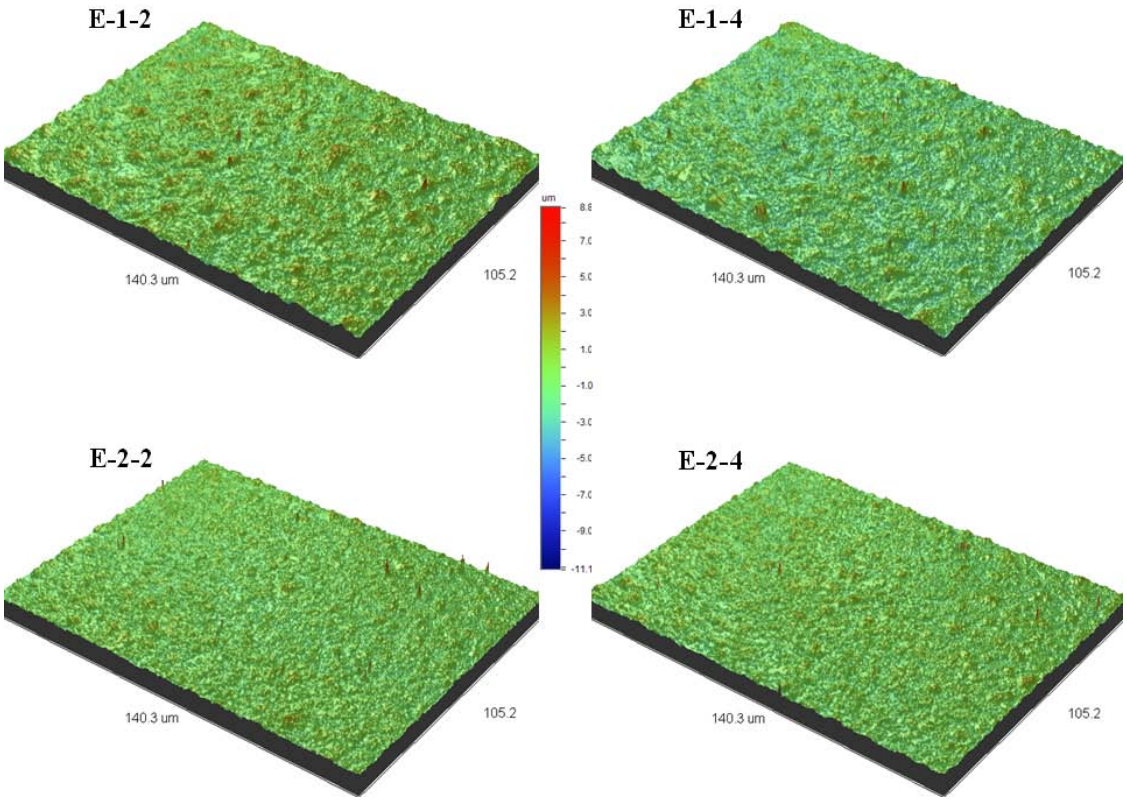

Figure 5.6. Surface texture maps corresponding to the diamond coated samples after surface pretreatments E-1-2, E-1-4, E-2-2, and E-2-4, where a characteristic surface is appreciated for each method with no dependence in the surface pretreatment etching time

The diamond crystal structures corresponding to the surfaces depicted in Figure 5.6 are characterized by SEM and shown in Figure 5.7. These images revealed no significant differences in the diamond crystal grain sizes for a pretreated surface with one particular method and minor differences in between both pretreatments as shown in Table 5.1 and Figure 5.6.

www.manaraa.com

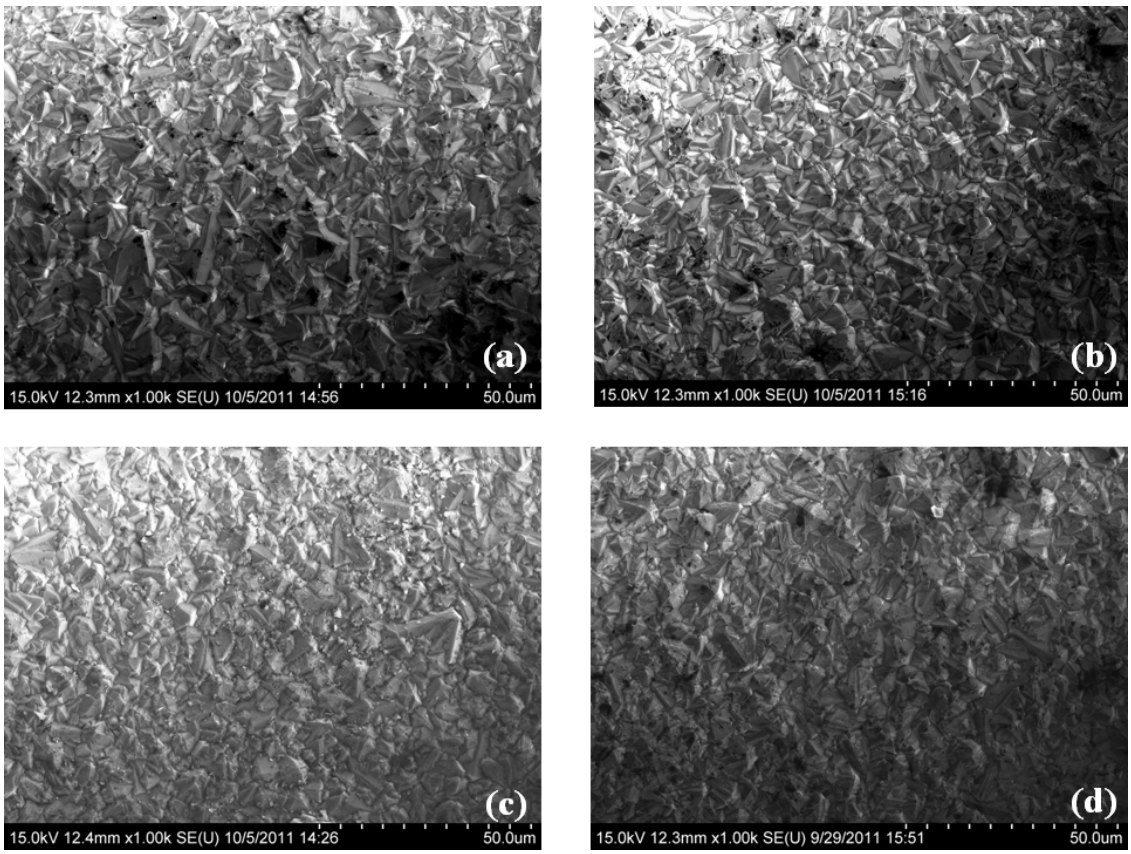

Figure 5.7. SEM micrographs corresponding to the diamond surface morphology of the coated samples (a) E-1-2, (b) E-1-4, (c) E-2-2, and (d) E-2-4, where a small difference in the diamond crystal grain size can be appreciated between both pretreatment methods

Adhesion evaluations were conducted on the diamond coatings deposited on all the surfaces resulting from the modified pretreatments. The first characteristic observed in the delamination mechanism of the diamond coatings after successive indentations was the progression of the diamond delamination from the substrate with respect to the indentation load, as shown in Figure 5.8(a) and Figure 5.8(b), corresponding to EPMA images of an oxygen distribution at the coated surface of sample E-2-3 after indentation loads of 45Kg and 100 Kg, respectively.

www.manaraa.com

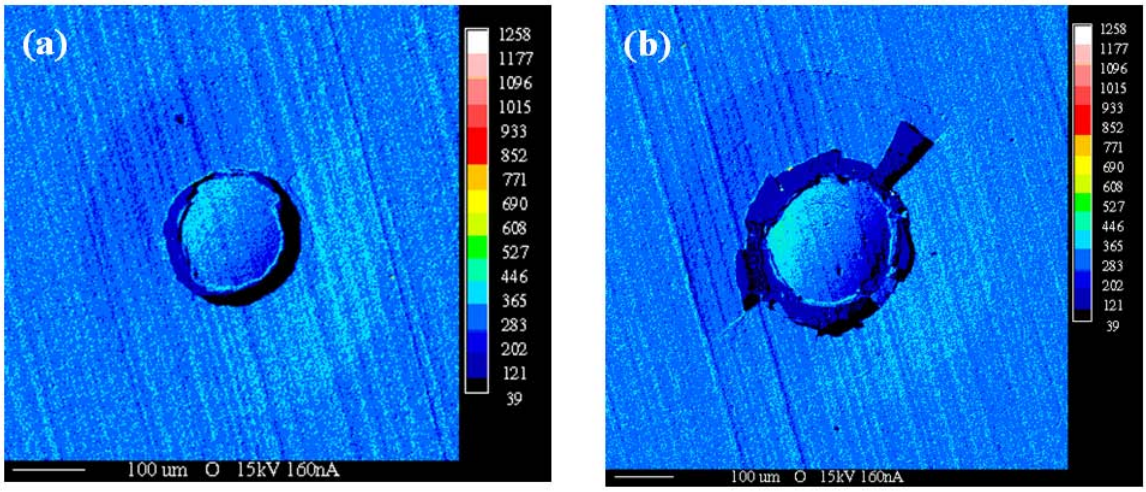

Figure 5.8. EPMA image from an oxygen map at the coated surface of sample E-2-3 after a Rockwell indentation with a force of (a) 45Kg and (b) 100 Kg

During lower indentation loads, the coating deformed with the substrate and a formation of circular marks developed concentrically to the Rockwell indentation imprint. This deformation was characterized by a contrasted area under the microscope, suggesting a lifting of the coating without peeling under a resolved tensile stress cause by a bending of the diamond coating [70,115] as shown in Figure 5.8(a), and produced by lateral cracks extending at the interface [116]. The small peeling area observed in Figure 5.8(a) is due to the higher tensile strain around the indenter geometry [117].

The concave shape of the lifted coating is an indication of the compressive nature of the initial biaxial residual stress present in the coating [118]. As the load increases, diamond will start to delaminate from the bent coatings when lateral cracks continue to propagate in a radial direction at the interface, now with a higher energy sufficient to peel the initial lifted and bent coating as shown, in Figure 5.8(b).

www.manaraa.com

A complete reconstruction of the crack propagations and diamond coating delaminations after successive Rockwell indentations at 45kKg, 60Kg, 100, and 150 Kg, is shown in Figure 5.9(a)-(d) on a diamond coated surface corresponding to sample E-2-3. This sample was chosen for this analysis due to the development of a progressive delamination mechanism visible on the SEM. The same mechanism was observed in the other coated surfaces but with different load progression dependence as an indication of different adhesion behaviors. This is expected due to the differences in the coating/substrate interfacial characteristics.

Figure 5.9(a) corresponds to the image of an indentation in the diamond coating at 45Kg. Radial cracks are present at the diamond coating surface with origins at the peeling ring around the indentation imprint. Small concentric cracks (arrow), also known as Hertzian ring cracks, start to form as the diamond coating starts to bend in a reference zone named 1. As the load increases to 60 Kg in Figure 5.9(b), the maximum concentric crack distance (MCCD) is more visible at approximately 260 μm colliding with the end of the radial cracks. Now the energy present in the lateral cracks peel the initial bent areas in zone 1 and bend a new coating area referenced as zone 2. Similarly in Figure 5.9(c) for a load of 100Kg, the zone 2 starts to peel (arrow) as confirmed by its MCCD value at approximately 258 μm. Additionally, a new bent coating is visible by the formation of a new maximum concentric crack located at a MCCD value of approximately 308 μm, defining a new area referenced as zone 3. After an indentation load of 150 Kg is applied, shown in Figure 5.9(d), the energy of the lateral cracks completely peeled zones 1, 2, and 3; the radial crack continues to propagate (arrow) at the end of zone 3 at a maximum peeled extension distance (MPED) of approximately 305 μm. No concentric cracks were

www.manaraa.com

found in the diamond coating. For this higher load, a substrate cohesive failure is observed and characterized by the apparition of lateral cracks on its surface, which is referenced as zone CF visible as a different contrast in the SEM image.

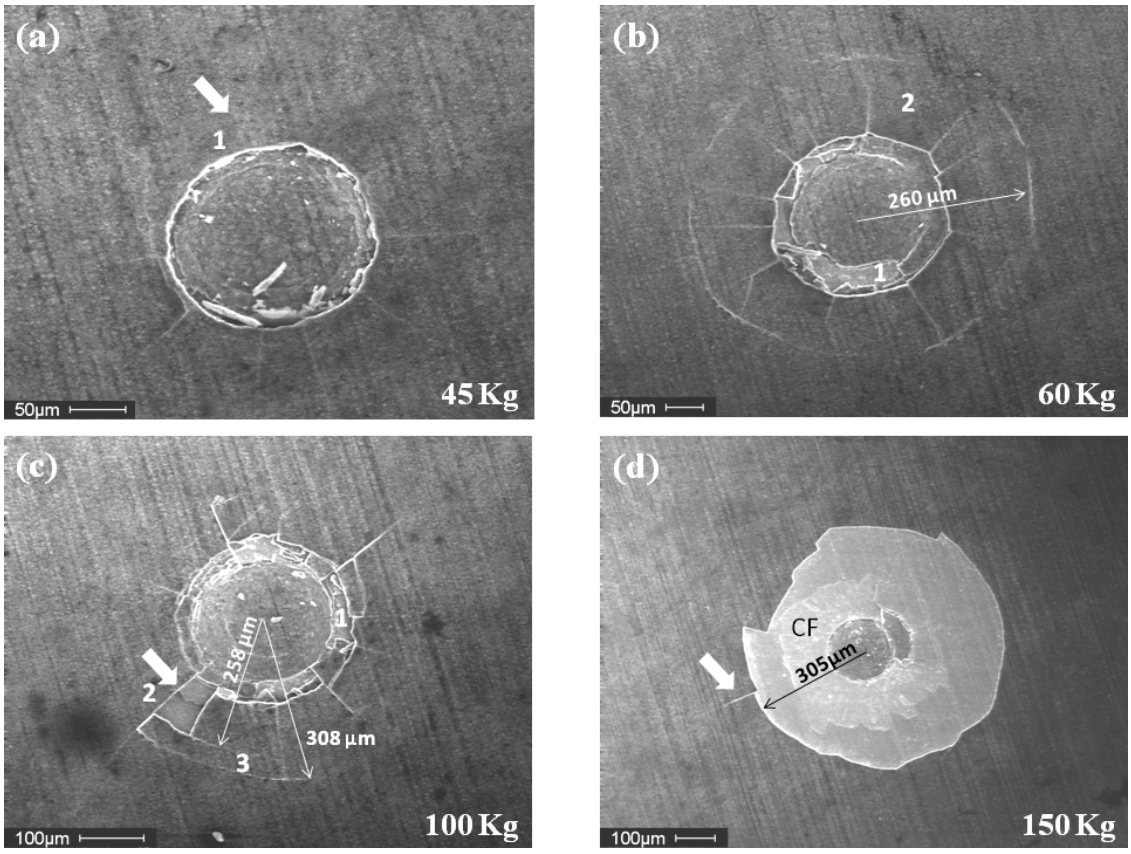

Figure 5.9. SEM micrographs corresponding to indentations in the diamond coated surface of sample E-2-3, depicting the failure of the coating for successive loads of (a) 45Kg, (b) 60Kg, (c) 100 Kg, and (d) 150 Kg

Details corresponding to the crack propagation mechanisms are depicted in Figure 5.10(a)-(d). The origin of the radial cracks from the outer ring around the indentation imprint is shown in Figure 5.10(a), including the formation of the initial concentric

www.manaraa.com

cracks. The crack energy is sufficient to promote an initial peeling of the coating around the imprint, exposing the substrate and pushing the peeled coating under the one which is lifted. Figure 5.10(b) shows the correspondence in direction between the lateral cracks developed at the interface and the radial cracks present at the lifted diamond coating. This initial delamination is characterized by the peeling area exposed from the origin of the radial cracks to the formation of the concentric crack, which develops the zone 1 discussed in Figure 5.9(a).

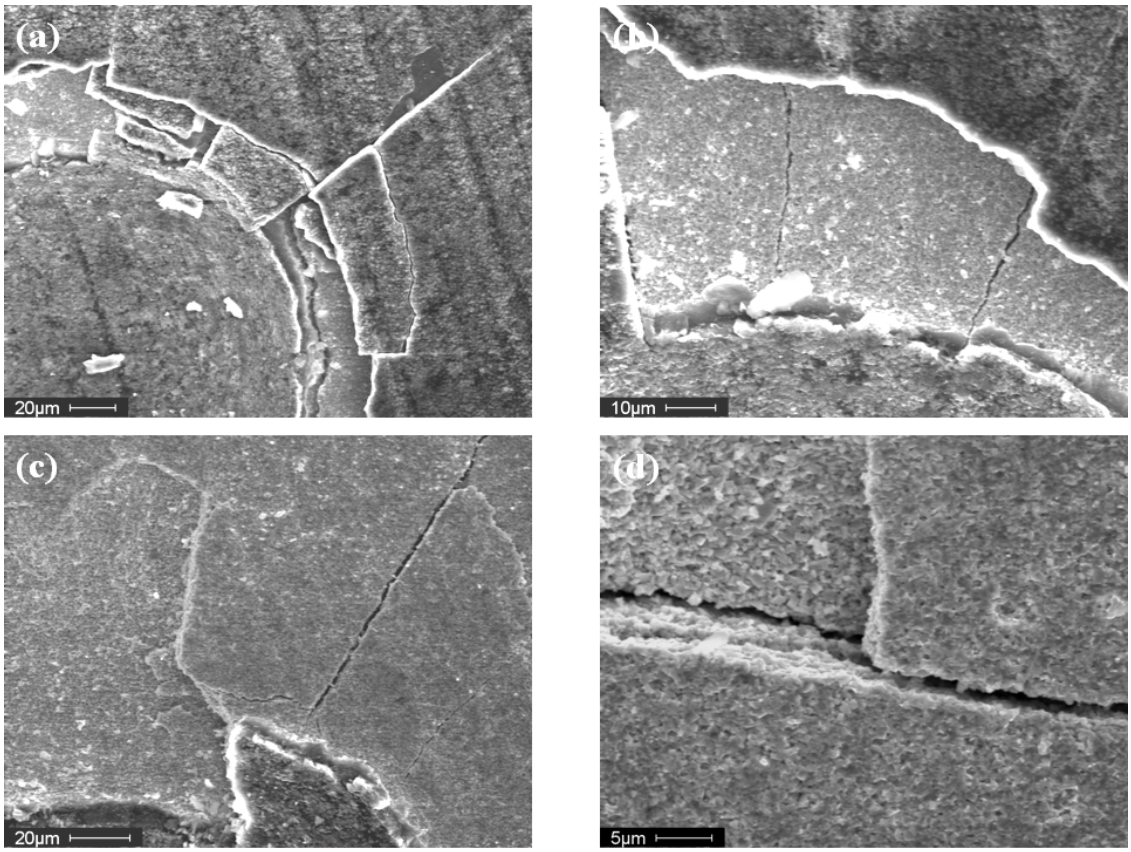

Figure 5.10. SEM micrographs corresponding to crack propagation mechanisms depicted in Figure 5.9 (a)-(d) for indentation loads of (a) 45 Kg, (b) 60 Kg, and (c)-(d) 150 Kg

www.manaraa.com

The cohesive failure of the substrate produced at an indentation load of 150 Kg is depicted in Figure 5.10(c). The presence of lateral cracks and the development of concentric cracks at the substrate exposed a new subsurface area, which is an indication that the force is sufficient to promote a cohesive failure of the top WC surface and the lateral crack runs at the interface between the original substrate and the Co depletion layer. These can be seen in detail in Figure 5.10(d), which depicts a lateral crack produced at the subsurface interface of the substrate causing its cohesive failure.

The same crack propagation mechanism was observed for the diamond coatings deposited on the CrN/Cr interlayer with differences in terms of the delamination interfaces. In this case, loads of 45Kg and 60 Kg produced a diamond delamination from the top Cr layer as shown in Figures 5.11(a) and 5.11(b) by the same abovementioned mechanisms. However, when a load of 100 Kg is applied, the crack energy is sufficient to produce a cohesive failure (CF) in the CrN/Cr interlayer, exposing the WC-Co substrate around the indentation imprint as shown in Figure 5.11(c). This cohesive failure zone is more visible at an indentation load of 150 Kg, partially shown in Figure 5.11(d), where the exposed WC-Co, CrN, and Cr surfaces are depicted. This zone is crossed by a lateral cracks and segmented by concentric cracks, which expose the WC-Co, CrN, and Cr surfaces.

www.manaraa.com

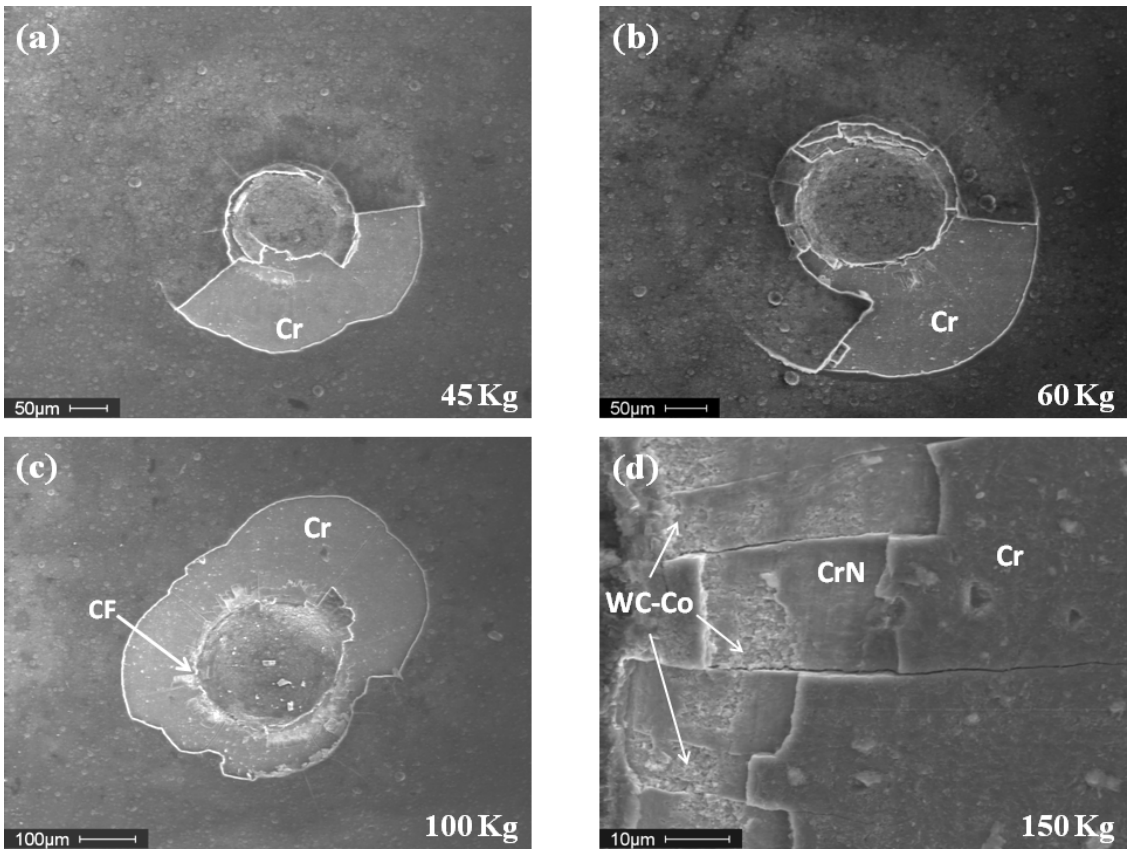

Figure 5.11. SEM micrographs corresponding to indentations in the diamond coated surface of sample I-1, depicting the failure of the coating for successive loads of (a) 45Kg, (b) 60Kg, (c) 100 Kg, and (d) 150 Kg

The delamination progression mechanisms analyzed from Figure 5.8 to Figure 5.11 confirms the statement mentioned earlier related to the fact that a direct diamond adhesion comparison between chemical etched pretreatments and interlayer approaches is not practical by indentation evaluation techniques. The lateral crack energies necessary to bend and peel the diamond coating are different in the two methods, and depend on the nucleation interface where the initial cracks originated. However, a comparison between different diamond coatings deposited on surfaces obtained by a similar cobalt suppression approach, etching or buffer interlayer, may be feasible.

www.manaraa.com

A diamond delamination analysis was done on the diamond coated modified pretreated samples after the successive Rockwell indentations with the aim to evaluate the effect of the substrate surface integrity and subsurface condition in the diamond adhesion. The maximum distance from the center of the indentation to the outermost coating concentric crack (MCCD) and to the extension of the peeled coating (MPED) was measured when present at different indentation loads. The maximum distance is used due to the non-circular morphology of the bent and peeled coating areas, as seen in previously. Table 5.2 contains the results of these measurements for samples E-1-1, E-1-4, E-2-1, E-2-4, and I-2. These results correspond to the highest MCCD and MPED values, both are present at the same time in a single indentation out of a set of four indentations per load.

It can be seen from Table 5.2 that the delamination progression mechanisms and crack lengths differ among the samples. A complete crack progression as seen in Figure 5.9(a)-(d) for sample E-1-3 was also obtained for sample E-1-4, which is characterized by a value of MCCD higher than the MPED value in all the indentation loads. This mechanism suggests that some portions of the coating still are adherent to the substrate at each individual indentation load, and a complete delamination will be achieved at a higher load. In the case of sample E-1-4, this load is higher than 150 Kg.

www.manaraa.com

Table 5.2. Maximum distance from the center of Rockwell indentation to the outermost concentric crack (MCCD) and to the final extension of the peeled area (MPED) when present on diamond coated samples at different indentation loads

E-1-1						**E-1-4**					
Load	**30Kg**	**45Kg**	**60Kg**	**100Kg**	**150Kg**	**Load**	**30Kg**	**45Kg**	**60Kg**	**100Kg**	**150Kg**
MCCD (µm)	NP	355.2	1126.7	1129.3	NP	**MCCD (µm)**	338.9	446.8	433.2	445.1	495.2
MPED (µm)	NP	NP	1146.8	1157.1	1166.2	**MPED (µm)**	316.6	272.7	288.4	283.9	353.2
E-2-1						**E-2-4**					
Load	**30Kg**	**45Kg**	**60Kg**	**100Kg**	**150Kg**	**Load**	**30Kg**	**45Kg**	**60Kg**	**100Kg**	**150Kg**
MCCD (µm)	NP	558.2	666.7	NP	NP	**MCCD (µm)**	428.7	489.4	471.9	441.8	NP
MPED (µm)	NP	303.4	516.4	684.4	719.8	**MPED (µm)**	377.7	441.0	524.1	386.5	414.7
I-2											
Load	**30Kg**	**45Kg**	**60Kg**	**100Kg**	**150Kg**						
MCCD (µm)	NP	253.1	269.0	1063.3	NP						
MPED (µm)	NP	103.7	126.0	265.8	1091.5						

MCCD: Maximum concentric crack distance

MPED: Maximum peeled extension distance

NP: No MCCD / No MPED

Diamond coating thickness:~ 30µm

A complete delamination is achieved at loads of 150 Kg in sample E-1-1 and E-2-4, and 100 Kg in E-1-1, which are all characterized by the absence of a MCCD value. The highest MPED value corresponds to sample E-1-1. The fully developed progression, which is characterized by the presence of both MCCD and MPED values in a single indentation starts at a load less than 30 Kg in sample E-1-4 and E-2-4, 60 Kg in sample

www.manaraa.com

E-1-1, 45 Kg in sample E-2-1, and 150 Kg in sample E-3. The beginning of the progression in sample I-2 is 45 Kg and a complete coating peeling area at 150 Kg.

Based on the results from Table 5.2, we defined the critical load in a delamination progression after successive Rockwell indentations as the minimum indentation load capable to produce a complete diamond coating delamination without creating an additional MCCD greater than the characteristic MPED present at that load. Furthermore, critical load value comparisons can only be conducted between coating/substrate systems with the same number of interfaces as a result of the nature of the crack developments and delamination progression discussed. In Table 5.2, the comparison can only be done between chemically etched samples E-1-1 and E-2-1, and samples E-1-4 and E-2-4, which have the same cobalt depletion layer thickness, so differences in adhesion will be solely attribute to variation in the superficial interface characteristics with the diamond coatings deposited under equal CVD deposition conditions. In interlayer cobalt suppression methods, a possible comparison could be achieved by independently modifying the interlayer thickness or material for the same number of interfaces; however, experimental results are necessary to validate this hypothesis.

A close look to the coating/substrate system failure under indentation load is presented in Figures 5.12, 5.13, and 5.14. Figure 5.12 corresponds to a SEM image of the cross section after fracture produced by a Rockwell C indentation (150 Kg) of a diamond coating surface deposited in a thickness of approximately 25 μm, over a modified cemented carbide turning insert by method E-1-3. In this figure, the deformation and stress distribution during the indentation depict the material volume displaced during the

www.manaraa.com

elastic-plastic contact [119] and the consequent elastoplastic indentation stress field [120].

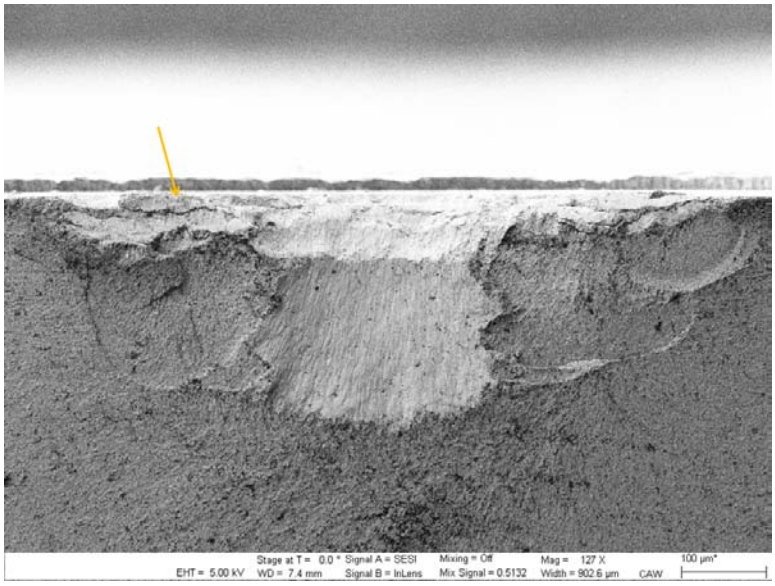

Figure 5.12. SEM micrographs corresponding to the fractured cross section of an indentation in the diamond coated surface of sample E-1-3, depicting the elastoplastic indentation strain field for a load of 150 Kg

It is evident the plastic deformation of the substrate is in a radial direction from the center of the indentation towards the bulk, and is divided into two fracture planes resulting from the two load conditions, the preload or minor load (10Kg) and the test load or major load (150Kg), during the Rockwell indentation. The formation of lateral cracks through the interface between the WC-Co original substrate and the cobalt depletion band are also present (arrow), which is responsible for the cohesive failure of the substrate discussed in Figure 5.10(c)-(d). This subsurface interfacial failure is depicted in Figure 5.13 at a zone close to the indentation imprint.

www.manaraa.com

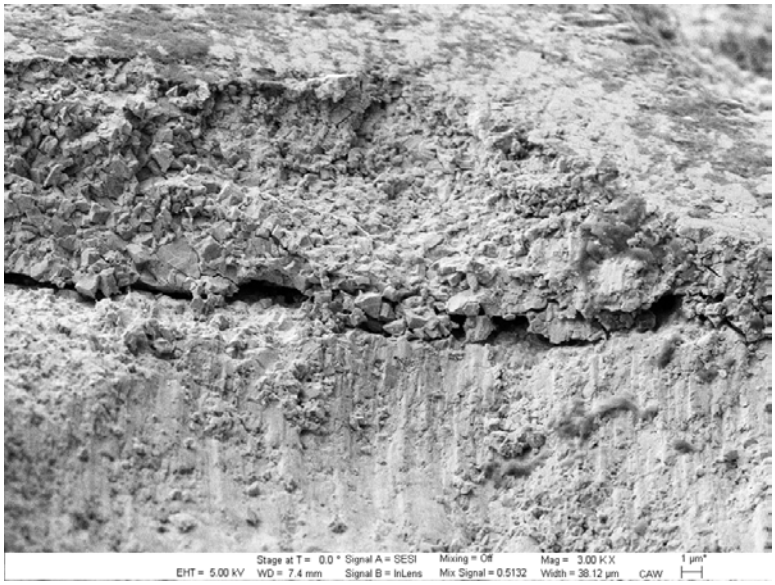

Figure 5.13. SEM micrographs corresponding to interfacial failure between the WC-Co bulk and the cobalt depletion layer during the indentation shown in Figure 5.12

The interfacial crack can be observed in between these two fracture surfaces, as a consequence of the difference in toughness between both, the WC-CO bulk and the cobalt free layer; here, the cobalt depletion layer can be distinguished by a different fracture texture when compared to the original WC-Co structured, which is characterized by the radial deformation flow discussed previously.

Figure 5.14 shows a SEM image at the end of the diamond peeled area, and corresponding to the cross section described in Figure 5.12. At this location, the interfacial failure is located between the coating and the substrate.

The fracture of the coatings is perpendicular to the substrate, which is expected due to the columnar growth direction of the diamond coating; however, a cohesive failure in the diamond coating is observed as an additional fracture surface parallel to the

www.manaraa.com

substrate. This region may correspond to the concentric cracks discussed earlier, which appear in a top view SEM image of the indentation showed in Figure 5.9(b)-(c).

This cohesive failure may be caused by the last bent portion of the peeled coating and the initial developing a new lifted zone ahead of the peeled zone continue with the delamination progression.

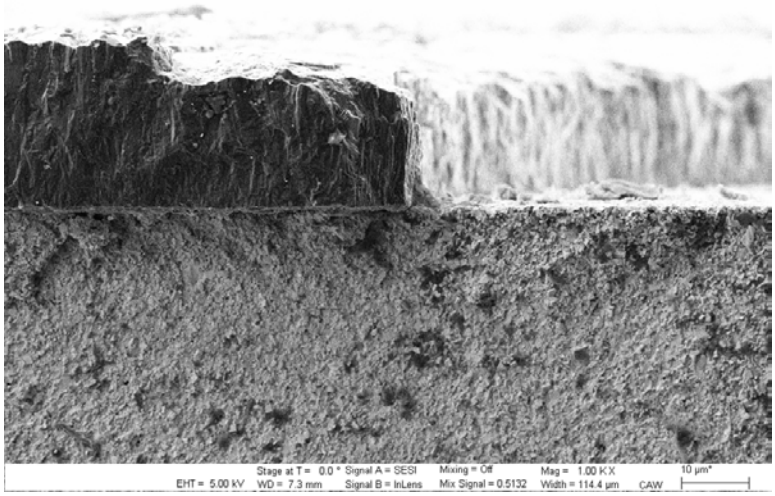

Figure 5.14. SEM micrographs corresponding to the transition between the end of the peeled diamond area and the adherent diamond coating during the indentation shown in Figure 5.12

www.manaraa.com

CHAPTER 6. MACHINING PERFORMANCE OF THE DIAMOND COATED TOOLS

6.1. Introduction

The ultimate goal of this research is to evaluate the dry machining performance of the diamond coated tool on the surface/subsurface modified WC-Co turning insert by the pretreatment methods described in Chapter 4. The results presented in this chapter will provide a direct correlation linking the effect of the surface and subsurface integrity of the pretreated WC-Co inserts, the adhesion behavior evaluated in Chapter 5, and the real machining performance of the diamond coatings in terms of wear behavior and tool life.

As summarized in Table 3.4, which is in regard to the experimental research works conducted to enhance diamond coated tools adhesion in dry machining applications during the last 10 years, there is no systematic work conducted to evaluate the effects of the tool substrate surface/subsurface characteristics on the dry machining performance, particularly, in high silicon aluminum alloy materials. The complex tool-coating-workpiece interactions developed during a dry cutting operation for a particular manufacturing chain require a real machining experimental scenario as the necessary evaluation criteria. This concludes the expected machining performance of the CVD diamond coatings.

www.manaraa.com

As mentioned in Chapter 1 and Chapter 2, high silicon aluminum alloys have a significant importance in the automobile and aerospace industries due to their high wear-resistant properties and fluidity, combined with a high strength to weight ratio [14]. In this research, a A390 aluminum alloy has been used for the machining performance tests conducted with the diamond coated tools. The workpiece material used correspond to cylinders of 110 mm in diameter and 200 mm long, and produced by initially casting A390 alloy bars with approximately 16 wt% silicon in the final cylindrical geometry. The chemical composition of the alloy is summarized in Table 6.1 measured by inductively coupled plasma mass spectrometry (ICP-MS).

Table 6.1. Chemical composition of the high-silicon aluminum alloys used for the machining performance test

Cr: 0.05%	**Cu**: 3.9%	**Fe**: 0.52%
Si: 16.3%	**Ti**: 0.06%	**Zn**: 1.1%
Mg: 0.44%	**Mn**: 0.18%	**Ni**: 0.14%

One of the big challenges in machining high-silicon aluminum alloys is the combination of a soft aluminum matrix capable to produce Al-BUE on the tool and the presence of high abrasive silicon particles and sludge. This sludge is characterized by the formation of hard intermetallic phases during the alloying process which combine with the precipitated silicon represent an aggressive abrasive condition which is detrimental to the tool life and performance.

Figure 6.1(a)-(b) shows optical images corresponding to the microstructure of the A390 alloy after metallographic preparation. Figure 6.1(a) depicts a 40x magnification of the general microstructure of the alloy. The presence of pores and voids in the workpiece material can be visualized in the micrograph. Figure 6.1(b) is an 80x micrograph where

www.manaraa.com

the typical microstructure of the alloy containing the coarse sludge intermetallic compounds. Figure 6.1(c) is a 160x micrograph depicting the distribution and morphology of the sludge in the soft aluminum matrix and the eutectic silicon. Figure 6.1(d) shows a micrograph at 400x detailing the eutectic silicon phase with some embedded Al_2O_3 particles.

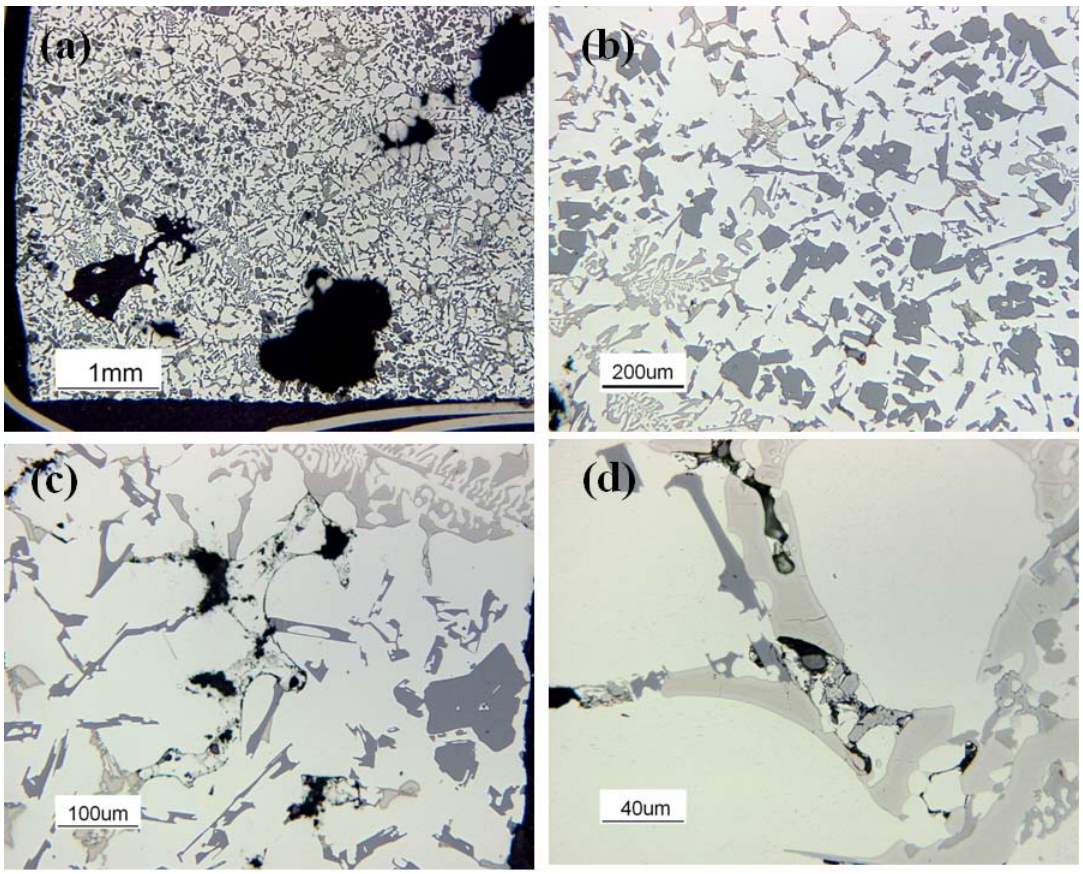

Figure 6.1. (a)-(d). Optical micrograph corresponding to the microstructure of the A390 high silicon aluminum alloy workpiece material used for the machining performance tests

www.manaraa.com

6.2. Experimental Conditions

Dry machining experiments were performed using a computer numerical control (CNC) lathe Hardinge Cobra 42 equipped with a Kistler dynamometer (9257B) to monitor the cutting forces during the machining at 500 scans/second, and a Kistler 8152B piezotron acoustic emission sensor to collect AE-RAW (raw data) and AE-RMS (root-mean-square) values at a 500 kHz sampling rate during the machining operation.

Figure 6.2 shows the dry machining performance test setup. Machining parameters were kept constant at a cutting speed of 10 m/sec, feed of 0.8 mm/rev, and a depth of cut of 1 mm. During the machining test, diamond coated inserts were periodically inspected to measure the flank wear-land by optical microscopy. The worn tools after testing were cleaned by 10 vol% hydrochloric acid to remove the aluminum alloy deposited in the cutting area and then examined by SEM and EPMA.

www.manaraa.com

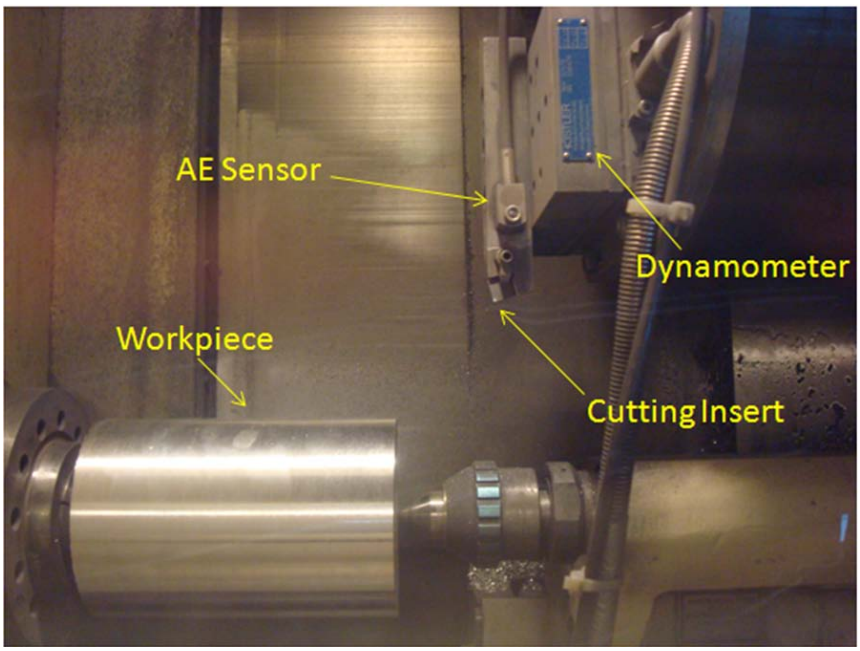

Figure 6.2. Dry machining performance setup used for the diamond coated tools experiments

6.3. The Dry Machining Performance Test after the Initial Surface Pretreatments

Figure 6.3 shows the flank wear-land width (VB) time evolution of diamond coated turning inserts pretreated under methods E-1, E-2, and I-1, and previous results of commercial MCD, PCD, and nano-diamond coated inserts [79]. The results indicated that samples I-1 showed an abrupt increase of wear-land in short period of times corresponding to 0.49 mm in 26 sec, which indicates that coating delamination occurred abruptly and resulted in rapid wear of the exposed interlayer/carbide substrate.

www.manaraa.com

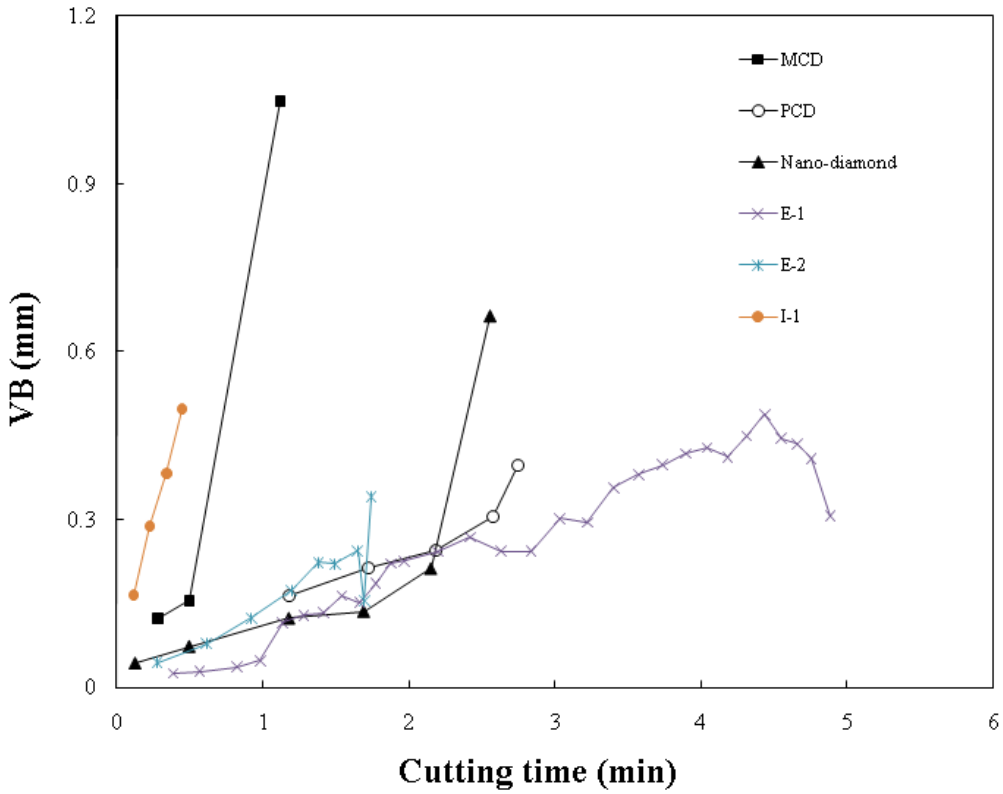

Figure 6.3. Flank wear-land (VB) time evolution of diamond coated turning inserts pretreated under methods E-1, E-2, and I-1

Perhaps the fluctuations observed in the wear-land width value (VB) shown in Figure 10 as the result of the accumulation of aluminum during the interrupted cutting operation, a better behavior was observed for samples E-1 and E-2, which failed at a lower VB levels and higher cutting times of 0.3 mm in 293 sec and 0.34 in 104 sec, respectively; the corresponding diamond film failure was detected as a change in the intensity of the AE-RAW signal when compared with the initial cutting pass. Thus, it is concluded that diamond coated turning inserts under the developed pretreatment method

www.manaraa.com

E-1 are more effective under the aforementioned dry machining conditions, and display a better performance compared to commercial tools.

Figure 6.4 shows SEM micrographs of the worn samples after the machining test. Coating delamination is the main failure for all samples. A gradual degradation of the diamond coating was observed for sample E-1 where flank wear-land is the major feature. Sample E-2 displays a sharp tool wear growth in contrast to sample I-1, which depicts a delamination the diamond and the interlayer coating, suggesting that the CrN/Cr interlayer detached from the substrate at early stages of the machining, which consequently exposed the carbide as the only remaining surface for cutting.

The abovementioned analysis was performed in order to get an estimate about the overall performance of the diamond coatings deposited under the main surface pretreatment approaches and compare them with the MCD, PCD, and NCD commercial tools. It was found that the adhesion of the coating can be significantly improved by the initial method E-1. However, it is still required to evaluate the failure mechanism associate with the surface and subsurface integrity for each method as proposed earlier.

www.manaraa.com

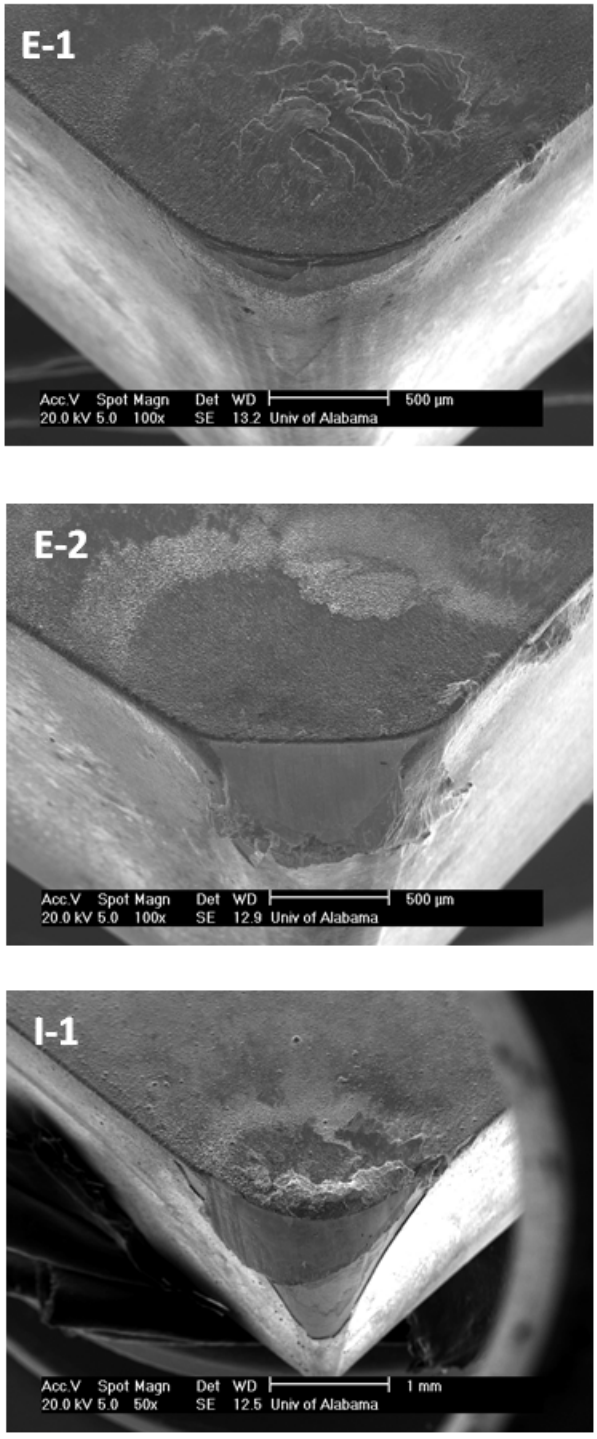

Figure 6.4. SEM micrographs of the worn samples after the machining test

www.manaraa.com

6.4. The Dry Machining Performance Test after the Modified Surface Pretreatments

Dry machining tests were conducted on the surface pretreated turning inserts described in Table 4.2 with the purpose to evaluate the effect of the etching time and the consequent surface/subsurface modifications with respect to the machining performance of diamond coated tools. Particularly, the key objective of these tests was to establish the correlation between the wear failure modes of the diamond coated tools and the surface/subsurface conditions, characterized in Chapter 4, in conjunction with the adhesion failures described in Chapter 5.

The machining tests were performed in samples E-1-1, E-1-3, and E-1-4 with the aim to evaluate the effect of the cobalt depletion layer in the mechanical and wear response of the diamond coated inserts during dry machining operations. A dry machining test was also performed in sample E-2-1 with the aim to correlate the effect of the surface and the resulting adhesion during dry machining when compared with sample E-1-1. These two samples have the same amount of subsurface damage in terms of the cobalt depletion thickness, as found in Chapter 4. Additionally, another test on sample I-1 was conducted to compare the wear behavior among all pretreatments under the same machining conditions.

Due to limitations in the amount of workpiece materials, and considering the possible outstanding performance of some diamond coated tools, a tool life criterion was established as the amount of wear when cutting until 2.5 minutes of interrupted cutting. The interrupted cutting condition was performed as a consequence of removing the tool at certain specific times during the cutting operation in order to measure the flank wear.

www.manaraa.com

Figure 6.5 summarize the tool wear progression of the different diamond coated tools until the 2.5 minutes of interrupted cutting by measuring the amount of flank wear on the tool at some points during cutting.

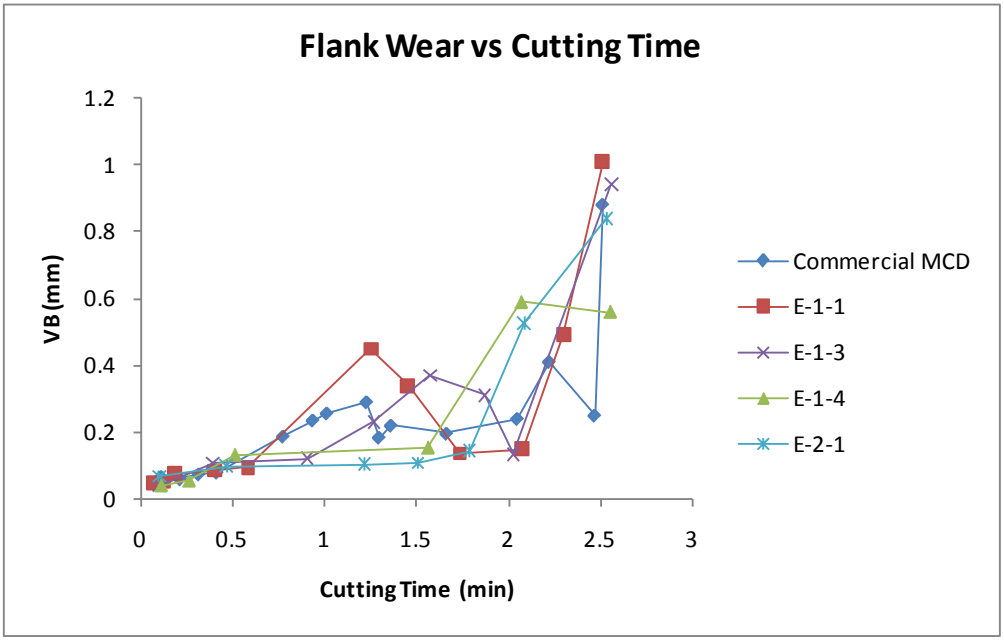

Figure 6.5. Flank wear-land (VB) time evolution of diamond coated turning inserts pretreated under methods E-1-1, E-1-3, E-1-4, and E-2-1

Sample I-1 corresponding to the CrN/Cr interlayer pretreatment method failed due to sudden delamination during the first pass displaying a VB wear value of 1.21mm occurred after 0.057 minutes of cutting. The lowest VB wearland corresponds to sample E-1-4 and the highest to sample E-1-1. However, due to the aluminum BUE observed during the dry machining, which is depicted as the fluctuations in the values of the wear land, samples were ultrasonically cleaned in an acetone solution to detach some of the

www.manaraa.com

aluminum present at the surface and obtaining a better wear land measurement at the end of the tests.

The final measurements of the VB wear land after the ultrasound cleaning cycle were 0.303 mm for the commercial MCD sample, 0.11 mm for sample E-1-1, 0.19 mm for sample E-1-3, 0.53 mm for sample E-1-4, and 0.83 mm for sample E-2-1. These results are included on the top of the images of the resulting flank surface for all tested tools shown in Figure 6.6. The values were measured at the cutting tip from the top surface of the tool to the final extension of the wear land. Measurements on the flank were difficult to perform due to the smeared aluminum on its surface.

The results from Figure 6.6 show the premature failure of sample I-1 due to a complete delamination of the diamond coating at the beginning of machining and the consequent exposure of the substrate. A microchipping failure was observed in sample E-1-1 and a gradual coating wear on samples E-1-3 and E-1-4. The extensive amount of wear measured in sample E-2-1 was associated with a flaking from the tool substrate after the final ultrasonic cleaning. A gradual wear failure mode was also observed on the commercial MCD sample. It is interesting to see how after the final ultrasound cleaning cycle, the wear land decreased for samples E-1-1, E-1-3, and MCD inserts, which suggests that the performance of sample E-1-4 is better than the rest in terms of the aluminum BUE deposited on the cutting tip.

In order to characterize the delamination mechanisms of the diamond coatings from the pretreated substrates, an additional ultrasonic cleaning cycle with a 10% HNO_3 solution was performed on all tools. A detailed analysis of the worn tool cutting edges

www.manaraa.com

after dry machining tests is shown in Figure 6.7 for samples E-1, E-2, and I-1; the results from digital microscopy images, EPMA backscattering electron (BSE) analysis, and chemical compositional maps are shown in columns from left to right, respectively.

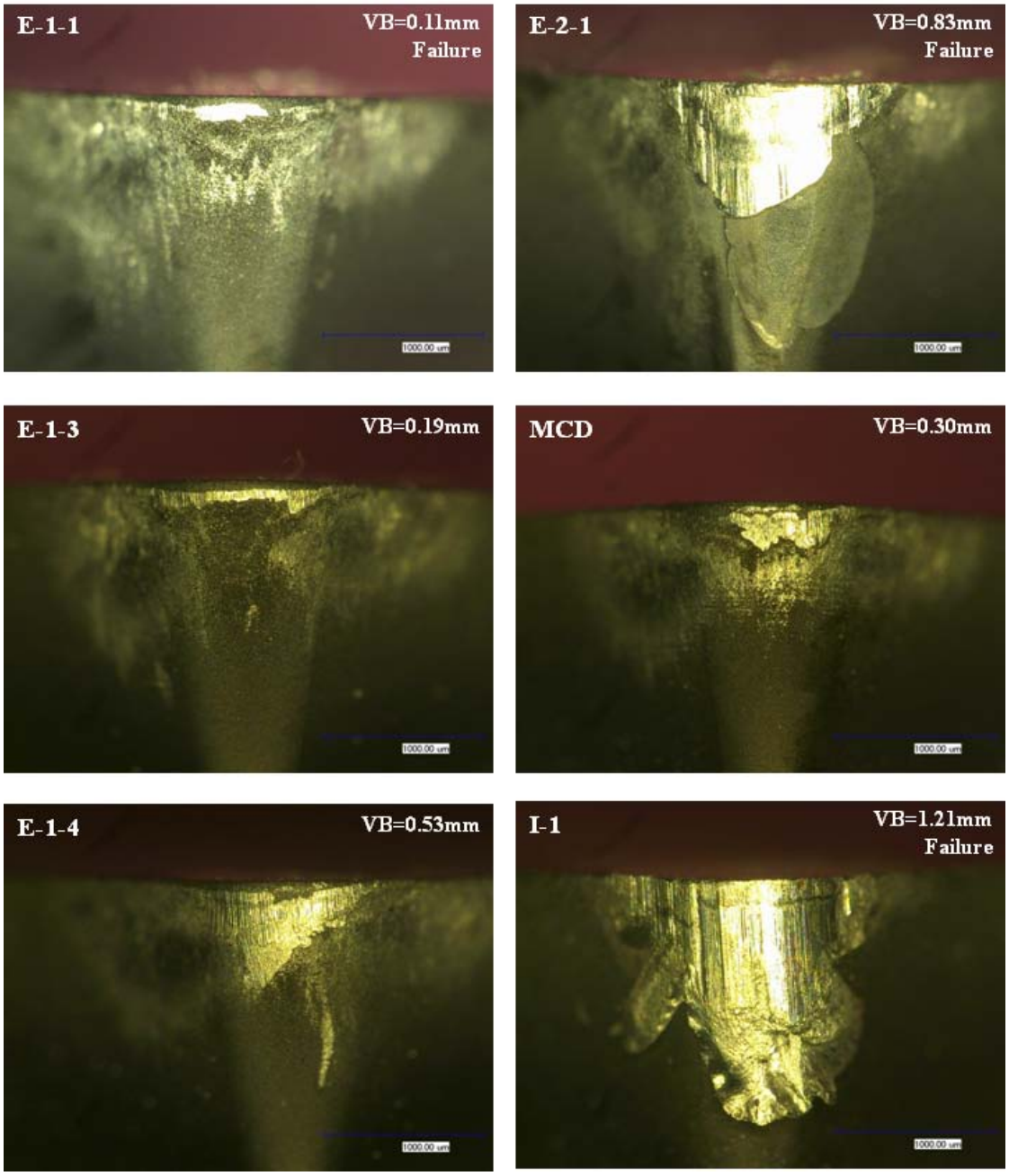

Figure 6.6. Wear morphology at the cutting tip of the pretreated diamond coated tools after 2.5 minutes of dry cutting

www.manaraa.com

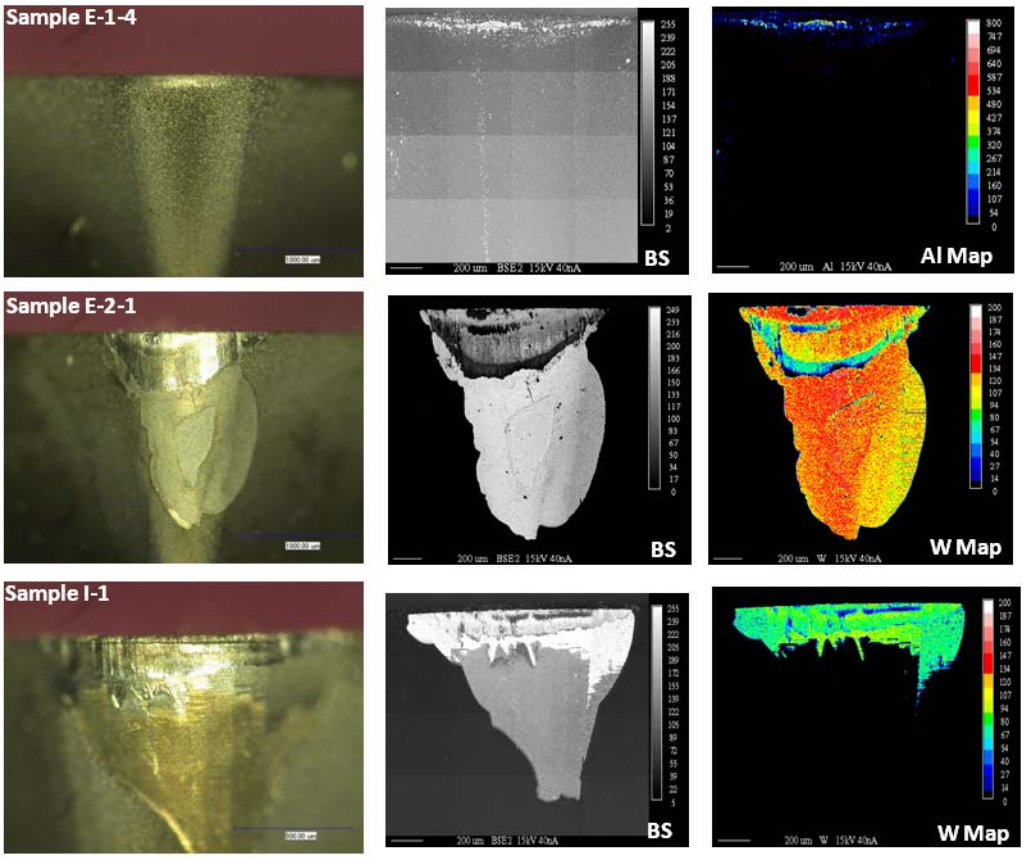

Figure 6.7. Digital microscopy images (left column), backscattering SEM micrographs and EPMA chemical composition mappings (center and right columns, respectively) corresponding to the worn cutting edges of samples E-1-4, E-2-1, and I-1

Results in Figure 6.7 evidenced that the sample E-1-4 displays a gradual wear-land formation, no diamond debonding, and some aluminum covering the wear land, typical characteristics of an adherent diamond coating. The results from the sample E-2-1 delamination patterns represent a tool failure characterized by an abrasion wear mechanism at the top of the cutting edge followed by a diamond peeling at the bottom of the flaking area. This wear pattern is associated with an early coating debonding at the top of the tool edge which promotes the subsequent abrasion of the WC substrate during

www.manaraa.com

the cutting operation, which is also confirmed by the W compositional maps. In sample I-1, the failure sequence is similar to the sample E-2-1; however, the initial diamond debonding begins at its interface with the top Cr interlayer promoting an abrasion of the latter followed by the CrN layer abrasion, and finally exposing the WC-Co substrate as confirmed by the BSE image and the W chemical map.

The failure of sample E-2-1 under dry machining conditions might be attributed to the undesirable directional surface features characterized in the texture maps shown in Chapter 4, which are perpendicular to the cutting direction at the tool edge. These directional features provide preferential paths for crack propagations which finally promote the diamond coating debonding as characterized from the indentions measurements and delamination evaluations discussed in Chapter 5.

The interlayer failure evidenced in sample I-1may be mainly originated from a weak chemical binding energy between the diamond coating and the top Cr surface where the blasted diamond particles are not sufficient enough to provide a strong bonding. Due to the wide difference in machining performance between the CrN/Cr interlayer and the chemical etching pretreated tools, any additional optimization in the distribution or amount of diamond blasted/impinged particles at the top of the interlayer could not be sufficient to get closer to the performance of chemical etched samples. This may constitute a reason of why there are still no commercial solutions in the market of diamond coated tools intended for high silicon aluminum dry machining applications which incorporate the use of CrN/Cr interlayers as an adhesion improvement method.

www.manaraa.com

The CrN/Cr lack of adhesion can also be attributed to its minimal carbide formation ability due to its interdiffusion with carbon and the formation of additional Cr multiphase compounds (Cr_3C_2, Cr_7C_3, and Cr_3C_6), which provide a preferential direction for crack propagation [121] and evidenced in the XRD patterns shown in Figure 5.2.

In order to characterize the progressive wear failure or the abrupt delamination observed in the diamond coated tools in terms of the cutting efficiency, the information from the force dynamometers was recorded during each cutting pass for all samples described in Figure 6.5. An example of the three cutting forces developed during one cutting length pass is shown in Figure 6.8. Due to the characteristics of the dry machining process and the workpiece material condition, there is a variation in the force signal during the cutting time. In order to estimate a value for these forces, an average value was taken for each of them in a time range between the beginning and the end of the cutting pass. These values are summarized in Table 6.2 and correspond to the first, intermediate (~ 1.2 min), and final pass during the machining performance test. Besides the three major force components, a ratio between the average axial force F_a (feed force) and the tangential force F_t (cutting force) was also included in Table 6.2. Differences in the values of the radial force component during the first pass among all samples are mainly caused by the differences in workpiece geometry in terms of its diameter and the resulting vibration modes.

www.manaraa.com

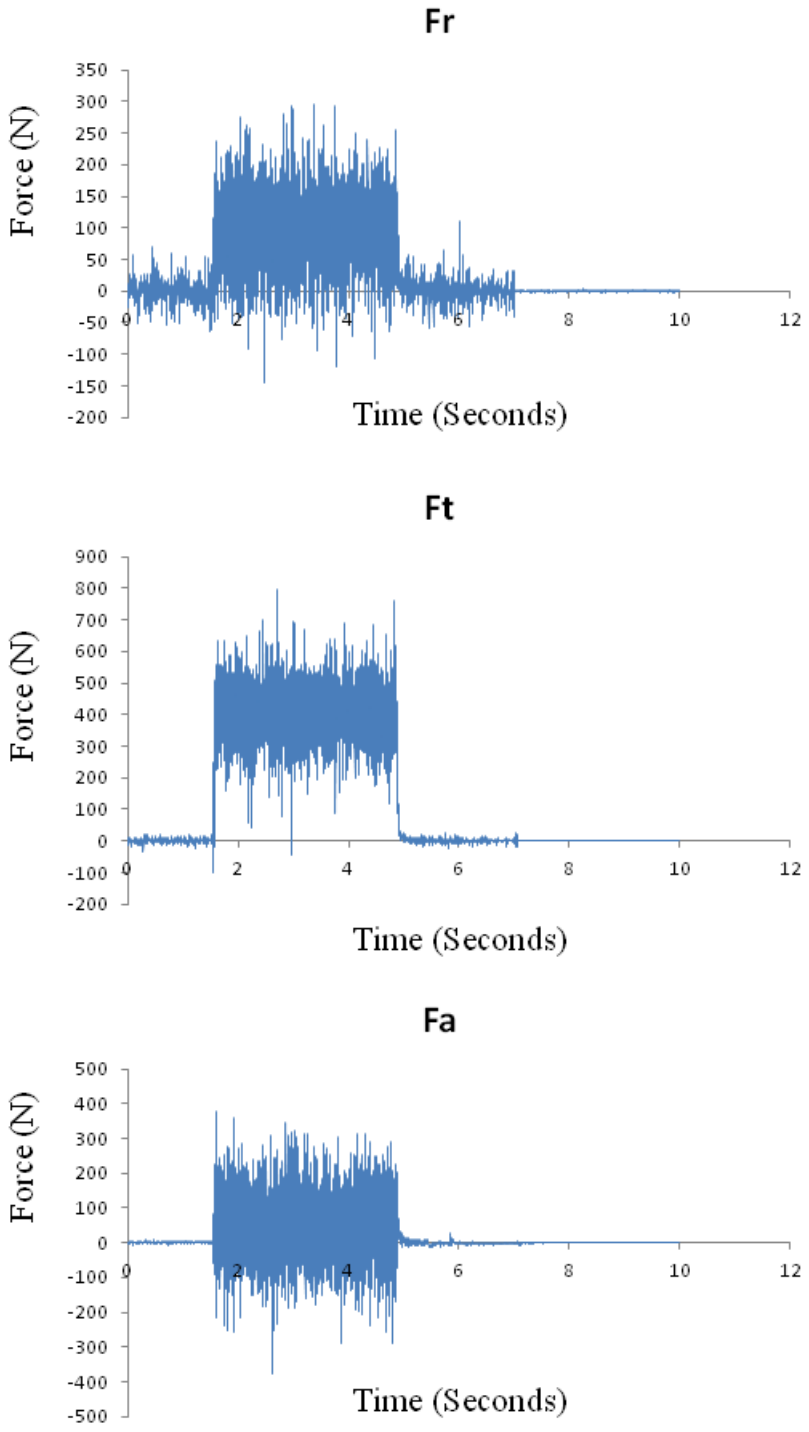

Figure 6.8. Example of the three cutting forces developed during one cutting length pass

www.manaraa.com

Table 6.2. Average values for the force components at three different cutting passes during the machine performance test

Sample	First Pass				Intermidiate Pass (~ 1.2 min)				Final Pass			
	Fr (N)	Ft (N)	Fa (N)	Fa/Ft	Fr (N)	Ft (N)	Fa (N)	Fa/Ft	Fr (N)	Ft (N)	Fa (N)	Fa/Ft
MCD	92.9	403.8	49.9	0.12	36.5	383.4	63.6	0.17	10.7	332.7	68.7	0.21
E-1-1	12.9	395.3	51.1	0.13	88.3	392.6	63.4	0.16	115.2	402.9	74.9	0.19
E-1-3	74.3	432.7	58.3	0.13	34.9	389.6	69.5	0.18	121.8	414.1	84.2	0.20
E-1-4	11.1	372.8	41.9	0.11	88.5	390.4	56.7	0.15	39.1	395.4	74.3	0.19
E-2-1	57.1	391.2	39.9	0.10	8.4	390.1	59.3	0.15	194.7	437.1	179.5	0.41

According to Table 6.2, the values of the forces F_t and F_a depend of the aluminum BUE amount at the tool cutting tip, however, the ratio F_a/F_t can be correlated to estimate the failure of the tool coating due to its gradual increase along with the cutting time. A failure in the coating can be also characterize by this ratio and found to be 0.41 for sample E-2-1.

www.manaraa.com

CHAPTER 7. CONCLUSIONS

The analysis and evaluation of diamond coatings deposited on cutting tool materials requires a systematic approach tailored in accordance with the particular manufacturing chain under consideration. Multiple research studies have been proposed in order to analyze the diamond adhesion and machining behavior, however, very few have been conducted by considering the correlation between the fundamental aspects of the diamond adhesion, the existent surface characteristics of the cutting tool, and the practical aspects encountered during dry machining operations. Moreover, any research study developed by using the cutting tool as a substrate, must consider its initial surface conditions and geometry aspects in order to optimize the diamond deposition process if machining performance is considered as the final output.

The main aspect to influence the diamond adhesion on surface pretreated WC-Co cutting tools is the surface/subsurface integrity of the substrate resulting from the cobalt suppression/halting approach applied. When chemical etching methods are used, the resulting roughness and surface texture in terms of preferential features play a key role in the diamond adhesion and machining performance as concluded by the results of the initial pretreatment evaluations. The selection of the processing variables during etching methods in terms of the chemical nature and immersion time must be related to the initial

www.manaraa.com

conditions encountered in the tool surface in order to achieve an optimal substrate condition.

During this research, the effect of the initial etching step using the Murakami reagent was analyzed in terms of the resulting texture and roughness parameter values. This etching stage is capable of producing a smoother surface at the substrate by minimizing the prior feed marks and surface damage. These features were successfully removed on the order of micro-scale roughness texture; however, other surface features were not removed completely after the highest immersion etching time (M4 treatment) as seen in Figure 4.7(d). Moreover, if longer Murakami etching times are used in an attempt to remove these remaining features, other surface defects will be created as seen in Figure 4.8. These resulting voids and craters significantly decrease the diamond adhesion and may have an impact in the tool geometry required for particular cutting operations. It is therefore important to specify an initial surface condition to the tool manufacturer when inserts are intended to be coated.

The amount of cobalt removed from the tool represented as the thickness of the cobalt depletion band depends on the immersion etching time as expected. The differences in this depletion band thickness are shown to have an effect on the formation of lateral cracks in the substrate. These cracks occurred during indentation evaluations performed to measure the initial adhesion of the diamond coatings. However, these values of the cobalt depletion thickness produced also prevented cobalt re-diffusion to the surface and did not appear to influence the final machining behavior of the diamond coated inserts during the dry machining operation.

www.manaraa.com

The fundamental chemical adhesion between the diamond coating and the CrN/Cr interlayer is the most important factor to consider if further optimization is to be attained through the use of this interlayer. The failure of the diamond coatings deposited when using this interlayer pretreatment approach is mostly associated with a delamination at the interface between the diamond and the top Cr layer as discussed in Chapters 5 and Chapter 6. Improvements by optimizing the shoot peening process may not have a significant impact on the adhesion due to its pure mechanical interlocking nature. An increase in the chemical bonding between the diamond and the interlayer is the key aspect to improve when considering new interlayer architectures. A better carbide formation without the formation of additional multiphase compounds is required to achieve an optimal adhesion behavior of the diamond coating.

The definition of adhesion refers to a system where the work or force of detachment is measured by the application of an external load capable of causing failure to the system under investigation. Based on this concept, different methodologies, which are essentially destructive, have been developed to characterize the adhesion, including Rockwell C indentation, scratch, bulge, and blister test. These methods are very useful for routine quality control. However, based on the experimental results of this research, it is not appropriate to correlate the adhesion measured by the Rockwell C indentation evaluation with the dry machining performance by using single indentations and comparing substrates with different interfacial characteristics. A more consistent adhesion evaluation for commercial microcrystalline diamond coating thicknesses (25-30 μm) was obtained by the critical load determination when using indentation progressions. The comparison of adhesion improvements in terms of critical loads is not valid when

www.manaraa.com

different interfaces (surface/subsurface) are present. Furthermore, the experimental results of this research work indicate that the evaluation of the adhesion of diamond coated cutting tools by pin-on-disc tribological tests, impact tests, scratch, indentation, or sand abrasion testing methods.

The machining performance of the interface engineered diamond coatings directly depends on the interfacial characteristics developed during the initial surface pretreatment methods. The failure of the CrN/Cr interlayer during the dry machining operation, suggest that the forces and stresses developed are considerably higher than the fundamental adhesion of the diamond coating. In terms of machining performance, the initial surface texture of the cutting tool determines the failure mode during cutting. In this manufacturing chain there is no evidence to believe that the subsurface integrity (cobalt depletion layer) has an influence in the machining performance.

When a particular surface condition is present on commercial carbide tools, any of the chemical etching methods can be used after a comprehensive optimization study of their effects. Through this extensive experimental work, there was no evidence of cobalt re-diffusion during the CVD growth that can potentially affect the resulting diamond adhesion. The CrN/Cr interlayer was not viable for dry machining applications and any optimization at the surface by peening methods will not increase the fundamental adhesion of the coating for machining applications.

An experimental protocol has been established to determine the critical load for commercial diamond coatings in an indentation progression and can be correlated to the expected dry machining performance. The coated tool insert produced by the chemical

www.manaraa.com

pretreatment E-1 performed significantly better in the dry machining of high silicon aluminum alloys and extensive experimentation was used to demonstrate the coating adhesion behavior and wear mechanisms involved.

www.manaraa.com

REFERENCES

[1] Mallika K, Komanduri R. Diamond coatings on cemented tungsten carbide tools by low-pressure microwave CVD. Wear 1999 2;224(2):245-66.

[2] INSPEC, INSPEC EMIS Group, Institution of Electrical Engineers, Nazaré MH, Neves AJ. Properties, growth, and applications of diamond. London: Institution of Electrical Engineers; 2001.

[3] Asmussin J, Reinhard DK. Diamond films handbook. New York: Marcel Dekker; 2002.

[4] Hall HT. Ultra-high Pressure Apparatus. Rev. Sci. Instr 1960;31(125).

[5] Bundy FP. Direct Conversion of Graphite to Diamond in Static Pressure Apparatus. Science 1962;137(3535):1057-8.

[6] Bundy FP, Hall HT, Strong HM, Wentorf RH,. Man-Made Diamonds. Nature 1955 07/09;176(4471):51-5.

[7] Trent EM, Wright PK. Metal cutting. 4th ed. Boston: Butterworth-Heinemann; 2000.

[8] Siniawski M, Bowman C. Metal working fluids: finding green in the manufacturing process. Industrial Lubrication and Tribology 2009;61(2):60.

[9] Sutherland K. Machinery and processing: Managing cutting fluids used in metal working. Filtration Sep. 2008;45(7):20-3.

[10] Jost HP. *Lubrication (Tribology) Education and Research,* A Report on the Present Position and Industry's Needs. 1966.

[11] Weinert K, Inasaki I, Sutherland JW, Wakabayashi T. Dry Machining and Minimum Quantity Lubrication. CIRP Ann.Manuf.Technol. 2004;53(2):511-37.

[12] UG Machining operations. 2011; (Surface Grinder and CNC Machine); Available at: http://www.thesurfacegrinder.com/2011/03/13/machining/.

www.manaraa.com

[13] Adler DP, Hii WW-, Michalek DJ, Sutherland JW. Examining the role of cutting fluids in machining and efforts to address associated environmental/health concerns. Mach.Sci.Technol. 2006 06/01; 2011/09;10(1):23-58.

[14] Roy P, Sarangi SK, Ghosh A, Chattopadhyay AK. Machinability study of pure aluminium and Al–12% Si alloys against uncoated and coated carbide inserts. International Journal of Refractory Metals and Hard Materials 2009 5;27(3):535-44.

[15] Gangopadhyay S, Acharya R, Chattopadhyay AK, Sargade VG. Effect of cutting speed and surface chemistry of cutting tools on the formation of BUL or BUE and surface quality of the generated surface in dry turning of AA6005 aluminium alloy. Mach.Sci.Technol. 2010 08/17; 2011/09;14(2):208-23.

[16] Köpf A, Feistritzer S, Udier K. Diamond coated cutting tools for machining of non-ferrous metals and fibre reinforced polymers. International Journal of Refractory Metals and Hard Materials 2006 9;24(5):354-9.

[17] Gat R, Swider S, Kelly E. CVD Diamond for Everyone. Cutting Tool Engineering 1995;47(2).

[18] Oles EJ, Inspektor A, Bauer CE. The new diamond-coated carbide cutting tools. Diamond and Related Materials 1996 5;5(6-8):617-24.

[19] Kalpakjian S, Schmid SR. Manufacturing engineering and technology. 4th ed. Upper Saddle River, NJ: Prentice Hall; 2001.

[20] Groover MP. Fundamentals of modern manufacturing : materials, processes, and systems. 2nd ed. New York: John Wiley & Sons; 2002.

[21] Alabi AGF, Ajiboye TK, Olusegun HD. Investigating the cutting forces in heat treated medium carbon steel when turning on a lathe machine. Journal of Engineering, Design and Technology 2010;8(1):80.

[22] Isakov E. DYNAMICS On GlobalSpec Available at: http://www.globalspec.com/reference/60600/203279/3-3-DYNAMICS. Accessed 11/3/2011, 2011.

[23] Kistler - Kistler Product Finder, Force Sensor, Force Transmitter Available at: http://www.kistler.com/us_en-us/131_Productfinder_ForceSensors/F1310.-.1/Product-Finder-Force.html. Accessed 9/4/2011, 2011.

[24] Shaw MC. Metal cutting principles. Oxford Oxfordshire; New York: Clarendon Press; Oxford University Press; 1984.

[25] Schey JA. Introduction to manufacturing processes. New York: McGraw-Hill; 1977.

www.manaraa.com

[26] Durante S. Dry machining solution for greener automotive production. 2003;EMO: 7d PRO-1 ECOSYSTEMS:1.

[27] Sreejith PS, Ngoi BKA. Dry machining: Machining of the future. J.Mater.Process.Technol. 2000 4/14;101(1-3):287-91.

[28] Canter N. The Possibilities and Limitations of Dry Machining. TLT 2009;67:40.

[29] Graham D, Huddle D, McNamara D. Machining Dry Is Worth A Try : Modern Machine Shop 2003; Available at: http://www.mmsonline.com/articles/machining-dry-is-worth-a-try. Accessed 9/8/2011, 2011.

[30] Smith PL. The 10 commandments of dry high-speed machining 1998; Available at: http://www.americanmachinist.com/304/Issue/Article/False/9131/Issue. Accessed 9/8/2011, 2011.

[31] Aronson RB. Why dry machining? Manufacturing Engineering 1995;2011.

[32] Torabian H, Pathak JP, Tiwari SN. Wear characteristics of Al-Si alloys. Wear 1994 2;172(1):49-58.

[33] Shanmugam DK, Chen FL, Siores E, Brandt M. Comparative study of jetting machining technologies over laser machining technology for cutting composite materials. Composite Structures 2002 7;57(1-4):289-96.

[34] Jianxin D, Taichiu L. Ultrasonic machining of alumina-based ceramic composites. Journal of the European Ceramic Society 2002 8;22(8):1235-41.

[35] Jain VK, Choudhary SK, Rajurkar KP. Experimental Investigations into Traveling Wire Electrochemical Spark Machining (TW-ECSM) of Composites. ASME Journal of Engineering for Industry 1991;113:75.

[36] Mohan B, Rajadurai A, Satyanarayana KG. Effect of SiC and rotation of electrode on electric discharge machining of Al–SiC composite. J.Mater.Process.Technol. 2002 6/20;124(3):297-304.

[37] Liu J, Kevin Chou Y. On temperatures and tool wear in machining hypereutectic Al–Si alloys with vortex-tube cooling. Int.J.Mach.Tools Manuf. 2007 3;47(3-4):635-45.

[38] Cline BL, Olson JM. CVD Diamond Solutions for Machining and Other Mechanical Applications. In: Asmussen J, Reinhard DK, editors. Diamond Films HandbookeBook ISBN: 978-0-203-91060-3: CRC Press; 2002.

[39] What is Chemical Vapor Deposition?; Innovation and Information for Sustainable Living. Available at : http://www.innovateus.net/science/what-chemical-vapor-deposition.

www.manaraa.com

[40] Pierson HO. Handbook of chemical vapor deposition : principles, technology and applications. 2nd ed. ed. Norwich, NY: Noyes Publications; 1999.

[41] Xu Z. Fabrication and optimization of microwave plasma assisted chemical vapor deposition system for growing diamond films. [electronic resource]. Tampa, Fla: University of South Florida; 2003.

[42] Celii FG, White Jr. D, Purdes AJ. Deposition of smooth, oriented diamond films using microwave plasma chemical vapor deposition. Thin Solid Films 1992 5/15;212(1-2):140-9.

[43] Buijnsters JG, Vázquez L, ter Meulen JJ. Substrate pre-treatment by ultrasonication with diamond powder mixtures for nucleation enhancement in diamond film growth. Diamond and Related Materials 2009 10;18(10):1239-46.

[44] Shing YH, Pool FS, Rich DH. Low-pressure microwave plasma nucleation and deposition of diamond films. Thin Solid Films 1992 5/15;212(1-2):150-5.

[45] Y. A. The effect of silicon surface preparation on the nucleation of diamond by chemical vapor deposition. Diamond and Related Materials 1992 3/25;1(2-4):216-9.

[46] Duncan Marshall R, Whitfield MD, Tracey S, Thompson DJ, Foord JS, Jackman RB. Optimising control of microwave plasma bias enhanced nucleation for heteroepitaxial chemical vapour deposition diamond. Diamond and Related Materials 1997 4;6(5-7):676-80.

[47] Davis RF. Diamond films and coatings : development, properties, and applications. Park Ridge, N.J: Noyes Pub; 1993.

[48] Belton DN, Schmieg SJ. Loss of epitaxy during diamond film growth on ordered Ni(100). J.Appl.Phys. 1989;66(9):4223-9.

[49] Xu Z. Synthesis, characterization, and applications of CVD micro- and nanocrystalline diamond thin films [electronic resource]. Tampa, Fla: University of South Florida; 2007.

[50] Gomez H, Kumar A, Jeedigunta S. Structural–property relationship of nanocrystalline diamond films and its applications. Int. J. Nanomanufacturing, 2009;4(1/2/3/4):317.

[51] Baidakova M, Vulâ€™ A, Golubev V, Grudinkin S, Melekhin V, Feoktistov N, et al. Growth of diamond films on crystalline silicon by hot-filament chemical vapor deposition. Semiconductors 2002;36(6):615-20.

www.manaraa.com

[52] Wang T, Xin HW, Zhang ZM, Dai YB, Shen HS. The fabrication of nanocrystalline diamond films using hot filament CVD. Diamond and Related Materials 2004 1;13(1):6-13.

[53] Zhang S. Materials characterization techniques / Sam Zhang, Lin Li, Ashok Kumar. Boca Raton: CRC Press; 2009.

[54] Haubner R. Comparison of sulfur, boron, nitrogen and phosphorus additions during low-pressure diamond deposition. Diamond and Related Materials 2005 7;14(3-7):355-63.

[55] Lin T. Compositional mapping of the argon-methane-hydrogen system for polycrystalline to nanocrystalline diamond film growth in a hot-filament chemical vapor deposition system. Appl.Phys.Lett. 2000;77(17):2692.

[56] Jeedigunta S, Xu Z, Hirai M, Spagnol P, Kumar A. Effects of plasma treatments on the nitrogen incorporated nanocrystalline diamond films. Diamond and Related Materials 2008 12;17(12):1994-7.

[57] Birrell J. Bonding structure in nitrogen doped ultrananocrystalline diamond. J.Appl.Phys. 2003;93(9):5606.

[58] Alam M, Peebles DE, Tallant DR. Diamond deposition onto WC-6%Co cutting tool material: coating structure and interfacial bond strength. Thin Solid Films 1997 5/28;300(1-2):164-70.

[59] Polini R, Marcheselli G, Mattei G, Traversa E. Nucleation and Growth of Diamond Films on Ni-Cemented Tungsten Carbide: II, Effects of Deposition Conditions. J Am Ceram Soc 1995;78(9):2431-6.

[60] Silva S, Mammana VP, Salvadori MC, Monteiro OR, Brown IG. WC-Co cutting tool inserts with diamond coatings. Diamond and Related Materials 1999 10;8(10):1913-8.

[61] Raghuveer MS, Yoganand SN, Jagannadham K, Lemaster RL, Bailey J. Improved CVD diamond coatings on WC–Co tool substrates. Wear 2002 12;253(11-12):1194-206.

[62] Huang Y, Xiao H, Ma Z, Wang J, Gao P. Effects of Cu and Cu/Ti interlayer on adhesion of diamond film. Surface and Coatings Technology 2007 11/15;202(1):180-4.

[63] Polini R, Barletta M. On the use of CrN/Cr and CrN interlayers in hot filament chemical vapour deposition (HF-CVD) of diamond films onto WC-Co substrates. Diamond and Related Materials 2008 3;17(3):325-35.

www.manaraa.com

[64] Tang W, Wang S, Lu F. Preparation and performance of diamond coatings on cemented carbide inserts with cobalt boride interlayers. Diamond and Related Materials 2000 10;9(9-10):1744-8.

[65] Glozman O, Halperin G, Etsion I, Berner A, Shectman D, Lee GH, et al. Study of the wear behavior and adhesion of diamond films deposited on steel substrates by use of a Cr–N interlayer. Diamond and Related Materials 1999 3;8(2-5):859-64.

[66] Lin CR, Kuo CT, Chang RM. Improvement in adhesion of diamond films on cemented WC substrate with Ti–Si interlayers. Diamond and Related Materials 1998 12;7(11-12):1628-32.

[67] Naguib NN, Elam JW, Birrell J, Wang J, Grierson DS, Kabius B, et al. Enhanced nucleation, smoothness and conformality of ultrananocrystalline diamond (UNCD) ultrathin films via tungsten interlayers. Chemical Physics Letters 2006 10/30;430(4-6):345-50.

[68] Polini R, Mantini FP, Barletta M, Valle R, Casadei F. Hot filament chemical vapour deposition and wear resistance of diamond films on WC-Co substrates coated using PVD-arc deposition technique. Diamond and Related Materials 2006 9;15(9):1284-91.

[69] Barletta M, Rubino G, Gisario A. Adhesion and wear resistance of CVD diamond coatings on laser treated WC–Co substrates. Wear 2011 7/29;271(9-10):2016-24.

[70] Amaral M, Almeida F, Fernandes AJS, Costa FM, Oliveira FJ, Silva RF. The role of surface activation prior to seeding on CVD diamond adhesion. Surface and Coatings Technology 2010 8/15;204(21-22):3585-91.

[71] Lin CR, Kuo CT, Chang RM. Application of heat treatment and dispersive strengthening concept in interlayer deposition to enhance diamond film adherence. Thin Solid Films 1997 10/31;308-309(0):273-8.

[72] Sommer M, Haubner R, Lux B. Diamond deposition on copper treated hardmetal substrates. Diamond and Related Materials 2000 5;9(3-6):351-7.

[73] Endler I, Leonhardt A, Scheibe H-, Born R. Interlayers for diamond deposition on tool materials. Diamond and Related Materials 1996 4;5(3-5):299-303.

[74] Sarangi SK, Chattopadhyay A, Chattopadhyay AK. Effect of pretreatment, seeding and interlayer on nucleation and growth of HFCVD diamond films on cemented carbide tools. International Journal of Refractory Metals and Hard Materials 2008 5;26(3):220-31.

[75] Almeida FA, Carrapichano JM, Fernandes AJS, Sacramento J, Silva RF, Oliveira FJ. Nanocrystalline CVD diamond coatings for drilling of WC-Co parts. International Journal of Refractory Metals and Hard Materials 2011 9;29(5):618-22.

www.manaraa.com

[76] Chou YK, Thompson RG, Kumar A. CVD-diamond technologies for dry drilling applications. Thin Solid Films 2010 10/1;518(24):7487-91.

[77] Zhang D, Shen B, Sun F. Study on tribological behavior and cutting performance of CVD diamond and DLC films on Co-cemented tungsten carbide substrates. Appl.Surf.Sci. 2010 2/1;256(8):2479-89.

[78] Kremer A, El Mansori M. Influence of nanostructured CVD diamond coatings on dust emission and machinability of SiC particle-reinforced metal matrix composite. Surface and Coatings Technology 2009 12/25;204(6-7):1051-5.

[79] Qin F, Hu J, Chou YK, Thompson RG. Delamination wear of nano-diamond coated cutting tools in composite machining. Wear 2009 6/15;267(5-8):991-5.

[80] Torres CD, Heaney PJ, Sumant AV, Hamilton MA, Carpick RW, Pfefferkorn FE. Analyzing the performance of diamond-coated micro end mills. Int.J.Mach.Tools Manuf. 2009 6;49(7-8):599-612.

[81] Chattopadhyay A, Sarangi SK, Chattopadhyay AK. Effect of negative dc substrate bias on morphology and adhesion of diamond coating synthesised on carbide turning tools by modified HFCVD method. Appl.Surf.Sci. 2008 12/30;255(5, Part 1):1661-71.

[82] Liang Q, Vohra YK, Thompson R. High speed continuous and interrupted dry turning of A390 Aluminum/Silicon Alloy using nanostructured diamond coated WC–6 wt.% cobalt tool inserts by MPCVD. Diamond and Related Materials 2008 12;17(12):2041-7.

[83] Almeida FA, Sacramento J, Oliveira FJ, Silva RF. Micro- and nano-crystalline CVD diamond coated tools in the turning of EDM graphite. Surface and Coatings Technology 2008 11/25;203(3-4):271-6.

[84] Meng XM, Tang WZ, Hei LF, Li CM, Askari SJ, Chen GC, et al. Application of CVD nanocrystalline diamond films to cemented carbide drills. International Journal of Refractory Metals and Hard Materials 2008 9;26(5):485-90.

[85] Martinho RP, Silva FJG, Baptista APM. Cutting forces and wear analysis of Si3N4 diamond coated tools in high speed machining. Vacuum 2008 8/8;82(12):1415-20.

[86] Cabral G, Gäbler J, Lindner J, Grácio J, Polini R. A study of diamond film deposition on WC–Co inserts for graphite machining: Effectiveness of SiC interlayers prepared by HFCVD. Diamond and Related Materials 2008 6;17(6):1008-14.

[87] Hu J, Chou YK, Thompson RG. Nanocrystalline diamond coating tools for machining high-strength Al alloys. International Journal of Refractory Metals and Hard Materials 2008 5;26(3):135-44.

www.manaraa.com

[88] Heaney PJ, Sumant AV, Torres CD, Carpick RW, Pfefferkorn FE. Diamond coatings for micro end mills: Enabling the dry machining of aluminum at the micro-scale. Diamond and Related Materials 2008 3;17(3):223-33.

[89] Cabral G, Reis P, Polini R, Titus E, Ali N, Davim JP, et al. Cutting performance of time-modulated chemical vapour deposited diamond coated tool inserts during machining graphite. Diamond and Related Materials 2006 10;15(10):1753-8.

[90] Riccardo P. Chemically vapour deposited diamond coatings on cemented tungsten carbides: Substrate pretreatments, adhesion and cutting performance. Thin Solid Films 2006 9/25;515(1):4-13.

[91] Sun FH, Zhang ZM, Chen M, Shen HS. Improvement of adhesive strength and surface roughness of diamond films on Co-cemented tungsten carbide tools. Diamond and Related Materials 2003 7;12(3-7):711-8.

[92] Chen M, Jian XG, Sun FH, Hu B, Liu XS. Development of diamond-coated drills and their cutting performance. J.Mater.Process.Technol. 2002 10/11;129(1-3):81-5.

[93] Polini R, Bravi F, Casadei F, D'Antonio P, Traversa E. Effect of substrate grain size and surface treatments on the cutting properties of diamond coated Co-cemented tungsten carbide tools. Diamond and Related Materials 2002 6;11(3-6):726-30.

[94] Burakowski T. Surface engineering of metals : principles, equipment, technologies / Tadeusz Burakowski, Tadeusz Wierzchoń. Boca Raton, Fla: CRC Press; 1999.

[95] Peng XiLing, Gan ZhaoPing. Morphologies and adhesion strength of diamond films deposited on WC-6%Co cemented carbides with different surface characteristics. Thin Solid Films 1994 2/15;239(1):47-50.

[96] Taher MA, Schmid WF, Malshe AP, Oles EJ, Inspektor A. The sate-of-the-art in adhesion of CVD diamond to carbide cutting inserts. In: Mittal KL, editor. Adhesion Aspects of Thin Films, Vol. 1.Boston: Utrecht ; Boston : VSP; 2001, p. 79.

[97] Ullram S, Haubner R. Temperature pre-treatments of hardmetal substrates to reduce the cobalt content and improve diamond deposition. Diamond and Related Materials 2006 8;15(4-8):994-9.

[98] Ken B. The rough edged secret of coating hardmetals with diamond layers. Metal Powder Report 2010 6;65(4):38-42.

[99] Vladimir I. G. Characterization of cascade arc assisted CVD diamond-coating technology: Part II. Coating properties and applications. Surface and Coatings Technology 2005 5/1;194(2-3):300-18.

www.manaraa.com

[100] Poon CY, Bhushan B. Comparison of surface roughness measurements by stylus profiler, AFM and non-contact optical profiler. Wear 1995 11;190(1):76-88.

[101] Shen B, Sun F. Deposition and friction properties of ultra-smooth composite diamond films on Co-cemented tungsten carbide substrates. Diamond and Related Materials 2009 3;18(2-3):238-43.

[102] Roy M, Ghodbane S, Koch T, Pauschitz A, Steinmüller–Nethl D, Tomala A, et al. Tribological investigation of nanocrystalline diamond films at low load under different tribosystems. Diamond and Related Materials 2011 4;20(4):573-83.

[103] Borrero-López O, Hoffman M, Bendavid A, Martin PJ. The use of the scratch test to measure the fracture strength of brittle thin films. Thin Solid Films 2010 6/30;518(17):4911-7.

[104] Buijnsters JG, Shankar P, van Enckevort WJP, Schermer JJ, ter Meulen JJ. The adhesion of hot-filament CVD diamond films on AISI type 316 austenitic stainless steel. Diamond and Related Materials 2004 8;13(4-8):848-57.

[105] Huu TL, Schmitt M, Paulmier D, Mamalis AG, Grabchenko A. Tribological properties of smooth diamond coatings for cutting tools. Wear 1999 4;225-229, Part 2(0):843-7.

[106] Amirhaghi S, Reehal HS, Wood RJK, Wheeler DW. Diamond coatings on tungsten carbide and their erosive wear properties. Surface and Coatings Technology 2001 1/15;135(2-3):126-38.

[107] Kamiya S, Takahashi H, D'Antonio P, Polini R, Traversa E. Quantitative comparison of adhesive toughness for various diamond films on co-cemented tungsten carbide. Diamond and Related Materials 2002 6;11(3-6):716-20.

[108] Deuerler F, Gruner H, Pohl M, Tikana L. Wear mechanisms of diamond-coated tools. Surface and Coatings Technology 2001 7;142-144(0):674-80.

[109] Deuerler F, Lemmer O, Frank M, Pohl M, Heßing C. Diamond films for wear protection of hardmetal tools. International Journal of Refractory Metals and Hard Materials 2002 3;20(2):115-20.

[110] Deuerler F, Pohl M, Heßing C. Micro- and nanostructured diamond films under wear charging in cavitation test. Surface and Coatings Technology 2003 10;174-175(0):732-7.

[111] Buijnsters JG, Shankar P, van Enckevort WJP, Schermer JJ, ter Meulen JJ. Adhesion analysis of polycrystalline diamond films on molybdenum by means of scratch, indentation and sand abrasion testing. Thin Solid Films 2005 3/1;474(1-2):186-96.

www.manaraa.com

[112] Zhu W, McCune RC, deVries JE, Tamor MA, Ng KYS. Investigation of adhesion of diamond films on Mo, W and carburized W substrates. Diamond and Related Materials 1995 4/1;4(3):220-33.

[113] Windischmann H, Gray KJ. Stress measurement of CVD diamond films. Diamond and Related Materials 1995 5/1;4(5-6):837-42.

[114] Cristofanilli G, Polini R, Barletta M. HF-CVD of diamond coatings onto Fluidized Bed (FB) treated CrN interlayers. Thin Solid Films 2010 12/30;519(5):1594-9.

[115] Chai H, Lawn BR. Fracture Mode Transitions in Brittle Coatings on Compliant Substrates as a Function of Thickness. J. Mater. Res 2004;19(6):1752.

[116] Evans AG, Hutchinson JW. On the mechanics of delamination and spalling in compressed films. Int.J.Solids Structures 1984;20(5):455-66.

[117] Wang JS, Sugimura Y, Evans AG, Tredway WK. The mechanical performance of DLC films on steel substrates. Thin Solid Films 1998 7/18;325(1-2):163-74.

[118] Gunnars J, Alahelisten A. Thermal stresses in diamond coatings and their influence on coating wear and failure. Surface and Coatings Technology 1996 4;80(3):303-12.

[119] Morris D, Cook R. Radial Fracture During Indentation by Acute Probes: I, Description by an Indentation Wedging Model. Int.J.Fract. 2005;136(1):237-64.

[120] Feng G, Qu S, Huang Y, Nix WD. An analytical expression for the stress field around an elastoplastic indentation/contact. Acta Materialia 2007 5;55(9):2929-38.

[121] Xiao X, Sheldon BW, Konca E, Lev LC, Lukitsch MJ. The failure mechanism of chromium as the interlayer to enhance the adhesion of nanocrystalline diamond coatings on cemented carbide. Diamond and Related Materials 2009 9;18(9):1114-7.

www.manaraa.com

ABOUT THE AUTHOR

Humberto Arturo Gomez Vega received his BSME in 2001 and MSME in 2003 from Universidad del Norte, Barranquilla, Colombia. In fall 2007, he began his doctoral research in the synthesis and characterization of nanocrystalline diamond films for multifunctional applications. In particular, he is interested in diamond coatings for dry machining applications. Additionally, he conducted significant research works on the synthesis and characterization of nanodiamond-polymer nanocomposite materials for energy and high stability applications. During the summers of 2010 and 2011, he joined the General Motors Global Research and Development Center at Warren-Michigan for a research visitor and graduate student intern position, respectively. Humberto has also published numerous papers in peer reviewed journals and conference proceedings. He has been the recipient of the Successful Latino Student Award 2011 in recognition of meritorious excellence, outstanding performance, and high scholastic achievement. Upon completion of his doctoral degree, Humberto will assume a faculty position in the Mechanical Engineering Department at Universidad del Norte.

www.manaraa.com